Western Graduate&PostdoctoralStudies

Western University
Scholarship@Western

Electronic Thesis and Dissertation Repository

4-18-2017 12:00 AM

Recruitment Strategies In Human Sympathetic Nerve Activity

Mark B. Badrov
The University of Western Ontario

Supervisor
Dr. J. Kevin Shoemaker
The University of Western Ontario

Graduate Program in Kinesiology
A thesis submitted in partial fulfillment of the requirements for the degree in Doctor of Philosophy
© Mark B. Badrov 2017

Follow this and additional works at: https://ir.lib.uwo.ca/etd

Part of the Systems and Integrative Physiology Commons

Recommended Citation

Badrov, Mark B., "Recruitment Strategies In Human Sympathetic Nerve Activity" (2017). *Electronic Thesis and Dissertation Repository*. 4493.
https://ir.lib.uwo.ca/etd/4493

This Dissertation/Thesis is brought to you for free and open access by Scholarship@Western. It has been accepted for inclusion in Electronic Thesis and Dissertation Repository by an authorized administrator of Scholarship@Western. For more information, please contact wlswadmin@uwo.ca.

Abstract

The overall objectives of the current dissertation were to 1) establish the neural coding principles employed by the sympathetic nervous system (SNS) in response to acute physiological stress; and 2) to determine the various mechanisms of control underlying these sympathetic neural recruitment strategies. This research tested the working hypothesis that efferent post-ganglionic muscle sympathetic nerve activity exhibits neural coding patterns reflecting increased firing of lower-threshold axons, recruitment of latent sub-populations of higher-threshold axons, as well as malleable synaptic delays, and further, that these strategies are governed by factors such as reflex-specificity, stress severity, perception of effort or stress, age, and cardiovascular disease. Specifically, we utilized a novel signal processing approach to study sympathetic action potential discharge patterning during periods of acute reflex-mediated sympathoexcitation. Overall, these studies support the working hypothesis and confirm that neural coding principles operate within the SNS. Specifically, in response to acute homeostatic perturbation, the SNS has options to increase the firing rate of already-active, lower-threshold axons, recruit sub-populations of previously silent (i.e., not present at baseline), larger-sized and faster conducting sympathetic axons, as well as modify acutely synaptic delays. *Study 1* demonstrated that the ability to recruit latent neural sub-populations represents a fixed, reflex-independent recruitment strategy, as this pattern was observed during chemoreflex- and baroreflex-mediated sympathoexcitation. In turn, this option appears reserved for severe stress scenarios. Furthermore, *study 2* suggests that central, perceptual features may play a specific role in modifying the synaptic delay aspect of efferent discharge timing, whereas peripheral-reflex mechanisms mediate the recruitment of latent axons. *Study 3* demonstrates that, while the ability to acutely modify synaptic delays appears

preserved, the ability to increase firing frequency of already-active axons, and importantly, the capacity of the SNS to recruit latent sub-populations of higher-threshold axons are reduced with healthy aging and perhaps lost altogether with cardiovascular disease. Finally, *study 4* suggests that the lack of ventilation itself, rather than the ever-increasing chemical drive, mediates the robust sympathetic neural recruitment observed during apnea. In conclusion, the series of studies contained herein confirm the presence of neural coding patterns in human efferent post-ganglionic sympathetic nerve activity.

Keywords

Action potential; Action potential detection; Aging; Baroreflex; Chemoreflex; Coronary artery disease; Exercise pressor reflex; Microneurography; Muscle sympathetic nerve activity; Sympathetic neural recruitment strategies

Co-Authorship Statement

Mark B. Badrov was the first author and Dr. J. Kevin Shoemaker was the senior author on all papers included in this thesis. The co-author on Chapter 2 was Charlotte W. Usselman. The co-author on Chapter 3 was T. Dylan Olver. The co-authors on Chapter 4 were Sophie Lalande, T. Dylan Olver, and Neville Suskin. The co-authors on Chapter 5 were Otto F. Barak, Tanja Mijacika, Leena N. Shoemaker, Lindsay J. Borrell, Mihajlo Lojpur, Ivan Drvis, and Zeljko Dujic.

Specific contributions to the papers are listed as follows:

Conception and design: Mark B. Badrov and J. Kevin Shoemaker

Data collection: Mark B. Badrov, Charlotte W. Usselman, T. Dylan Olver, Sophie Lalande, Otto F. Barak, Tanja Mijacika, Mihajlo Lojpur, Ivan Drvis, and J. Kevin Shoemaker

Data analysis and interpretation: Mark B. Badrov, Leena N. Shoemaker, Lindsay J. Borrell, Zeljko Dujic, and J. Kevin Shoemaker

Writing and revisions: Mark B. Badrov with revisions and feedback from all co-authors

Dedication

To mom and Tata … I love you

Acknowledgments

I would like to acknowledge Jennifer Vording and Arlene Fleischhauer for their assistance with *Study 3* of this dissertation.

Table of Contents

Abstract i

Keywords iii

Co-Authorship Statement iv

Dedication v

Acknowledgments vi

Table of Contents vii

List of Tables xi

List of Figures xiii

List of Abbreviations xvi

Chapter 1 1

1 Introduction 1

1.1 Overview 1

1.2 Autonomic Nervous System 9

1.2.1 Parasympathetic Nervous System 10

1.2.2 Sympathetic Nervous System 11

1.3 Sympathetic Neural Control of the Circulation 14

1.3.1 Baroreflex 14

1.3.2 Chemoreflex 16

1.3.3 Exercise Pressor Reflex 18

1.4 Muscle Sympathetic Nerve Activity 19

1.5 References 34

Chapter 2 49

2 Sympathetic neural recruitment strategies: responses to severe chemoreflex and baroreflex stress 49

2.1 Introduction 49

2.2 Methods 51
2.2.1 Participants 51
2.2.2 Experimental Protocol 51
2.2.3 Sympathetic Neural Recordings 53
2.2.4 Integrated MSNA Analysis 54
2.2.5 Action Potential Detection and Analysis 55
2.2.6 Test-Retest Repeatability of Action Potential Detection 57
2.2.7 Statistical Analysis 58
2.3 Results 58
2.4 Discussion 76
2.5 References 82
Chapter 3 86
3 Central vs. peripheral determinants of sympathetic neural recruitment: insights from static handgrip exercise and postexercise circulatory occlusion 86
3.1 Introduction 86
3.2 Methods 89
3.2.1 Participants 89
3.2.2 Experimental Protocol 89
3.2.3 Experimental Measures 90
3.2.4 Data Analysis 90
3.2.5 Statistical Analysis 92
3.3 Results 93
3.4 Discussion 104
3.5 References 110
Chapter 4 116
4 Effects of aging and coronary artery disease on sympathetic neural recruitment strategies during end-inspiratory and end-expiratory apnea 116

4.1 Introduction 116
4.2 Methods 118
4.2.1 Participants 118
4.2.2 Experimental Protocols 119
4.2.3 Experimental Measures 120
4.2.4 Data Analysis 120
4.2.5 Statistical Analysis 122
4.3 Results 122
4.4 Discussion 142
4.5 References 148
Chapter 5 153
5 Ventilation inhibits sympathetic action potential recruitment even during severe chemoreflex stress 153
5.1 Introduction 153
5.2 Methods 157
5.2.1 Participants 157
5.2.2 Experimental Protocol 157
5.2.3 Experimental Measures 159
5.2.4 Data Analysis 159
5.2.5 Statistical Analysis 162
5.3 Results 163
5.4 Discussion 180
5.5 References 186
Chapter 6 192
6 General Discussion 192
6.1 Overview 192

6.2 Major Findings 192
6.3 Perspectives and Significance 197
6.4 Conclusion 199
6.5 References 200
Appendix A: Ethics Approval 203
Appendix B: Rights of Authors of APS Articles 209
Curriculum Vitae 211

List of Tables

Table 2.1: Hemodynamic parameters at baseline and during maximal end-inspiratory apnea 62

Table 2.2: Integrated MSNA and action potential indices at baseline and during maximal end-inspiratory apnea 63

Table 2.3: Hemodynamic parameters at baseline and during −80 mmHg lower body negative pressure 64

Table 2.4: Integrated MSNA and action potential indices at baseline and during −80 mmHg lower body negative pressure 65

Table 2.5: Proportional and fixed bias outcomes for action potential detection determined from the Bland-Altman method of differences during baseline, maximal end-inspiratory apnea, and −80 mmHg lower body negative pressure protocols 66

Table 3.1: Hemodynamic responses to SHG and PECO 96

Table 3.2: Integrated MSNA and action potential responses to SHG and PECO 97

Table 4.1: Participant characteristics 129

Table 4.2: Hemodynamic responses to end-inspiratory and end-expiratory apnea 130

Table 4.3: Integrated MSNA and action potential indexes at baseline and during maximal end-inspiratory apnea 131

Table 4.4: Integrated MSNA and action potential indexes at baseline and during maximal end-expiratory apnea 133

Table 5.1: Hemodynamic responses to FRC_{Apnea} and $RBR_{Matched}$ protocols 169

Table 5.2: Integrated MSNA responses to FRC_{Apnea} and $RBR_{Matched}$ protocols 170

Table 5.3: Hemodynamic responses to FRC_{Apnea} and RBR_{End} protocols 171

Table 5.4: Integrated MSNA responses to FRC_{Apnea} and RBR_{End} protocols 172

Table 5.5: Hemodynamic responses to the FRC-RBR_{alt} protocol..... 173

Table 5.6: Integrated MSNA responses to the FRC-RBR_{alt} protocol 174

List of Figures

Figure 1.1: Schematic representation of action potential (AP) detection and classification. . 28

Figure 2.1: Schematic representation of action potential (AP) detection and classification. . 67

Figure 2.2: Representative sample of data from one subject collected at baseline, during rebreathe, maximal end-inspiratory apnea, and recovery. 68

Figure 2.3: Total detected clusters (A) and active clusters/burst (B) at baseline and during maximal end-inspiratory apnea. 69

Figure 2.4: Histogram representing action potential (AP) content as a function of normalized cluster number at baseline and during maximal end-inspiratory apnea. 70

Figure 2.5: Mean action potential cluster latency across participants as a function of normalized cluster number at baseline and during maximal end-inspiratory apnea. 71

Figure 2.6: Representative sample of data from one subject collected at baseline and during −80 mmHg lower body negative pressure (LBNP) and recovery. 72

Figure 2.7: Total detected clusters (A) and active clusters/burst (B) at baseline and during −80 mmHg lower body negative pressure (LBNP). 73

Figure 2.8: Histogram representing action potential (AP) content as a function of normalized cluster number at baseline and −80 mmHg lower body negative pressure (LBNP). 74

Figure 2.9: Mean action potential cluster latency across participants as a function of normalized cluster number at baseline and −80 mmHg lower body negative pressure (LBNP). 75

Figure 3.1: Representative sample of data collected from one subject at baseline (BSL) and during static handgrip and postexercise circulatory occlusion (PECO). 98

Figure 3.2: Hemodynamic responses to static handgrip (HG) and postexercise circulatory occlusion (PECO). 99

Figure 3.3: Integrated muscle sympathetic nerve activity (MSNA) responses to static handgrip (HG) exercise and postexercise circulatory occlusion (PECO). 100

Figure 3.4: Sympathetic action potential (AP) responses to static handgrip (HG) exercise and postexercise circulatory occlusion (PECO). 101

Figure 3.5: Action potential (AP) cluster latency as a function of AP cluster size at baseline (BSL), minutes one to five of static handgrip (HG), and post-exercise circulatory occlusion (PECO). 102

Figure 4.1: Representative recordings of the integrated muscle sympathetic nerve activity (MSNA) neurogram and detected action potentials (APs) from one young healthy (YH) individual (A), one older healthy (OH) individual (B), and one coronary artery disease (CAD) patient (C) at baseline and during end-inspiratory (EI) and end-expiratory (EE) apnea. 135

Figure 4.2: Action potential (AP) content per burst (A), total clusters (B), and active clusters per burst (C) in young healthy (YH), older healthy (OH), and coronary artery disease (CAD) patients at baseline and during end-inspiratory (EI) apnea. 136

Figure 4.3: Action potential (AP) cluster latency as a function of normalized cluster number (i.e., size) at baseline and during end-inspiratory (EI) apnea in young healthy (YH; left panel), older healthy (OH; middle panel), and coronary artery disease patients (CAD; right panel). 138

Figure 4.4: Action potential (AP) content per burst (A), total clusters (B), and active clusters per burst (C) in young healthy (YH), older healthy (OH), and coronary artery disease (CAD) patients at baseline and during end-expiratory (EE) apnea. 139

Figure 4.5: Action potential (AP) cluster latency as a function of normalized cluster number (i.e., size) at baseline and during end-expiratory (EE) apnea in young healthy (YH; left panel), older healthy (OH; middle panel), and coronary artery disease patients (CAD; right panel). 141

Figure 5.1: Representative recordings of the integrated muscle sympathetic nerve activity (MSNA) neurogram and detected action potentials (APs) (and associated chemoreflex stimuli) from one individual during the functional residual capacity (FRC) apnea and rebreathing protocols. 175

Figure 5.2: Sympathetic action potential (AP) recruitment during baseline (BSL), initial rebreathe (RBR), and maneuver (MAN) periods of the FRC_{Apnea} and $RBR_{Matched}$ protocols. 176

Figure 5.3: Sympathetic action potential (AP) recruitment during baseline (BSL), initial rebreathe (RBR), and maneuver (MAN) periods of the FRC_{Apnea} and RBR_{End} protocols. ... 177

Figure 5.4: Representative recordings of the integrated muscle sympathetic nerve activity (MSNA) neurogram and detected action potentials (APs) (and associated chemoreflex stimuli) from one individual during the alternating functional residual capacity (FRC) apnea and rebreathe (RBR) protocol (i.e., FRC-RBR_{ALT}). 178

Figure 5.5: Sympathetic action potential (AP) recruitment during baseline (BSL) and alternating periods of apnea at functional residual capacity (FRC) and rebreathe (RBR). .. 179

List of Abbreviations

AP – Action potential

ACh – Acetylcholine

ANOVA – Analysis of variance

ANS – Autonomic nervous system

ATP – Adenosine triphosphate

AU – Arbitrary units

BMI – Body mass index

CAD – Coronary artery disease

cAMP – Cyclic adenosine monophosphate

CNS – Central nervous system

CO – Cardiac output

CVLM – Caudal ventrolateral medulla

CWT – Continuous wavelet transform

EE – End-expiratory

EI – End-inspiratory

FRC – Functional residual capacity

GABA – ɣ-aminobutyric-acid

hb – Heartbeats

HbSat – Hemoglobin saturation

HR – Heart rate

IML – Intermediolateral cell column

LBNP – Lower body negative pressure

LVEF – Left ventricular ejection fraction

MAP – Mean arterial pressure

MI – Myocardial infarction

MSNA – Muscle sympathetic nerve activity

MVC – Maximal voluntary contraction

NE – Norepinephrine

NPY – Neuropeptide Y

NS – Not significant

NTS – Nucleus tractus solitarius

OH – Older healthy

PCO_2 – Partial pressure of carbon dioxide

PECO – Post-exercise circulatory occlusion

$P_{ET}CO_2$ – End-tidal partial pressure of carbon dioxide

$P_{ET}O_2$ – End-tidal partial pressure of oxygen

PNS – Parasympathetic nervous system

PO_2 – Partial pressure of oxygen

RBR - Rebreathe

RVLM – Rostral ventrolateral medulla

SD – Standard deviation

SE – Standard error

SHG – Static handgrip

SNR – Signal-to-noise ratio

SNS – Sympathetic nervous system

SV – Stroke volume

TPR – Total peripheral resistance

YH – Young healthy

Chapter 1

1 Introduction

1.1 Overview

The foundation of ‘integrative physiology’ as we know it today may well be rooted in the seminal workings of Claude Bernard (1813-1878), a French physiologist who noted, “…all of the vital mechanisms, however varied they may be, have always one goal, to maintain the uniformity of the conditions of life in the internal environment [*milieu intérieur*]…the constancy of the internal environment is the condition for free and independent life…” (Bernard, 1974). In this sense, the concept of ‘homeostasis’, a fundamental principle of physiology, was born, the term being devised sometime later by Walter B. Cannon (1871-1945), an American physiologist (Cannon, 1929). Homeostasis, therefore, represents the tendency of an organism to regulate its internal stability, owing largely to a coordinated system of feedback controls, so as to stabilize its health and functioning in the face of external challenge. As such, the concept of ‘homeostasis’ has become somewhat synonymous with the domain of ‘physiology’. In this regard, a full understanding of, and appreciation for, the integrative regulation and functioning (i.e., physiology) of the human body, requires that integrative physiologists break down the individual phenomena, or ‘parts’, that together constitute the existence of living beings.

Certainly, the autonomic nervous system (ANS), and especially, its sympathetic division, is of fundamental importance in both the short- and long-term regulation and maintenance of the cardiovascular system in humans. Indeed, the bidirectional

relationship that exists between autonomic dysregulation and numerous cardiovascular disease-related pathologies represents perhaps the best evidence for the fundamental role played by the ANS in maintaining cardiovascular homeostasis (Esler, 2010; Malpas, 2010). For example, sympathetic nervous system (SNS) dysregulation represents a hallmark of, among others, essential hypertension (Grassi *et al.* 2010; Parati & Esler, 2012), coronary artery disease (CAD) (Graham *et al.* 2002; Graham *et al.* 2004), heart failure (Floras, 2009; Triposkiadis *et al.* 2009), obstructive sleep apnea (Somers *et al.* 1995; Narkiewicz & Somers, 2003), and even, increasing age (Seals & Esler, 2000). Therefore, as mentioned above, a thorough understanding of the pathophysiology of these (or any) disease and/or aging process requires the careful study of the individual 'parts' that together comprise the dysfunctional system. But first, one must understand the 'normal' processes in health.

The SNS represents a major medium through which homeostatic adjustments to stress are achieved, occurring mostly as a result of its vasoconstrictor actions, and thus, control of blood pressure and distribution of blood flow (Shoemaker *et al.* 2016). This process has been largely referred to as sympathetic neural control of the circulation. In brief, sympathetic neural control involves central integration of sensory afferent and cortical/subcortical signals within the brainstem autonomic nuclei and spinal cord (Barman & Gebber, 2000), synapses at peripheral sympathetic ganglia (Jänig & McLachlan, 1992), efferent post-ganglionic nerve activity, neurotransmitter release, and ultimately, the end-organ effect (Shoemaker *et al.* 2016). As such, each of these individual junctures, or 'parts', offer unique sites of control in which sympathetic outflow can be coded and modified in response to homeostatic challenge. The focus of

the series of studies in this dissertation is on the patterns of sympathetic neural coding and the recruitment strategies used by the efferent SNS to increase sympathetic drive in the face of physiological stress.

Indeed, patterns of neural coding form the basis of all stimulus-response processes requiring exchange and processing of neural information. Specifically, these can include variations in the frequency or rate of neuron firing (i.e., rate coding), recruitment of additional, higher-threshold neurons (i.e., population coding), as well as variations in the timing of activity amongst neurons (i.e., temporal coding). To date, limited access to direct neural recordings in humans, as well as technological limitations, have precluded a definitive understanding of the neural coding principles used by the ANS, as opposed to more well-known and defined patterns in other peripheral organ systems. For example, rate- and population coding patterns exist in the somatic nervous system during the generation of ever-increasing muscular contraction force (i.e., Henneman's size principle) (Henneman *et al.* 1965). However, whether the SNS operates in a similar manner remains largely unknown.

With the introduction of the microneurographic technique (Hagbarth & Vallbo, 1968; Vallbo *et al.* 2004), direct neural recordings from the populations of post-ganglionic sympathetic axons innervating the skeletal muscle vasculature (i.e., muscle sympathetic nerve activity; MSNA) are possible in humans. Indeed, this tool has proven instrumental in understanding sympathetic neural control of the circulation in both health and disease (Wallin & Charkoudian, 2007; Charkoudian & Rabbitts, 2009; Shoemaker *et al.* 2016; Joyner *et al.* 2015). Traditionally, due to an inherently noisy signal, analysis of this multi-fibre MSNA signal has been largely constrained to the

integrated neurogram that exposes the timing and location of sympathetic ‘bursts’ that, in turn, reflect periods of efferent action potential (AP) synchronization (i.e., sympathetic APs firing more or less at the same time) (Delius *et al.* 1972). Nonetheless, inferences regarding central neural recruitment strategies have been drawn from the integrated MSNA neurogram. That is, early observations that larger integrated sympathetic bursts expressed shorter reflex latencies (i.e., faster neural conduction rates) led Wallin *et al.* (1994) to hypothesize that potential may exist for malleable synaptic delays and/or the ability to recruit sub-populations of neurons with varying recruitment thresholds and conduction velocities. Indeed, the strength of any given burst reflects both the number (Ninomiya *et al.* 1993) and size (Salmanpour *et al.* 2011*a*) of axons recruited within that burst. Therefore, variations in the strength (i.e., size) of sympathetic bursts represent the discharge patterns used by the SNS to elevate efferent neural drive. In this regard, these axonal recruitment patterns ultimately represent the strategies used by the central nervous system (CNS) to fine-tune efferent sympathetic nerve activity and control the cardiovascular system, and, by extension, maintain homeostasis.

With the use of these features, the concept of neural coding in the SNS was advanced by Macefield *et al.* (1994) with the introduction of single-axon sympathetic recordings. These data indicated that, when active, a given axon will fire generally once per integrated sympathetic burst at rest (Macefield *et al.* 1994; Macefield & Wallin, 1999), but perhaps more (i.e., two to three times) during periods of acute (Macefield & Wallin, 1999; Elam & Macefield, 2001; Murai *et al.* 2006) or chronic (Elam *et al.* 2002; Ashley *et al.* 2010) sympathoexcitation. However, information regarding the

populations of axons available for recruitment, and therefore, the neural recruitment strategies available to the SNS to alter efferent outflow, cannot be extracted from single-unit recordings, but instead require a multi-unit approach.

Recently, technological advancements have been made that allow for the extraction, quantification, and morphological classification of the populations of sympathetic APs comprising each integrated MSNA burst (Salmanpour *et al.* 2010). With the use of this approach, Steinback *et al.* (2010*b*) reported increased firing rates of axons already-active at baseline, as well as recruitment of previously silent (i.e., not active at baseline) sub-populations of larger-sized, faster conducting sympathetic axons during voluntary apnea-induced sympathoexcitation. In contrast, recruitment of latent neural sub-populations was not observed during baroreceptor unloading induced via −60 mmHg lower body negative pressure (LBNP) (Salmanpour *et al.* 2011*a*). In this scenario, increases in sympathetic outflow were achieved through increased firing rate of axons already-active at baseline. The reasons for the observed difference in recruitment patterns between studies are unknown, but could involve varying thresholds for recruitment of these latent axons (i.e., stress severity), interindividual variability, and/or reflex-specific neural recruitment strategies. Therefore, additional data are needed, in the same individuals, on the reflex-specific neural recruitment strategies available to the SNS to alter efferent post-ganglionic outflow in response to physiologic stress. This background formed the rationale for *Study 1* of this dissertation. Briefly, sympathetic neural recruitment strategies were studied during both chemoreflex- (i.e., as inferred from voluntary apnea) and baroreflex- (i.e., −80 mmHg LBNP) mediated sympathoexcitation in the same individuals.

Furthermore, in preliminary studies, Salmanpour *et al.* (2011*b*) demonstrated an acute downward shift in the AP cluster size-latency relationship during reflex-mediated stress. That is, all APs at baseline displayed shorter reflex latency during a subsequent Valsalva maneuver, providing evidence perhaps for the possibility of acute synaptic delay modifications somewhere within the reflex pathway, as previously hypothesized (Wallin *et al.* 1994). However, in addition to reflex-specific recruitment strategies, a persistent question remains, particularly with the apnea data (Steinback *et al.* 2010*b*; Breskovic *et al.* 2011), as to whether or not these neural coding patterns are influenced by a central (i.e., perception of effort or stress) phenomena, or by the reflex stress itself (i.e., a peripheral-reflex mechanism). Specifically, voluntary apnea and the Valsalva maneuver, as opposed to lower body suction, exhibit a certain level of volitional stress that is likely related to perception of effort or stress and/or individual tolerance for the maneuver. As such, the exact central versus peripheral elements of these sympathetic neural coding principles requires investigation. This background formed the rationale for *Study 2* of this dissertation, in which sympathetic neural recruitment patterns were investigated during fatiguing static handgrip (SHG) exercise and a subsequent period of post-exercise circulatory occlusion (PECO). Specifically, this model (i.e., exercise pressor reflex) was used as the physiologic response to fatiguing exercise (and PECO) represents a unique scenario in which the central and peripheral features of the reflex can be studied separately as they occur over time.

Furthermore, the majority of studies to date have investigated young, healthy populations, and therefore, the malleability of these recruitment strategies with increasing age and cardiovascular disease remains unknown. As such, this formed the

rationale for *Study 3* of this dissertation. Briefly, CAD patients completed maximal voluntary apneas, which served as a stimulus for sympathoexcitation, and neural recruitment patterns were compared to that of young healthy and older healthy individuals to account for the concurrent effect of age.

Finally, while voluntary apnea appears to provide the most powerful stimulus for sympathetic axonal recruitment (Steinback *et al.* 2010*b*), the exact mechanisms mediating this robust sympathetic response are uncertain and appear diverse. Specifically, the roles played by ventilation (or the lack thereof in the case of apnea) versus the chemoreflex activation itself in eliciting the recruitment response are unknown. This formed the rationale for *Study 4* of this dissertation, in which sympathetic neural discharge patterns were studied during prolonged voluntary apnea (i.e., absence of ventilation) and during asphyxic rebreathing (i.e., presence of ventilation) in trained breath-hold divers. In this sense, we studied the dissociated influences of chemoreceptor stimuli (i.e., hypoxia and hypercapnia) and ventilation on sympathetic AP recruitment patterns during varying levels of high chemoreflex stress.

As such, the overall objectives of the research contained herein are to 1) Establish the neural coding principles employed by the SNS in response to acute physiological (i.e., homeostatic) stress; and 2) To determine the various mechanisms of control underlying these sympathetic neural recruitment strategies. The **working hypothesis** to be tested is that efferent post-ganglionic MSNA exhibits neural coding patterns reflecting increased firing rates of lower-threshold axons, latent sub-populations of higher-threshold axons, as well as malleable synaptic delays and/or central processing times, and further, that these are modified by factors such as reflex-

specificity, stress severity, perception of effort or stress, age, and cardiovascular disease.

Study 1. Sympathetic neural recruitment strategies: responses to severe chemoreflex and baroreflex stress

Objective: To test the hypothesis that neural coding strategies exist within the SNS and to determine reflex-specific neural recruitment strategies during severe chemoreflex- and baroreflex-mediated stress.

Study 2. Central vs. peripheral determinants of sympathetic neural recruitment: insights from static handgrip exercise and postexercise circulatory occlusion

Objective: To investigate the varying roles played by central versus peripheral elements in the control of sympathetic neural recruitment during acute physiological stress.

Study 3. Effects of aging and coronary artery disease on sympathetic neural recruitment strategies during end-inspiratory and end-expiratory apnea

Objective: To test the hypothesis that cardiovascular disease impairs sympathetic neural recruitment.

Study 4. Ventilation inhibits sympathetic action potential recruitment even during severe chemoreflex stress

Objective: To determine the influence of ventilation on sympathetic neural recruitment during varying levels of high chemoreflex stress.

1.2 Autonomic Nervous System

The ANS represents a highly complex, multi-faceted neural network that, in an involuntary manner (i.e., without conscious control), maintains and controls most visceral organs within the body's internal environment. In this sense, the ANS coordinates numerous bodily functions and is critical to the maintenance of physiologic homeostasis, and by extension, many life-sustaining outcomes. Of great importance, and a focus of this dissertation, is the ANS control of the cardiovascular system, occurring largely through the reflexive regulation of blood pressure and distribution of blood flow (Shoemaker *et al.* 2016). In this sense, these variables are tonically, and reflexively, regulated to ensure adequate perfusion and delivery of oxygen throughout the body in an attempt to meet the metabolic demands of all organs and tissues. Specifically, the ANS is comprised of two main branches; that is, the parasympathetic nervous system (PNS) and the SNS. The PNS and SNS function antagonistically, synergistically, and/or independently to regulate cardiovascular function, among other effector systems, both at rest and in the face of physiological perturbation. Importantly, dysregulation of the ANS represents the basis for, or a consequence of, many chronic cardiovascular disease-related pathologies (Somers *et al.* 1995; Narkiewicz & Somers, 2003; Floras, 2009; Esler, 2010; Grassi *et al.* 2010; Malpas, 2010; Parati & Esler, 2012), highlighting its fundamental role in homeostatic cardiovascular control. Thus, an appreciation for, and thorough understanding of, the intricate nature of autonomic neural control in both health and disease represents a critical endeavor in the understanding of 'normal' homeostatic mechanisms, as well as the pathophysiological basis of many chronic disease states.

1.2.1 Parasympathetic Nervous System

The PNS involves a two-neuron efferent system with pre-ganglionic neurons situated in the CNS and post-ganglionic neurons located at peripheral ganglia (Shields, 1993). The PNS consists of long, myelinated or unmyelinated pre-ganglionic fibres that synapse onto unmyelinated post-ganglionic fibres near or within the target organ (Wehrwein *et al.* 2016). In general, cell bodies of PNS pre-ganglionic fibres originate within regions of the brainstem, as well as in the sacral spinal cord (Wehrwein *et al.* 2016). Within these regions, the oculomotor (CN III), facial (CN VII), glossopharyngeal (CN IX), and vagus (CN X) nerves form the pre-ganglionic parasympathetic nerves which, in turn, synapse with post-ganglionic neurons through the binding of acetylcholine (ACh) onto nicotinic cholinergic receptors (Shields, 1993; Wehrwein *et al.* 2016). With respect to cardiac function, PNS control is mediated via the vagus nerve through the binding of ACh onto muscarinic receptors located within the heart (Brodde & Michel, 1999). Although several subtypes of muscarinic receptors have been identified (Brodde & Michel, 1999), the predominant receptor found in the human heart is the M_2 receptor subtype (Peralta *et al.* 1987; Hulme *et al.* 1990). In brief, activation of M_2 receptors via ACh binding, coupling to an inhibitory G-protein, leads to inhibition of adenylate cyclase activity, which subsequently inhibits intracellular cyclic adenosine monophosphate (cAMP), resulting in decreased intracellular calcium (Ca^{2+}) levels. Furthermore, binding of ACh to M_2 receptors causes increased outward, hyperpolarizing potassium (K^+) currents, which decreases sinoatrial node firing rate and slows conduction within the atrioventricular node. Therefore, the net result of vagal (i.e., PNS) stimulation of the heart is reduced cardiac contractility

and conduction velocity, and importantly, decreased heart rate. While the importance of parasympathetic neural control of the circulation cannot be understated, its effects are limited to the heart, and therefore, cardiac function, whereas the SNS innervates the heart, blood vessels, and other visceral organs to provide widespread control of cardiac and vascular function. In this sense, the SNS exerts considerable control over cardiovascular homeostasis. Thus, neuro-circulatory control in the context of the SNS, and more specifically, sympathetic neural control of the vasculature, represents the focus of this dissertation.

1.2.2 Sympathetic Nervous System

Similar to the PNS, the peripheral elements of the SNS also operate via a two-neuron efferent system to effectively modulate homeostatic cardiovascular control; that is, short, myelinated pre-ganglionic neurons originating in the CNS synapse with post-ganglionic neurons located at peripheral ganglia, whose long, unmyelinated axons travel to visceral targets within the periphery to exert appropriate end-organ responses (Shields, 1993; Wehrwein *et al.* 2016). Specifically, the cell bodies of SNS pre-ganglionic neurons lie in the intermediolateral (IML) cell column within the first thoracic to the first two lumbar regions of the spinal cord (i.e., T1-L2) (Shields, 1993). Here, the SNS pre-ganglionic fibres exit via the ventral root to form the white rami, where they synapse with post-ganglionic neurons within prevertebral ganglia and/or paravertebral ganglia located at the sympathetic chains (Wehrwein *et al.* 2016). At these peripheral ganglia, pre-ganglionic neurons release ACh, which binds to nicotinic cholinergic receptors located on post-ganglionic neuron cell-bodies which, in turn, stimulates an AP in the post-ganglionic neuron. The AP descends along the axon until it

reaches the distal end of the neuron. Sympathetic post-ganglionic axons that innervate cardiovascular tissue (i.e., cardiac and vascular smooth muscle) branch extensively, coming into close contact with several regional effector cells. Here, sympathetic post-ganglionic fibres become beaded with enlargements known as varicosities, in which they release their neurotransmitters from. Specifically, once the AP arrives at the varicosity, the ensuing depolarization initiates the opening of voltage-gated Ca^{2+} channels, resulting in an influx of Ca^{2+} and the exocytosis of synaptic vesicles containing neurotransmitters. Sympathetic post-ganglionic neurons release several neurotransmitters, including norepinephrine (NE), neuropeptide Y (NPY), and adenosine triphosphate (ATP) (Burnstock, 1990; Lundberg *et al.* 1990) that, in turn, stimulate receptors located on the effector organs and tissues, as described below. Additionally, sympathetic pre-ganglionic fibres can also travel to the medullary portion of the adrenal gland, where they release ACh onto nicotinic cholinergic receptors located on chromaffin cells. In this scenario, the adrenal medulla releases NE and epinephrine, in an approximate 1:4 ratio (Jänig, 2008), into the circulation, where they can bind to receptors located on effector targets.

Of importance to neuro-cardiovascular control are receptors located at the heart, and perhaps more importantly, on smooth muscle cells of the vasculature within skeletal muscle and other visceral organs. Briefly, at the heart, NE and epinephrine bind to β_1- and β_2-adrenergic receptors, which, through a stimulatory G-protein, activates adenylate cyclase, thereby catalyzing the conversion of ATP to cAMP. This causes increases in cAMP-dependent protein-kinase A activity, thus activating L-type Ca^{2+} channels. The net result is increased intracellular Ca^{2+} levels, and thus, increased heart

rate and cardiac contractility. Within blood vessels, neurally released NE and epinephrine bind to α_1-adrenergic receptors which, through a Gq-protein, stimulates phospholipase C, leading to the formation of inositol triphosphate and diacylglycerol, and, in turn, increased intracellular Ca^{2+} and protein kinase C activation, respectively. The rise in Ca^{2+} activates calmodulin-dependent myosin light chain kinase to increase myosin ATPase activity, causing myosin and actin binding, and therefore, vascular smooth muscle contraction. Therefore, the net result is overall vasoconstriction. Similarly, activation of α_2-adrenergic receptors via NE binding is coupled to an inhibitory G-protein which inhibits adenylate cyclase and decreases cAMP levels. Briefly, this causes less myosin light chain kinase inhibition and greater intracellular Ca^{2+} levels. Again, the net result is vasoconstriction. In addition to NE, as mentioned above, vascular sympathetic nerves also co-release NPY and ATP (Burnstock, 1990; Lundberg *et al.* 1990). Both neurotransmitters can cause net vasoconstriction through the activation of NPY Y_1 receptors, via NPY, and purinergic $P2X_1$ receptors, via ATP, which act to increase intracellular Ca^{2+} levels, and therefore, vascular smooth muscle contraction. The release of these co-transmitters and the subsequent contribution to the functional sympathetic vasoconstrictor response may ultimately depend on the patterning and rate of sympathetic discharge that, in turn, likely exerts important influences on end-organ homeostatic stress responses (Huidobro-Toro & Donoso, 2004). In this sense, technological advancements allowing for direct recordings of sympathetic post-ganglionic vasoconstrictor discharge (i.e., microneurography; described in detail later) has initiated an exciting era of research with respect to sympathetic neurovascular control.

1.3 Sympathetic Neural Control of the Circulation

Overall, the concept of sympathetic neurovascular control represents a highly integrative and multi-faceted process of regulation that involves central integration of sensory signals within the brainstem and spinal cord (Barman & Gebber, 2000), synapses at peripheral ganglia (Jänig & McLachlan, 1992), recruitable efferent post-ganglionic sympathetic nerve traffic, neurotransmitter release, and finally, the end-organ response (Shoemaker *et al.* 2016). Ultimately, each of these elements offer unique and complex levels of regulation, that combined, represent a key mechanism of control over cardiovascular homeostasis. Therefore, to fully appreciate the complexity and integrative nature of sympathetic neuro-circulatory control in health, and perhaps more importantly, in disease, a thorough and systematic understanding of each individual element of control, or 'part', is critical. In line with this, recruitment patterns in efferent sympathetic nerve activity form the scope of this dissertation. For detailed information on other regulatory segments within the sympathetic neural control complex, such as the central and ganglionic features (McAllen & Malpas, 1997; Jänig & Häbler, 2003; McLachlan, 2003), or the efferent nerve activity–vascular contraction integration (Shoemaker *et al.* 2016), the reader is referred to existing comprehensive reviews. Nonetheless, the concept of sympathetic neurovascular control has been well-studied in three fundamental reflexes; that is, the baroreflex, chemoreflex, and exercise pressor reflex. These efforts are described briefly in the sections below.

1.3.1 Baroreflex

The arterial baroreflex provides short-term regulation of arterial blood pressure around a set-point (determined by the state of the individual), via a negative feedback

control system that responds to beat-to-beat changes in blood pressure by reflexively altering ANS (i.e., PNS and SNS) activity. The arterial baroreflex consists of baroreceptors located in the carotid sinus, at the bifurcation of the internal and external carotid artery, as well as the aortic arch (Dampney, 1994). The carotid and aortic baroreceptors are composed of mechanosensitive afferent neurons located within the medial-adventitial wall of the vessel that respond to stretch or distortion of the arterial wall due to changes in blood pressure, or more specifically, transmural pressure (Dampney, 1994). Afferent baroreceptor discharge is relayed from the carotid sinus (via the glossopharyngeal nerve) and the aortic arch (via the vagus nerve) to the nucleus tractus solitarius (NTS) in the medulla oblongata region of the brainstem (Dampney, 1994; Aicher *et al.* 2000). Here, NTS neurons project to and excite (via the release of glutamate) the caudal ventrolateral medulla (CVLM). CVLM neurons are interneurons in the baroreflex pathway and project to the rostral ventrolateral medulla (RVLM), and through the release of ɣ-aminobutyric-acid (GABA), inhibit the RVLM. The RVLM represents the primary regulator of the SNS, sending excitatory messages to sympathetic pre-ganglionic neurons located in the IML of the spinal cord, as mentioned above. As such, when baroreceptors are activated (i.e., by increased blood pressure), the NTS activates the CVLM, thus inhibiting the RVLM, which, in turn, inhibits sympathetic nerve activity to decrease blood pressure (i.e., vasodilation) back to its set-point. In this scenario, PNS activity is simultaneously increased to cause reductions in heart rate and cardiac contractility. On the other hand, when blood pressure levels decrease, less afferent baroreceptor discharge causes less excitation of the NTS, less activation of the CVLM, and therefore, disinhibition (i.e., activation) of the RVLM.

This, in turn, causes increases in efferent sympathetic nerve activity to the periphery, and therefore, vasoconstriction (i.e., to increase blood pressure).

Orthostatic (i.e., postural) stress represents a common method of studying baroreflex-mediated neuro-circulatory control due to reductions in venous return, cardiac output, and thus, blood pressure. This results in baroreceptor 'unloading', reductions in afferent discharge to central sympathetic sites, and therefore, as described above, increases in sympathetic nerve activity and peripheral vascular resistance to maintain arterial blood pressure (Sundlöf & Wallin, 1978*a*; Victor & Leimbach, 1987). In a laboratory setting, orthostatic stress is often simulated using LBNP, although other methods are often utilized. In brief, during LBNP, participants lie supine with their lower body sealed within a chamber at the level of the iliac crest. Next, negative suction is created, such that blood is shunted away from the thoracic cavity and into the capacitance vessels of the lower body, thereby unloading the baroreceptors. Indeed, LBNP elicits robust and graded (i.e., with severity) increases in efferent sympathetic nerve outflow, vasoconstriction, and, by extension, total vascular resistance (Rea & Wallin, 1989; Taylor *et al.* 1992; Ryan *et al.* 2011). Furthermore, the patterning of sympathetic discharge may differ with LBNP stress severity, such that both rate and strength of firing increase at lower levels of suction (i.e., up to approximately −30 mmHg), whereas, at higher levels of LBNP, the strength of sympathetic discharge appears emphasized (Ichinose *et al.* 2004; Ichinose *et al.* 2006).

1.3.2 Chemoreflex

The chemoreflex represents a highly complex and coordinated homeostatic response to systemic hypoxia and/or hypercapnia that ultimately serves to regulate

cardiorespiratory function to maintain and defend perfusion to the body's critical organs and tissues. Briefly, the chemoreflex includes peripheral chemoreceptors, located primarily in the carotid bodies, but also, the aortic bodies, as well as the central chemoreceptors, located within the brainstem. In general, peripheral chemoreceptors respond primarily to hypoxia, but also to hypercapnia/H^+ concentration (Marshall, 1994), while central chemoreceptors respond to increased brain interstitial hypercapnia/H^+ concentration (Nattie & Li, 2012). The net result of peripheral and/or central chemoreceptor activation is reflex-induced increases in respiration, as well as autonomic circulatory arousal. Indeed, the homeostatic response to chemoreflex activation involves large increases in post-ganglionic sympathetic nerve activity (Saito *et al.* 1988; Morgan *et al.* 1995; Leuenberger *et al.* 2005), mediated through an excitatory NTS to RVLM to IML neural reflex arc (Koshiya *et al.* 1993), to influence systemic vascular resistance and distribution of blood flow, and ultimately, maintain brain perfusion.

Importantly, when the effects of hypoxia and hypercapnia are combined, such as occurs during asphyxic rebreathing or breathing a hypoxic-hypercapnic gas mixture, a synergistic effect occurs, such that the sympathoexcitatory response is potentiated (Somers *et al.* 1989*a*; Jouett *et al.* 2015). Furthermore, voluntary apnea (i.e., absence of active ventilation) appears to elicit an even more robust sympathetic response (Somers *et al.* 1989*b*; Steinback *et al.* 2010*a*), reflecting increases in both frequency and strength of sympathetic discharge.

1.3.3 Exercise Pressor Reflex

The exercise pressor reflex is of fundamental importance in mediating the necessary neural cardiovascular adjustments to fatiguing exercise, which include increases in blood pressure and elevated sympathetic drive. In brief, mechanically- and metabolically-sensitive sensory afferent fibres within active skeletal muscle provide feedback to cardiovascular control centers within the brain stem in response to mechanical and chemical stimuli, respectively (Alam & Smirk, 1937; McCloskey & Mitchell, 1972; Kaufman *et al.* 1983; Mitchell *et al.* 1983). Specifically, muscle mechanoreflex sensory afferents are comprised of Type III sensory neurons and respond primarily to mechanical stretch and deformation induced by muscular contraction (Mitchell *et al.* 1983). On the other hand, muscle metaboreflex sensory afferents are comprised of Type IV sensory neurons and are stimulated via the build-up of metabolites (i.e., chemical stimuli) produced by the working skeletal muscle (Mitchell *et al.* 1983). However, this organization is not absolute, as some Type III fibres respond to metabolic stimuli, whereas some Type IV fibres respond the mechanical stimuli. Nonetheless, the exercise pressor reflex elicits large increases in sympathetic nerve activity (Mark *et al.* 1985; Seals *et al.* 1988; Victor *et al.* 1988; Wallin *et al.* 1989; Shoemaker *et al.* 2007), albeit after a delay (Mark *et al.* 1985), the timing of which depends on exercise intensity (Hashimoto *et al.* 1998). Furthermore, sympathetic outflow remains elevated during PECO, which serves to trap exercise-induced metabolites within the previously-active skeletal muscle (thereby, isolating the metaboreflex) (Alam & Smirk, 1937), suggesting a dominant role for the muscle metaboreflex in eliciting the robust sympathetic response.

1.4 Muscle Sympathetic Nerve Activity

In the late 1960s (Hagbarth & Vallbo, 1968), the study of sympathetic neuro-circulatory control was greatly advanced in humans with the development of the microneurographic technique by Hagbarth and Vallbo in Uppsala, Sweden (Vallbo *et al.* 2004). Specifically, microneurography allows for direct real-time recordings from the populations of post-ganglionic sympathetic axons innervating the skeletal muscle vasculature (i.e., MSNA) in human peripheral nerves. The recordings are referred to as "multi-unit" in that several axons are recorded from simultaneously. Sympathetic outflow directed to skeletal muscle, as opposed to skin (Hagbarth *et al.* 1972), is related to blood pressure and accurately reflects both age-related and pathological states (Sundlöf & Wallin, 1978*b*; Wallin & Charkoudian, 2007); thus, MSNA represents the neural signal of interest in this dissertation. Advantages of the microneurographic technique versus other measures of sympathetic nerve activity (i.e., plasma catecholamine levels, NE spillover, etc.) include its direct and continuous nature and its excellent temporal resolution. Disadvantages include the technical demands of the skill and its pseudo-invasive nature (thereby, limiting its practicality), its focus on one regional vascular bed, as well as uncertainty over how best, and how accurately, to interpret and analyze the recorded signal (White *et al.* 2015; Joyner, 2016). In general, however, levels of MSNA reflect levels of sympathetic outflow to the heart and other visceral beds (Wallin *et al.* 1992; Wallin *et al.* 1996; Lambert *et al.* 1997; Grassi & Esler, 1999), reinforcing the relevance of this important neural signal. Indeed, over the past 50 years or so, microneurography has proven an invaluable research tool in the study of sympathetic neurovascular control at rest, and in response to physiological

stress, in both health and disease (Wallin & Charkoudian, 2007; Charkoudian & Rabbitts, 2009; Shoemaker *et al.* 2016; Joyner *et al.* 2015).

In theory, any accessible peripheral nerve can be used for microneurographic recordings; however, the most widely used is likely the peroneal nerve at or just proximal to the fibular head, as it is readily accessible and close to the skin, relatively large, and fairly easy to stabilize (i.e., the lower limb) for long durations of time (White *et al.* 2015). Certainly, the peroneal nerve, along with other human mixed nerves, contains unmyelinated efferent sympathetic axons (i.e., C-fibers), albeit in a mix of other sensory and motor fibres. Though limited data exist in humans on the anatomical arrangement and distribution of these sympathetic fibres within peripheral nerves, Tompkins *et al.* (2013) demonstrated, using immunohistochemical techniques, that sympathetic fibres were dispersed throughout approximately 25 to 38 fascicles within the human peroneal nerve. Throughout these fascicles, sympathetic fibres existed either individually or in bundled groups of approximately two- to 44 axons, although the distribution favoured smaller bundles (i.e., median value of five axons/bundle). Finally, the axons also displayed variations in size, with diameters ranging from approximately 0.5 to 2 µm. Therefore, within the human peroneal nerve, post-ganglionic sympathetic fibres exist in bundles of axons that vary both in number and size.

As such, microneurography involves the manual manipulation and positioning of a recording electrode into an active bundle of efferent sympathetic axons within the peroneal nerve. Specifically, the technique entails the use of two electrodes. First, a ‘reference’ electrode is positioned subcutaneously approximately 1-3 cm from the recording site. Next, a tungsten ‘recording’ electrode (35 mm long, 200 µm in diameter,

and tapered to a 1-5 µm uninsulated tip) is inserted percutaneously into the nerve and is manually, and carefully, manipulated until an adequate MSNA recording site is located. This is confirmed by the presence of a characteristic pulse-synchronous burst pattern, absence of skin paresthesia, and a signal that increases in response to voluntary apnea, but not during arousal to loud noise (Delius *et al.* 1972). The recorded raw neural signal is first preamplified with a gain of 1000 (using preamplifier and isolation amplifier; gain of 100 and 10, respectively) and further amplified with a gain of 75 (using a variable gain amplifier; gain of 0.1-99). The neural activity is then band-pass filtered (bandwidth of 700-2000 Hz) before being rectified and integrated (using a leaky integrator; 0.1 s time constant) to obtain a mean voltage neurogram. These steps ultimately reduce background noise to expose both the timing and location of sympathetic 'bursts' that, in turn, reflect periods of efferent AP synchronization (Delius *et al.* 1972). In this sense, variations in the size and number of APs within and between sympathetic bursts is lost in the integration process. Nonetheless, MSNA is characterized by spontaneously, and irregularly, occurring bursts of pulse-synchronous impulses (i.e., APs) that are separated by periods of neural silence (Hagbarth & Vallbo, 1968). These integrated sympathetic bursts are entrained to the cardiac cycle via a baroreflex mechanism, in that they are initiated during diastole and turned off during systole (Sundlöf & Wallin, 1978*b*). Indeed, Fagius *et al.* (1985) demonstrated that baroreceptor deafferentation via temporary bilateral block of the vagus and glossopharyngeal nerves led to marked increases in muscle sympathetic outflow and a loss of MSNA cardiac rhythmicity. Confirmation that these recorded bursts indeed represent efferent post-ganglionic sympathetic outflow is evidenced by their conduction

velocities (~1 m/s) (Hagbarth & Vallbo, 1968; Fagius & Wallin, 1980), as well as their complete abolishment following ganglionic blockade (Delius *et al.* 1972).

Sympathetic bursts are identified from the integrated MSNA neurogram if: 1) they exhibit pulse-synchrony; 2) they have a signal-to-noise ratio of at least 2:1 with respect to the previous period of neural silence between bursts; 3) they present with characteristic rising and falling slopes; and 4) APs are visible in the corresponding raw and filtered neurograms. The level of integrated sympathetic nerve activity is most commonly quantified using burst frequency and/or burst incidence. Burst frequency gives an indication of overall firing frequency and is expressed as the number of bursts per minute, whereas burst incidence involves the 'normalization' of burst frequency to heart rate, and therefore, is expressed as the number of bursts per 100 heartbeats. Furthermore, the level of total integrated activity (i.e., total MSNA) is often calculated as the product of burst frequency and burst amplitude (or area), although interpretation of the latter amplitude component is more complicated, as described below. Therefore, integrated burst frequency represents the most-widely reported MSNA index in the literature due to its relative ease of calculation and interpretation, and because it is highly reproducible over time (Sundlöf & Wallin, 1977; Kimmerly *et al.* 2004). In contrast, burst size demonstrates less test-retest reproducibility, presumably due to the fact that absolute burst size voltages are influenced by proximity of the recording electrode tip in relation to the active group of axons, a factor that is likely to differ between individuals and between recording sites. In this sense, interindividual comparisons of absolute burst amplitude are limited, and therefore, normalization procedures are often utilized. A commonly used approach is to normalize all bursts

within the recording period to the largest burst at baseline (or throughout the recording), which is assigned a value of 100 arbitrary units, although other methods are often employed (White *et al.* 2015). Another approach, developed by Sverrisdóttir and colleagues (Sverrisdóttir *et al.* 1998; Sverrisdóttir *et al.* 2000), involves the normalization of burst amplitude as above, followed by the creation of a relative burst amplitude distribution spectra or plot that describes the relative proportion of 'small' versus 'large' bursts within the integrated neurogram. Importantly, this method has demonstrated to be a more sensitive and specific indicator of altered MSNA (Sverrisdóttir *et al.* 1998), is reproducible (Kimmerly *et al.* 2004), and furthermore, has shown to independently discriminate clinical conditions (i.e., heart failure) with elevated, but similar, burst frequency (Sverrisdóttir *et al.* 2000). Therefore, burst amplitude offers unique insight into sympathetic neural control of the circulation above and beyond that of burst frequency or burst incidence. In this sense, burst size represents an important independent variable of interest, as outlined below.

Certainly, it has been hypothesized for some time that burst size is regulated in a differential manner as compared to burst frequency, thereby representing its own level of control (Malpas, 1995; Kienbaum *et al.* 2001). Highlighting this point, several studies have observed alterations in burst amplitude, without accompanying changes in burst frequency, in response to both baroreflex- (DiBona *et al.* 1997; Kimmerly & Shoemaker, 2003) and chemoreflex- (Malpas & Ninomiya, 1992; Malpas *et al.* 1996) induced stress. As such, changes in burst frequency alone may not adequately represent reflex-mediated sympathetic vasomotor control. Furthermore, changes in burst amplitude, reflecting altered AP discharge patterns, may be independently relevant for

neurovascular control (Malpas, 1998). Indeed, Fairfax *et al.* (2013) demonstrated that burst size alone, independent of burst pattern or frequency (i.e., single versus multiple bursts), influences directly the magnitude of decrease in leg vascular conductance (i.e., vasoconstriction). The importance of the burst amplitude index likely lies in the fact that the size of each integrated burst represents the true neural content of that burst; that is, burst size is reflective of both the number (Ninomiya *et al.* 1993; Salmanpour *et al.* 2011*a*) and size (Salmanpour *et al.* 2011*a*) of axons recruited within that burst. Therefore, the content and variability of APs within and between integrated bursts reflect the recruitment patterns and strategies used by the CNS to fine-tune sympathetic outflow, and ultimately, control systemic vascular resistance and blood pressure at rest and in the face of physiological challenge. While the efforts outlined above for normalizing burst amplitude have proven somewhat fruitful (Kimmerly & Shoemaker, 2003), considerable information is lost within the integrated neural signal. Specifically, the integration process eliminates all AP information (i.e., number and morphology), precluding the study of sympathetic neural discharge patterning. As such, investigation into the neural coding patterns utilized by the SNS has been limited over the years due to technical limitations in extracting AP information from raw MSNA recordings due to high levels of background noise.

Nonetheless, early hypotheses regarding central recruitment strategies have been inferred from the integrated MSNA neurogram. For instance, Wallin *et al.* (1994) observed an inverse relationship between integrated burst amplitude and baroreflex latency; that is, larger sympathetic bursts expressed shorter reflex latencies. Baroreflex latency, as determined from the time-delay between the peak of the integrated burst and

the preceding R-wave related to that burst (Fagius & Wallin, 1980), has been found to be approximately 1.2 to 1.5 seconds in human peroneal nerve recordings (Fagius & Wallin, 1980). In turn, this reflex latency reflects the sum of time of all conduction components, including baroreceptor sensory afferent processing, central integration, spinal conduction time, and pre- and post-ganglionic efferent nerve segments. In this sense, the finding that larger sympathetic bursts expressed shorter conduction latencies was hypothesized to be due to either malleability of synaptic delays between the brain stem and peripheral nerve (i.e., 'shortcuts' in the neural pathway), and/or the presence of sub-populations of sympathetic fibres with varying conduction velocities and thresholds for recruitment (Wallin *et al.* 1994).

The question of neural coding in human efferent sympathetic nerve activity was advanced by Macefield *et al.* (1994) with the introduction of single sympathetic fibre recordings. The single-unit approach uses the same methodology as outlined above for multi-unit recordings; however, the electrode has a much higher impedance and thus limits the overall area from which the neural signal is recorded. Data from this work indicates that, in general, when active at rest, a given axon will fire approximately once per sympathetic burst (Macefield *et al.* 1994; Macefield & Wallin, 1999), but perhaps more in certain pathological states (Elam *et al.* 2003; Lambert *et al.* 2008). Indeed, a shift towards greater likelihood of multiple firing of individual axons per burst has been demonstrated in hypertension (Lambert *et al.* 2007), obstructive sleep apnea syndrome (Elam *et al.* 2002), and chronic obstructive pulmonary disease (Ashley *et al.* 2010), but not in congestive heart failure (Macefield *et al.* 1999). Furthermore, multiple within-burst firing has been observed during acute states of autonomic arousal, such as the

Valsalva maneuver (Murai *et al.* 2006), voluntary apnea (Macefield & Wallin, 1999), and following cardiac dysrhythmia (Elam & Macefield, 2001). Therefore, these data indicate that increased firing probability, and also, an increase in the within-burst firing of single axons, represent mechanisms by which sympathetic drive is elevated during physiological stress. However, given that only approximately 40% of bursts during apnea were associated with multiple spikes, Macefield and colleagues hypothesized that recruitment of additional neurons (along with increased firing probability) may be the primary mechanism by which sympathetic activation is achieved (Macefield & Wallin, 1999). However, recruitment of new axons cannot be determined from single-fibre recordings. As such, information regarding the several recruitment strategies available to the SNS to alter efferent outflow in response to homeostatic challenge cannot be extracted using single-unit analyses, but instead, require a multi-unit analysis approach.

Indeed, patterns of neural coding represent a fundamental feature of all neural exchange and processing. These patterns, among others, can include variations in the frequency, or rate, of individual spike firing (i.e., rate coding), varying thresholds for recruitment of additional neurons (i.e., population coding), and also, variations in the timing of neuronal activity (i.e., temporal coding). These coding patterns exist in the control of many bodily systems. For example, the recruitment strategies used by the skeletal motor system to respond to ever-increasing muscular contraction force follow Henneman's size principle, whereby smaller motor units are recruited first, followed by recruitment of larger, faster conducting motor units as load intensity and force production increase (Henneman *et al.* 1965). Furthermore, once active, these units increase their firing rate (Westgaard & De Luca, 2001). Therefore, neural coding

patterns exist in the control of muscular activation. Whether these principles operate in the SNS, which regulates numerous homeostatic outcomes, is less clear in humans due to limited access to direct neural recordings, and furthermore, limitations in extracting multi-unit AP activity from the sympathetic neurogram.

More recently, the investigation of neural coding in efferent sympathetic nerve activity has been furthered by technological advancements enabling the extraction and morphological classification of multi-unit APs from raw MSNA recordings (Salmanpour *et al.* 2010). One such method, developed by Salmanpour *et al.* (2010), and used in many subsequent experiments (Steinback *et al.* 2010*b*; Breskovic *et al.* 2011; Salmanpour *et al.* 2011*a*,*b*; Maslov *et al.* 2012; Salmanpour & Shoemaker, 2012; Maslov *et al.* 2014*a*,*b*), uses wavelet-base methodology to detect and extract sympathetic APs from the noisy raw MSNA signal, thereby enabling the study of multi-unit post-ganglionic neural discharge (Figure 1.1).

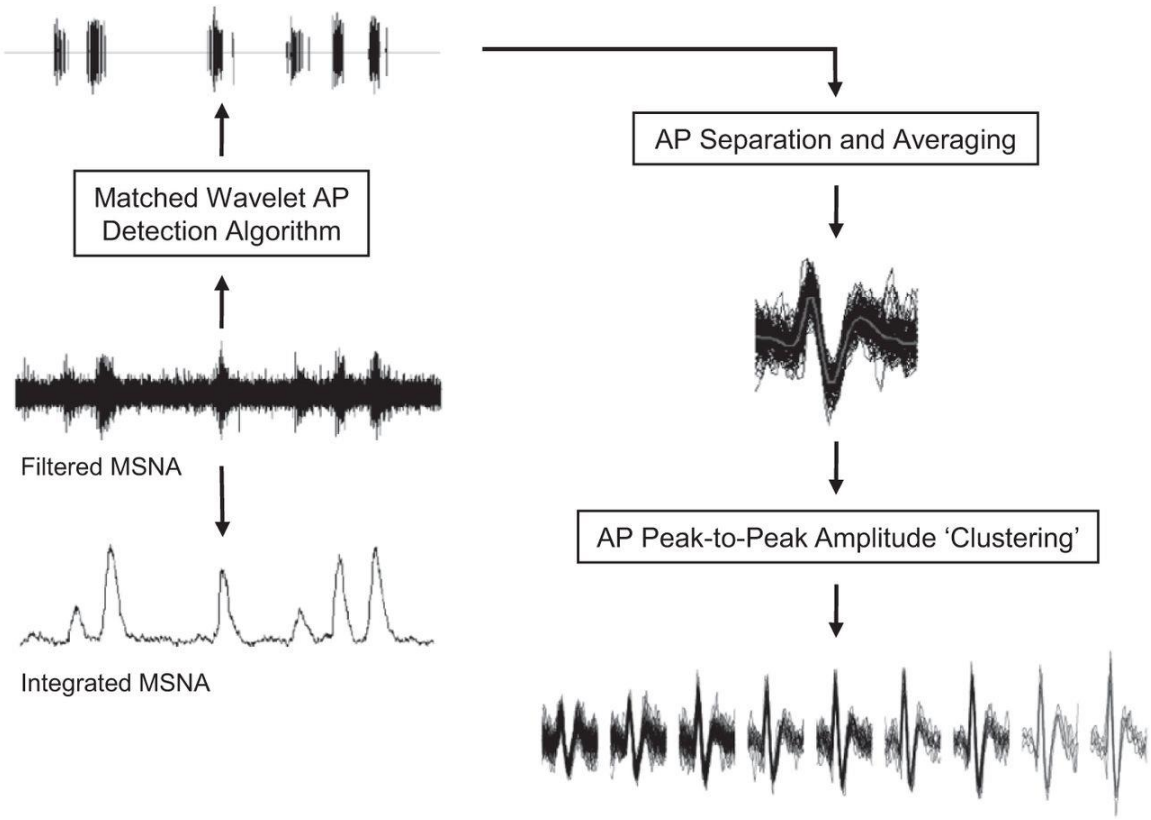

Figure 1.1: Schematic representation of action potential (AP) detection and classification.

MSNA, muscle sympathetic nerve activity. Reproduced with permission from the American Physiological Society: "Badrov MB, Usselman CW & Shoemaker JK (2015). Sympathetic neural recruitment strategies: responses to severe chemoreflex and baroreflex stress. *Am J Physiol Regul Integr Physiol* 309: R160-168."

This technique has proven invaluable in the testing of early hypotheses proposed by Wallin *et al.* (1994) and Macefield and colleagues (Macefield *et al.* 1994; Macefield & Wallin, 1999), among others (Tsukahara & Mano, 1997; Xie *et al.* 1999). With the use of this approach, an ordered pattern of recruitment was observed within the SNS during baseline rest, whereby larger axons with faster conduction velocities (i.e., shorter reflex latencies) are hierarchically recruited as integrated sympathetic bursts become stronger (i.e., larger) (Steinback *et al.* 2010*b*; Salmanpour *et al.* 2011*a*). This pattern was also observed during baroreflex- and chemoreflex-mediated sympathoexcitation (Steinback *et al.* 2010*b*; Salmanpour *et al.* 2011*a*). Furthermore, in response to prolonged voluntary apnea, Steinback *et al.* (2010*b*), and later, Breskovic *et al.* (2011), observed increased firing rates of sympathetic fibres already-active at baseline, and also, recruitment of previously silent (i.e., not present at baseline) sub-populations of higher-threshold, faster conducting (therefore, larger) sympathetic axons. Importantly, these larger, latent axons accounted for approximately 74% of the apnea-induced increase in sympathetic nerve activity (Steinback *et al.* 2010*b*). Therefore, it appears that increased sympathetic drive in response to physiological stress may be achieved predominantly through the recruitment of additional, larger sympathetic neurons, as previously hypothesized (Macefield & Wallin, 1999). However, in contrast to the discharge patterns observed during apnea (Steinback *et al.* 2010*b*; Breskovic *et al.* 2011), recruitment of latent neural sub-populations was not observed during moderate levels of baroreceptor unloading (i.e., −60 mmHg LBNP) in approximately 70% of participants, whereby sympathetic activation was achieved primarily through increased firing rates of those axons already recruited as baseline (Salmanpour *et al.* 2011*a*).

Discrepancy in recruitment strategies between the two studies (or reflexes) may be due to stress severity (i.e., varying thresholds for recruitment) and/or differences between the reflexes themselves (i.e., ‘chemoreflex’ versus ‘baroreflex’). However, these two studies were conducted in different samples of individuals, thereby limiting conclusions as to the roles played by these factors. Therefore, reflex-specific neural recruitment strategies within the SNS, as well as the issue of stress severity and threshold for recruitment of these latent axons, require further investigation.

Furthermore, a consistent finding to date has been an inverse relationship between AP size and AP latency; that is, larger APs express shorter reflex latencies (i.e., faster conduction velocities) (Steinback *et al.* 2010*b*; Salmanpour *et al.* 2011*a*,*b*). This finding forms the basis of the assumption that these larger APs reflect recruitment of larger axons. While this relationship has been observed at rest and during sympathoexcitatory stimuli (Steinback *et al.* 2010*b*; Salmanpour *et al.* 2011*a*), Salmanpour *et al.* (2011*b*) demonstrated that all APs active at baseline were recruited with a shorter reflex latency during a subsequent Valsalva maneuver, evidence perhaps for acute malleability of synaptic delays within the neural reflex arc. In contrast, in a preliminary manner, Salmanpour *et al.* (2011*a*) observed an acute upward-shift of the AP size-latency profile during −60 mmHg LBNP, such that lower-threshold axons were recruited with a slower latency during moderate levels of simulated orthostatic stress. Nonetheless, these observations appear to support the concept, initially proposed by Wallin *et al.* (1994), of acute synaptic delay variations, although additional data are required. Furthermore, the exact mechanism(s) for the reduction in neural activation latency during the Valsalva maneuver (Salmanpour *et al.* 2011*b*), but the increase

during LBNP-induced baroreceptor unloading (Salmanpour *et al.* 2011*a*), are unknown, but may reflect a central, perceptual component that is likely more pronounced during the Valsalva maneuver. As such, in addition to the study of reflex-specific discharge patterns, the exact roles played by central, perceptual components versus peripheral-reflex mechanisms in mediating these sympathetic neural recruitment responses remain to be determined.

Additionally, the majority of studies to date on sympathetic AP discharge properties have been conducted in young, healthy populations, and therefore, whether these neural coding strategies persist with increasing age and cardiovascular disease remains largely uncertain. Preliminary work in healthy aged-individuals and chronic heart failure patients suggests a comparable pattern, but perhaps slightly diminished in heart failure, of sympathetic neural recruitment in response to voluntary apnea (Maslov *et al.* 2014*b*) and premature ventricular contractions (Maslov *et al.* 2012). However, direct comparisons to a young, healthy group were not made. Furthermore, AP latency variations, reflecting synaptic delay modifications, were not studied in these investigations. Therefore, the malleability of these sympathetic neural recruitment strategies with increasing age and cardiovascular disease requires further study.

Finally, voluntary apnea appears to provide the most powerful stimulus for sympathetic axonal recruitment (Steinback *et al.* 2010*b*). Yet, the exact mechanisms mediating the robust sympathetic response are uncertain and appear diverse. Indeed, one fundamental issue involves the roles played by ventilation (or the lack thereof) versus chemoreceptor activation in eliciting the recruitment response. For example, the chemoreflex stimulus to typical 20- to 30-second apneas in untrained breath-hold

performers is rather ordinary (Leuenberger *et al.* 2005; Heusser *et al.* 2009; Seitz *et al.* 2013), raising the concern that additional factors are likely at play. Furthermore, voluntary apnea has shown to potentiate the sympathetic response to isocapnic hypoxia (Somers *et al.* 1989*a*,*b*), indicating the sympathoinhibitory nature of breathing. Therefore, the influence of chemoreflex stress *per se*, as opposed to the absence of ventilation itself, on sympathetic axonal discharge during apneic stress remains to be determined.

Nonetheless, the existing multi-unit data, albeit limited, appear to support earlier hypotheses (Wallin *et al.* 1994; Macefield & Wallin, 1999) that, in response to acute homeostatic stress, the SNS has options to increase the firing rate of already-active, lower-threshold axons, recruit latent, higher-threshold neural sub-populations, as well as modify acutely synaptic delays and/or central processing times. In turn, it appears that these strategies may differ across reflexes and/or with stress severity, which may perhaps reflect a perceptual component. Therefore, as outlined above, many questions/issues remain regarding the mechanisms of control underlying the neural recruitment strategies used by the SNS, which include, among others: (1) the reflex-specific recruitment strategies in efferent sympathetic nerves, (2) the threshold for recruitment of these neural sub-populations (i.e., stress severity), (3) the central, perceptual versus peripheral-reflex elements of sympathetic neural coding, (4) the effects of age and disease on neural discharge properties, and (5) the role of chemoreflex stress versus ventilation (or the lack thereof) in the apneic neural response. These important, but yet unanswered issues, form the basis of this dissertation.

Therefore, the overall objectives of this dissertation are to 1) Establish the neural recruitment strategies available to the SNS to respond to acute homeostatic challenge; and 2) To determine the various mechanisms of control underlying these neural coding patterns. The research contained herein tested the **working hypothesis** that efferent post-ganglionic MSNA exhibits neural coding strategies reflecting increased firing rates of lower-threshold axons, recruitment of latent, higher-threshold axons, and acute synaptic delays modifications, and further, that these are modified by factors such as reflex-specificity, stress severity, perception of effort or stress, age, and cardiovascular disease.

1.5 References

Aicher SA, Milner TA, Pickel VM & Reis DJ (2000). Anatomical substrates for baroreflex sympathoinhibition in the rat. *Brain Res Bull* **51,** 107-110.

Alam M & Smirk FH (1937). Observations in man upon a blood pressure raising reflex arising from the voluntary muscles. *J Physiol* **89,** 372-383.

Ashley C, Burton D, Sverrisdottir YB, Sander M, McKenzie DK & Macefield VG (2010). Firing probability and mean firing rates of human muscle vasoconstrictor neurones are elevated during chronic asphyxia. *J Physiol* **588,** 701-712.

Barman SM & Gebber GL (2000). "Rapid" rhythmic discharges of sympathetic nerves: sources, mechanisms of generation, and physiological relevance. *J Biol Rhythms* **15,** 365-379.

Bernard C (1974). Lectures on the phenomena of life common to animals and plants (HE Hoff, R Guillemin, & L Guillemin, Trans.). Charles C Thomas, Springfield.

Breskovic T, Steinback CD, Salmanpour A, Shoemaker JK & Dujic Z (2011). Recruitment pattern of sympathetic neurons during breath-holding at different lung volumes in apnea divers and controls. *Auton Neurosci* **164,** 74-81.

Brodde OE & Michel MC (1999). Adrenergic and muscarinic receptors in the human heart. *Pharmacol Rev* **51,** 651-690.

Burnstock G (1990). Noradrenaline and ATP as cotransmitters in sympathetic nerves. *Neurochem Int* **17,** 357-368.

Cannon WB (1929). Organization of physiological homeostasis. *Physiol Rev* **9,** 399-431.

Charkoudian N & Rabbitts JA (2009). Sympathetic neural mechanisms in human cardiovascular health and disease. *Mayo Clin Proc* **84,** 822-830.

Dampney R (1994). Functional organization of central pathways regulating the cardiovascular system. *Physiol Rev* **74,** 323-364.

Delius W, Hagbarth KE, Hongell A & Wallin BG (1972). General characteristics of sympathetic activity in human muscle nerves. *Acta Physiol Scand* **84,** 65-81.

DiBona GF, Jones SY & Sawin LL (1997). Reflex effects on renal nerve activity characteristics in spontaneously hypertensive rats. *Hypertension* **30,** 1089-1096.

Elam M & Macefield VG (2001). Multiple firing of single muscle vasoconstrictor neurons during cardiac dysrhythmias in human heart failure. *J Appl Physiol* **91,** 717-724.

Elam M, McKenzie D & Macefield VG (2002). Mechanisms of sympathoexcitation: single-unit analysis of muscle vasoconstrictor neurons in awake OSAS subjects. *J Appl Physiol* **93,** 297-303.

Elam M, Sverrisdottir Y, Rundqvist B, McKenzie D, Wallin BG & Macefield VG (2003). Pathological sympathoexcitation: how is it achieved? *Acta Physiol Scand* **177,** 405-411.

Esler M (2010). The 2009 Carl Ludwig Lecture: pathophysiology of the human sympathetic nervous system in cardiovascular diseases: the transition from mechanisms to medical management. *J Appl Physiol* **108,** 227-237.

Fagius J & Wallin BG (1980). Sympathetic reflex latencies and conduction velocities in normal man. *J Neurol Sci* **47,** 433-448.

Fagius J, Wallin BG, Sundlof G, Nerhed C & Englesson S (1985). Sympathetic outflow in man after anaesthesia of the glossopharyngeal and vagus nerves. *Brain* **108,** 423-438.

Fairfax ST, Padilla J, Vianna LC, Davis MJ & Fadel PJ (2013). Spontaneous bursts of muscle sympathetic nerve activity decrease leg vascular conductance in resting humans. *Am J Physiol Heart Circ Physiol* **304,** H759-H766.

Floras JS (2009). Sympathetic nervous system activation in human heart failure. *J Am Coll Cardiol* **54,** 375-385.

Graham LN, Smith PA, Stoker JB, Mackintosh AF & Mary DA (2004). Sympathetic neural hyperactivity and its normalization following unstable angina and acute myocardial infarction. *Clin Sci* **106,** 605-611.

Graham LN, Smith PA, Stoker JB, Mackintosh AF & Mary DA (2002). Time course of sympathetic neural hyperactivity after uncomplicated acute myocardial infarction. *Circulation* **106,** 793-797.

Grassi G & Esler M (1999). How to assess sympathetic activity in humans. *J Hypertens* **17,** 719-734.

Grassi G, Seravalle G & Quarti-Trevano F (2010). The 'neuroadrenergic hypothesis' in hypertension: current evidence. *Exp Physiol* **95,** 581-586.

Hagbarth KE, Hallin RG, Hongell A, Torebjörk HE & Wallin BG (1972). General characteristics of sympathetic activity in human skin nerves. *Acta Physiol Scand* **84,** 164-176.

Hagbarth KE & Vallbo AB (1968). Pulse and respiratory grouping of sympathetic impulses in human muscle nerves. *Acta Physiol Scand* **74,** 96-108.

Hashimoto I, Miyamura M & Saito M (1998). Initiation of increase in muscle sympathetic nerve activity delay during maximal voluntary contraction. *Acta Physiol Scand* **164,** 293-297.

Henneman E, Somjen G & Carpenter DO (1965). Functional significance of cell size in spinal motoneurons. *J Neurophysiol* **28,** 560-580.

Heusser K, Dzamonja G, Tank J, Palada I, Valic Z, Bakovic D, Obad A, Ivancev V, Breskovic T, Diedrich A, Joyner MJ, Luft FC, Jordan J & Dujic Z (2009). Cardiovascular regulation during apnea in elite divers. *Hypertension* **53,** 719-724.

Huidobro-Toro JP & Donoso MV (2004). Sympathetic co-transmission: the coordinated action of ATP and noradrenaline and their modulation by neuropeptide Y in human vascular neuroeffector junctions. *Eur J Pharmacol* **500,** 27-35.

Hulme E, Birdsall N & Buckley N (1990). Muscarinic receptor subtypes. *Annu Rev Pharmacol Toxicol* **30,** 633-673.

Ichinose M, Saito M, Fujii N, Kondo N & Nishiyasu T (2006). Modulation of the control of muscle sympathetic nerve activity during severe orthostatic stress. *J Physiol* **576,** 947-958.

Ichinose M, Saito M, Ogawa T, Hayashi K, Kondo N & Nishiyasu T (2004). Modulation of control of muscle sympathetic nerve activity during orthostatic stress in humans. *Am J Physiol Heart Circ Physiol* **287,** H2147-H2153.

Jänig W (2008). Integrative action of the autonomic nervous system: Neurobiology of homeostasis. Cambridge University Press, Cambridge.

Jänig W & Häbler HJ (2003). Neurophysiological analysis of target-related sympathetic pathways–from animal to human: Similarities and differences. *Acta Physiol Scand* **177,** 255-274.

Jänig W & McLachlan EM (1992). Characteristics of function-specific pathways in the sympathetic nervous system. *Trends Neurosci* **15,** 475-481.

Jouett NP, Watenpaugh DE, Dunlap ME & Smith ML (2015). Interactive effects of hypoxia, hypercapnia and lung volume on sympathetic nerve activity in humans. *Exp Physiol* **100,** 1018-1029.

Joyner MJ (2016). Preclinical and clinical evaluation of autonomic function in humans. *J Physiol* **594,** 4009-4013.

Joyner MJ, Barnes JN, Hart EC, Wallin BG & Charkoudian N (2015). Neural control of the circulation: how sex and age differences interact in humans. *Compr Physiol* **5,** 193-215.

Kaufman MP, Longhurst JC, Rybicki KJ, Wallach JH & Mitchell JH (1983). Effects of static muscular contraction on impulse activity of groups III and IV afferents in cats. *J Appl Physiol* **55,** 105-112.

Kienbaum P, Karlsson T, Sverrisdottir YB, Elam M & Wallin BG (2001). Two sites for modulation of human sympathetic activity by arterial baroreceptors? *J Physiol* **531,** 861-869.

Kimmerly DS, O'Leary DD & Shoemaker JK (2004). Test–retest repeatability of muscle sympathetic nerve activity: influence of data analysis and head-up tilt. *Auton Neurosci* **114,** 61-71.

Kimmerly DS & Shoemaker JK (2003). Hypovolemia and MSNA discharge patterns: assessing and interpreting sympathetic responses. *Am J Physiol Heart Circ Physiol* **284,** H1198-H1204.

Koshiya N, Huangfu D & Guyenet PG (1993). Ventrolateral medulla and sympathetic chemoreflex in the rat. *Brain Res* **609,** 174-184.

Lambert E, Dawood T, Schlaich M, Straznicky N, Esler M & Lambert G (2008). Single-unit sympathetic discharge pattern in pathological conditions associated with elevated cardiovascular risk. *Clin Exp Pharmacol Physiol* **35,** 503-507.

Lambert E, Straznicky N, Schlaich M, Esler M, Dawood T, Hotchkin E & Lambert G (2007). Differing pattern of sympathoexcitation in normal-weight and obesity-related hypertension. *Hypertension* **50,** 862-868.

Lambert GW, Thompson JM, Turner AG, Cox HS, Wilkinson D, Vaz M, Kalff V, Kelly MJ, Jennings GL & Esler M (1997). Cerebral noradrenaline spillover and its relation to muscle sympathetic nervous activity in healthy human subjects. *J Auton Nerv Syst* **64,** 57-64.

Leuenberger UA, Brubaker D, Quraishi S, Hogeman CS, Imadojemu VA & Gray KS (2005). Effects of intermittent hypoxia on sympathetic activity and blood pressure in humans. *Auton Neurosci* **121,** 87-93.

Lundberg JM, Franco-Cereceda A, Lacroix JS & Pernow J (1990). Neuropeptide Y and sympathetic neurotransmissiona. *Ann N Y Acad Sci* **611,** 166-174.

Macefield VG, Rundqvist B, Sverrisdottir YB, Wallin BG & Elam M (1999). Firing properties of single muscle vasoconstrictor neurons in the sympathoexcitation associated with congestive heart failure. *Circulation* **100,** 1708-1713.

Macefield VG & Wallin BG (1999). Firing properties of single vasoconstrictor neurones in human subjects with high levels of muscle sympathetic activity. *J Physiol* **516,** 293-301.

Macefield VG, Wallin BG & Vallbo AB (1994). The discharge behaviour of single vasoconstrictor motoneurones in human muscle nerves. *J Physiol* **481,** 799-809.

Malpas SC (1995). A new model for the generation of sympathetic nerve activity. *Clin Exp Pharmacol Physiol* **22,** 11-16.

Malpas SC (1998). The rhythmicity of sympathetic nerve activity. *Prog Neurobiol* **56,** 65-96.

Malpas SC (2010). Sympathetic nervous system overactivity and its role in the development of cardiovascular disease. *Physiol Rev* **90,** 513-557.

Malpas SC, Bendle RD, Head GA & Ricketts JH (1996). Frequency and amplitude of sympathetic discharges by baroreflexes during hypoxia in conscious rabbits. *Am J Physiol Heart Circ Physiol* **271,** H2563-H2574.

Malpas SC & Ninomiya I (1992). Effect of asphyxia on the frequency and amplitude modulation of synchronized renal nerve activity in the cat. *J Auton Nerv Syst* **40,** 199-205.

Mark AL, Victor RG, Nerhed C & Wallin BG (1985). Microneurographic studies of the mechanisms of sympathetic nerve responses to static exercise in humans. *Circ Res* **57,** 461-469.

Marshall JM (1994). Peripheral chemoreceptors and cardiovascular regulation. *Physiol Rev* **74,** 543-594.

Maslov PZ, Shoemaker JK & Dujic Z (2014*a*). Firing patterns of muscle sympathetic neurons during apnea in chronic heart failure patients and healthy controls. *Auton Neurosci* **180,** 66-69.

Maslov PZ, Breskovic T, Brewer DN, Shoemaker JK & Dujic Z (2012). Recruitment pattern of sympathetic muscle neurons during premature ventricular contractions in heart failure patients and controls. *Am J Physiol Regul Integr Comp Physiol* **303,** R1157-R1164.

Maslov PZ, Shoemaker JK & Dujic Z (2014*b*). Firing patterns of muscle sympathetic neurons during apnea in chronic heart failure patients and healthy controls. *Auton Neurosci* **180,** 66-69.

McAllen RM & Malpas SC (1997). Sympathetic burst activity: characteristics and significance. *Clin Exp Pharmacol Physiol* **24,** 791-799.

McCloskey DI & Mitchell JH (1972). Reflex cardiovascular and respiratory responses originating in exercising muscle. *J Physiol* **224,** 173-186.

McLachlan E (2003). Transmission of signals through sympathetic ganglia–modulation, integration or simply distribution? *Acta Physiol Scand* **177,** 227-235.

Mitchell JH, Kaufman MP & Iwamoto GA (1983). The exercise pressor reflex: its cardiovascular effects, afferent mechanisms, and central pathways. *Annu Rev Physiol* **45,** 229-242.

Morgan BJ, Crabtree DC, Palta M & Skatrud JB (1995). Combined hypoxia and hypercapnia evokes long-lasting sympathetic activation in humans. *J Appl Physiol* **79,** 205-213.

Murai H, Takata S, Maruyama M, Nakano M, Kobayashi D, Otowa K, Takamura M, Yuasa T, Sakagami S & Kaneko S (2006). The activity of a single muscle sympathetic vasoconstrictor nerve unit is affected by physiological stress in humans. *Am J Physiol Heart Circ Physiol* **290,** H853-H860.

Narkiewicz K & Somers V (2003). Sympathetic nerve activity in obstructive sleep apnoea. *Acta Physiol Scand* **177,** 385-390.

Nattie E & Li A (2012). Central chemoreceptors: locations and functions. *Compr Physiol* **2,** 221-254.

Ninomiya I, Malpas SC, Matsukawa K, Shindo T & Akiyama T (1993). The amplitude of synchronized cardiac sympathetic nerve activity reflects the number of activated pre- and postganglionic fibers in anesthetized cats. *J Auton Nerv Syst* **45,** 139-147.

Parati G & Esler M (2012). The human sympathetic nervous system: its relevance in hypertension and heart failure. *Eur Heart J* **33,** 1058-1066.

Peralta EG, Ashkenazi A, Winslow JW, Smith DH, Ramachandran J & Capon DJ (1987). Distinct primary structures, ligand-binding properties and tissue-specific expression of four human muscarinic acetylcholine receptors. *EMBO J* **6,** 3923-3929.

Rea RF & Wallin BG (1989). Sympathetic nerve activity in arm and leg muscles during lower body negative pressure in humans. *J Appl Physiol* **66,** 2778-2781.

Ryan KL, Rickards CA, Hinojosa-Laborde C, Cooke WH & Convertino VA (2011). Arterial pressure oscillations are not associated with muscle sympathetic nerve activity in individuals exposed to central hypovolaemia. *J Physiol* **589,** 5311-5322.

Saito M, Mano T, Iwase S, Koga K, Abe H & Yamazaki Y (1988). Responses in muscle sympathetic activity to acute hypoxia in humans. *J Appl Physiol* **65,** 1548-1552.

Salmanpour A, Brown LJ & Shoemaker JK (2010). Spike detection in human muscle sympathetic nerve activity using a matched wavelet approach. *J Neurosci Methods* **193,** 343-355.

Salmanpour A, Brown LJ, Steinback CD, Usselman CW, Goswami R & Shoemaker JK (2011*a*). Relationship between size and latency of action potentials in human muscle sympathetic nerve activity. *J Neurophysiol* **105,** 2830-2842.

Salmanpour A, Frances MF, Goswami R & Shoemaker JK (2011*b*). Sympathetic neural recruitment patterns during the Valsalva maneuver. *Conf Proc IEEE Eng Med Biol Soc* **2011,** 6951-6954.

Salmanpour A & Shoemaker JK (2012). Baroreflex mechanisms regulating the occurrence of neural spikes in human muscle sympathetic nerve activity. *J Neurophysiol* **107,** 3409-3416.

Seals DR, Chase PB & Taylor JA (1988). Autonomic mediation of the pressor responses to isometric exercise in humans. *J Appl Physiol* **64,** 2190-2196.

Seals DR & Esler MD (2000). Human ageing and the sympathoadrenal system. *J Physiol* **528,** 407-417.

Seitz MJ, Brown R & Macefield VG (2013). Inhibition of augmented muscle vasoconstrictor drive following asphyxic apnoea in awake human subjects is not affected by relief of chemical drive. *Exp Physiol* **98,** 405-414.

Shields RW (1993). Functional anatomy of the autonomic nervous system. *J Clin Neurophysiol* **10,** 2-13.

Shoemaker JK, Badrov MB, Al-Khazraji BK & Jackson DN (2016). Neural control of vascular function in skeletal muscle. *Compr Physiol* **6,** 303-329.

Shoemaker JK, Mattar L, Kerbeci P, Trotter S, Arbeille P & Hughson RL (2007). WISE 2005: stroke volume changes contribute to the pressor response during ischemic handgrip exercise in women. *J Appl Physiol* **103,** 228-233.

Somers VK, Dyken ME, Clary MP & Abboud FM (1995). Sympathetic neural mechanisms in obstructive sleep apnea. *J Clin Invest* **96,** 1897-1904.

Somers VK, Mark AL, Zavala DC & Abboud FM (1989*a*). Contrasting effects of hypoxia and hypercapnia on ventilation and sympathetic activity in humans. *J Appl Physiol* **67,** 2101-2106.

Somers VK, Mark AL, Zavala DC & Abboud FM (1989*b*). Influence of ventilation and hypocapnia on sympathetic nerve responses to hypoxia in normal humans. *J Appl Physiol* **67,** 2095-2100.

Steinback CD, Breskovic T, Frances M, Dujic Z & Shoemaker JK (2010*a*). Ventilatory restraint of sympathetic activity during chemoreflex stress. *Am J Physiol Regul Integr Comp Physiol* **299,** R1407-R1414.

Steinback CD, Salmanpour A, Breskovic T, Dujic Z & Shoemaker JK (2010*b*). Sympathetic neural activation: an ordered affair. *J Physiol* **588,** 4825-4836.

Sundlöf G & Wallin BG (1977). The variability of muscle nerve sympathetic activity in resting recumbent man. *J Physiol* **272,** 383-397.

Sundlöf G & Wallin BG (1978*a*). Effect of lower body negative pressure on human muscle nerve sympathetic activity. *J Physiol* **278,** 525-532.

Sundlöf G & Wallin BG (1978*b*). Human muscle nerve sympathetic activity at rest. Relationship to blood pressure and age. *J Physiol* **274,** 621-637.

Sverrisdóttir YB, Rundqvist B & Elam M (1998). Relative burst amplitude in human muscle sympathetic nerve activity: a sensitive indicator of altered sympathetic traffic. *Clin Auton Res* **8,** 95-100.

Sverrisdóttir YB, Rundqvist B, Johannsson G & Elam M (2000). Sympathetic neural burst amplitude distribution: A more specific indicator of sympathoexcitation in human heart failure. *Circulation* **102,** 2076-2081.

Taylor JA, Hand GA, Johnson DG & Seals DR (1992). Sympathoadrenal-circulatory regulation of arterial pressure during orthostatic stress in young and older men. *Am J Physiol Regul Integr Comp Physiol* **263,** R1147-R1155.

Tompkins RP, Melling CW, Wilson TD, Bates BD & Shoemaker JK (2013). Arrangement of sympathetic fibers within the human common peroneal nerve: implications for microneurography. *J Appl Physiol* **115,** 1553-1561.

Triposkiadis F, Karayannis G, Giamouzis G, Skoularigis J, Louridas G & Butler J (2009). The sympathetic nervous system in heart failure: physiology, pathophysiology, and clinical implications. *J Am Coll Cardiol* **54,** 1747-1762.

Tsukahara R & Mano T (1997). The recruitment pattern of single vasoconstrictor neurons in human. *J Auton Nerv Syst* **66,** 26-34.

Vallbo AB, Hagbarth KE & Wallin BG (2004). Microneurography: how the technique developed and its role in the investigation of the sympathetic nervous system. *J Appl Physiol* **96,** 1262-1269.

Victor RG, Bertocci LA, Pryor SL & Nunnally RL (1988). Sympathetic nerve discharge is coupled to muscle cell pH during exercise in humans. *J Clin Invest* **82,** 1301-1305.

Victor RG & Leimbach W (1987). Effects of lower body negative pressure on sympathetic discharge to leg muscles in humans. *J Appl Physiol* **63,** 2558-2562.

Wallin BG, Burke D & Gandevia S (1994). Coupling between variations in strength and baroreflex latency of sympathetic discharges in human muscle nerves. *J Physiol* **474,** 331-338.

Wallin BG & Charkoudian N (2007). Sympathetic neural control of integrated cardiovascular function: insights from measurement of human sympathetic nerve activity. *Muscle Nerve* **36,** 595-614.

Wallin BG, Esler M, Dorward P, Eisenhofer G, Ferrier C, Westerman R & Jennings G (1992). Simultaneous measurements of cardiac noradrenaline spillover and sympathetic outflow to skeletal muscle in humans. *J Physiol* **453,** 45-58.

Wallin BG, Thompson JM, Jennings GL & Esler MD (1996). Renal noradrenaline spillover correlates with muscle sympathetic activity in humans. *J Physiol* **491,** 881-887.

Wallin BG, Victor RG & Mark AL (1989). Sympathetic outflow to resting muscles during static handgrip and postcontraction muscle ischemia. *Am J Physiol Heart Circ Physiol* **256,** H105-H110.

Wehrwein EA, Orer HS & Barman SM (2016). Overview of the anatomy, physiology, and pharmacology of the autonomic nervous system. *Compr Physiol* **6,** 1239-1278.

Westgaard R & De Luca C (2001). Motor control of low-threshold motor units in the human trapezius muscle. *J Neurophysiol* **85,** 1777-1781.

White DW, Shoemaker JK & Raven PB (2015). Methods and considerations for the analysis and standardization of assessing muscle sympathetic nerve activity in humans. *Auton Neurosci* **193,** 12-21.

Xie A, Skatrud JB, Puleo DS & Morgan BJ (1999). Arousal from sleep shortens sympathetic burst latency in humans. *J Physiol* **515,** 621-628.

Chapter 2

2 Sympathetic neural recruitment strategies: responses to severe chemoreflex and baroreflex stress

(Published in Am J Physiol Regul Integr Comp Physiol 309: R160-R168, 2015)

2.1 Introduction

Patterns of neural coding form the basis of all neural processes requiring information exchange and processing. Neural coding patterns include variations in firing rate of single neurons (rate coding), the timing of activity amongst synchronized or pseudo-synchronized neurons (temporal coding), and varying thresholds for recruitment of sub-populations (population coding). Although established largely in intracerebral neural processing, these coding patterns exist in the control of peripheral organs as well, such as during the generation of ever-increasing muscular force (Henneman *et al.* 1965). Conversely, the neural strategies employed by the autonomic nervous system, which regulates homeostatic and life-sustaining outcomes, remain unclear, particularly in humans where access to direct neural recordings is limited. The multiple sites of control through which efferent sympathetic outflow can be modified include the brainstem autonomic nuclei (Barman & Gebber, 2000), spinal cord, and paraspinal ganglia (Jänig & McLachlan, 1992; McAllen & Trevaks, 2003). These junctures introduce opportunities for modifiable synaptic delays and latent neuronal sub-populations.

Using microneurographic techniques (Hagbarth & Vallbo, 1968), direct recordings are made from the populations of post-ganglionic sympathetic neurons innervating the skeletal muscle vasculature (muscle sympathetic nerve activity; MSNA)

in humans. The measured bursts of activity reflect periods of efferent action potential synchronization (Delius *et al.* 1972*b*). The size of any given burst is determined by the proximity of the recording electrode to the individual neurons within the respective bundle of sympathetic axons (Tompkins *et al.* 2013), as well as the number (Ninomiya *et al.* 1993) and size (Salmanpour *et al.* 2011*a*) of action potentials. With the use of these features, the question of neural coding in efferent sympathetic nerve activity was advanced by the introduction of single fibre recordings (Macefield *et al.* 1994), which indicated that a given axon will fire approximately once per burst and perhaps two to three times during states of elevated sympathetic drive (Macefield & Wallin, 1999; Elam *et al.* 2002). To further study the existence of latent neuronal sub-populations and/or modifiable synaptic delays, our laboratory developed a technique that quantifies and classifies the populations of axons comprising each sympathetic burst (Salmanpour *et al.* 2010). With the use of this approach, a fundamental pattern was exposed within the sympathetic nervous system, whereby larger neurons with faster conduction velocities are hierarchically recruited as sympathetic bursts become stronger (i.e., larger), an observation made under baseline conditions (Salmanpour *et al.* 2011*a*) and during chemoreceptor activation (Steinback *et al.* 2010). Importantly, Steinback *et al.* (2010) documented recruitment of latent sub-populations of larger neurons during maximal end-inspiratory apnea, which were absent under baseline conditions. However, in a preliminary study, recruitment of latent axons was not observed during moderate baroreceptor unloading using −60 mmHg lower body negative pressure [LBNP; (Salmanpour *et al.* 2011*a*)]. Discrepancy in neuronal recruitment patterns between

studies may be due to reflex-specific strategies, varying thresholds for sub-population recruitment, and/or interindividual variations.

To further understand rate and population coding within the efferent sympathetic nervous system, this study tested the hypothesis of reflex-specific sympathetic neural recruitment strategies during periods of high sympathetic stress in the same individuals, and whether these recruitment patterns demonstrated test-retest repeatability.

2.2 Methods

2.2.1 Participants

Eleven normotensive individuals (6 males, 5 females) participated in the current investigation. Participants were aged 25 ± 3 years (mean ± SD) and were 173 ± 8 cm in height and 70 ± 9 kg in weight (body mass index = 24 ± 2 kg/m^2). Participants were regular exercisers, non-smokers, and free of any overt cardiovascular or respiratory disease (as assessed by a standardized health questionnaire). All protocols in the current investigation were submitted to, and approved by, the Health Sciences Research Ethics Board at Western University in Canada. All participants provided written informed consent and were familiarized to all experimental procedures before study participation.

2.2.2 Experimental Protocol

All testing was conducted following at least a 3-hour fast and a 12-hour abstinence from alcohol, caffeine, and other stimulants. Female participants were tested during the early follicular menstrual cycle phase. Participants voided their bladder immediately prior to testing commencement to minimize the effect of bladder distention

on sympathetic nerve activity (Fagius & Karhuvaara, 1989). Experimentation entailed two protocols as follows.

In the first protocol, the impact of progressive chemoreflex stress was studied in which data were obtained in the supine position during a 5-minute period of baseline (spontaneous breathing) and during a maximal end-inspiratory apnea, which was preceded by a rebreathing period designed to maximize the severity of chemoreflex stimulation through progressive hypoxia and hypercapnia [described previously in detail; (Usselman *et al.* 2015)]. Briefly, participants were fitted with a mouthpiece (series 9060, Hans Rudolph, Kansas City, MO) attached to a three-way valve allowing them to breathe either room air, or through a Y-connector (VacuMed, Ventura, CA) leading to two 3-liter breathing bags. Before the start of the protocol, participants expired into the breathing bags to fill them with air for the ensuing rebreathing period. After five minutes of baseline collection, the three-way valve was turned to initiate rebreathing. Once end-tidal partial pressure of oxygen ($P_{ET}O_2$) reached 70 Torr, participants performed an end-inspiratory apnea of maximal voluntary duration. Upon cessation, participants breathed twice into and out of the bags to allow for the measurement of end-apnea $P_{ET}O_2$ and end-tidal partial pressure of carbon dioxide ($P_{ET}CO_2$). Blood gases were analyzed using an infrared carbon dioxide sensor and optical oxygen detector fed from a damped micro-vacuum sampling pump (ML206 Gas Analyzer, ADInstruments, Colorado Springs, CO). Values were calibrated using ambient air pressure values and converted to online measurements of $P_{ET}O_2$ and $P_{ET}CO_2$.

In the second protocol, the impact of severe baroreceptor unloading was studied. Data were collected in the supine position during a 5-minute period of baseline (spontaneous breathing) and during three minutes of −80 mmHg LBNP. One individual exhibited presyncopal symptoms (i.e., systolic blood pressure <90 mmHg) during the −80 mmHg LBNP protocol; however, data used for this participant included the first 170 seconds of LBNP, prior to the onset of presyncopal symptoms.

Heart rate was measured using a standard three-lead electrocardiogram. Continuous beat-to-beat mean arterial blood pressure was obtained through finger photoplethysmography (Finometer; Finapres Medical Systems, Amsterdam, The Netherlands). Finometer blood pressures were validated and calibrated to manual sphygmomanometer blood pressure measurements taken throughout the protocol. Stroke volume and cardiac output were obtained using the Finometer Modelflow algorithm. Participant sex, age, height, and weight were input manually into the Finometer to optimize estimation of stroke volume and cardiac output. Total peripheral resistance was calculated as mean arterial pressure divided by cardiac output. Data were collected using LabChart6 and PowerLab data acquisition system (ADInstruments).

2.2.3 Sympathetic Neural Recordings

Efferent post-ganglionic sympathetic outflow was measured in the fibular (peroneal) nerve of the right leg by microneurography (Hagbarth & Vallbo, 1968). Specifically, a tungsten microelectrode (35 mm long, 200 μm in diameter, and tapered to a 1-5 μm uninsulated tip) was inserted percutaneously into the nerve just posterior to the fibular head. A reference electrode was positioned subcutaneously 1-3 cm from the recording site. A suitable recording site was searched for by manually manipulating the

microelectrode until a characteristic pulse-synchronous burst pattern was observed. Confirmation of an MSNA site was determined by the absence of skin paresthesia and a signal that increased firing frequency in response to voluntary apnea, but not during arousal to loud noise (Delius *et al.* 1972*a*). The MSNA neurogram was measured with a nerve traffic analysis system (662C-3; Bioengineering of University of Iowa, Iowa City, IA). The neural signal was first preamplified with a gain of 1,000 (using preamplifier and isolation amplifier; gain of 100 and 10, respectively) and further amplified with a gain of 75 (using a variable gain amplifier; gain of 0.1-99). The neural activity was then band-pass filtered (bandwidth of 700-2,000 Hz) before being rectified and integrated (using a leaky integrator; 0.1 s time constant) to obtain a mean voltage neurogram. The raw, filtered, and integrated MSNA signals were sampled at a frequency of 10,000 Hz and stored for further offline analysis (PowerLab Software, ADInstruments).

2.2.4 Integrated MSNA Analysis

Integrated bursts of MSNA were included in the analysis if they exhibited pulse-synchrony, had a signal-to-noise ratio of at least 2:1 with respect to the previous period of neuronal silence between bursts, and had characteristic rising and falling slopes. Occurrence of integrated sympathetic bursts was confirmed by visually inspecting the corresponding raw and filtered neurograms.

Integrated sympathetic nerve activity was expressed both as burst frequency (the number of bursts per minute) and burst incidence (the number of bursts per 100 heart beats). Burst amplitudes during baseline and sympathoexcitatory maneuvers were normalized to the largest recorded burst during each relevant baseline and maneuver

period, which was given a value of 100. Total MSNA was quantified as the product of mean normalized burst amplitude and burst frequency.

2.2.5 Action Potential Detection and Analysis

Action potentials were detected and extracted from the filtered raw MSNA signal using the techniques developed in our laboratory and described previously in detail [See Figure 2.1; (Salmanpour *et al.* 2010)]. Briefly, this approach detects individual action potentials using a continuous wavelet transform (CWT). The CWT uses a 'mother wavelet' that was adapted to an actual average action potential waveform constructed from (and with the same morphology as) physiological recordings of efferent post-ganglionic sympathetic action potentials (Salmanpour *et al.* 2010). The CWT was applied to the filtered raw MSNA signal to generate a resemblance index (i.e., wavelet coefficient) between the signal of interest (i.e., an action potential) and the mother wavelet, such that the wavelet coefficient was the greatest in the presence of action potentials and negligible when applied to noise. Wavelet coefficients related to action potentials and noise were separated based on thresholding analysis (Johnstone & Silverman, 1997). The exact location of the negative peak for each action potential was then detected by isolating the largest suprathreshold wavelet coefficient. With the use of this location information, the action potential waveforms were obtained from the original filtered raw MSNA signal by setting the estimated location of action potentials in the center of a predefined window (3.2 ms). As such, the amplitude and morphology of each extracted action potential remained unaltered. Extracted action potentials were then ordered based on their peak-to-peak amplitude, and histogram analysis was performed to separate action potentials

into ‘clusters’ (i.e., bins or groups of action potentials with similar peak-to-peak amplitudes) defined by Scott’s rule (Scott, 1979). Scott’s rule proposes the optimal histogram bin width to minimize the integrated mean square error by defining bin width based on the sample size and an estimate of the SD of the data. As such, the number of total clusters varied by participant. To enable comparisons within maneuvers and individuals, bin characteristics across conditions (i.e., baseline vs. apnea; baseline vs. LBNP) were manipulated within each individual to ensure that minimum histogram bin width, maximum bin center, and total number of bins would be identical across conditions. This bin normalization ensured that corresponding clusters at baseline and subsequent sympathoexcitatory maneuvers contained action potentials with similar peak-to-peak amplitudes. As such, new clusters detected during sympathoexcitatory maneuvers represent recruitment of new, larger action potentials not present during baseline.

Action potential indices assessed include action potential frequency (the number of action potentials per minute), action potential incidence (the number of action potentials per 100 heart beats), and the mean action potential content per integrated burst. Additionally, the number of total clusters detected and the number of active clusters per integrated burst were assessed. The conduction latency of each individual action potential was established as the time delay between the R-wave of the ECG of the preceding cardiac cycle and the negative peak of the action potential waveform. As such, action potential cluster latency was determined as the mean latency of all action potentials contained within each cluster. As the number of total clusters varied by individual, normalization procedures were completed when assessing action potential

content and latency as a function of cluster number between individuals (i.e., Figures 2.4, 2.5, 2.8, and 2.9). Specifically, each participants' number of total clusters was normalized to 10 total clusters (i.e., bins), each containing a 10% range of the largest detected cluster (i.e., 0-10%, 10-20%, etc.), which was given a value of 100%. For example, cluster 0-10% contained an average of all cluster numbers that were 0-10% of the largest cluster. This procedure was then repeated for the nine remaining clusters.

2.2.6 Test-Retest Repeatability of Action Potential Detection

To assess the test-retest repeatability of this technique to detect and extract action potentials from the filtered raw MSNA signal, male participants (n = 6) were studied a second time approximately one month following their initial testing day. All repeat testing was conducted at the same time of day as initial testing. Successful microneurographic recordings were obtained in both test dates in five participants, who are thus included in the test-retest repeatability analysis (chemoreflex protocol; n = 4). Test-retest repeatability of selected action potential variables (action potential frequency and active clusters per burst) was assessed using the Bland-Altman method of differences (Altman & Bland, 1983; Bland & Altman, 1986). To determine systematic differences or biases between the two test dates, we assessed measures of fixed bias and proportional bias. Fixed bias occurs when one test produces values that are consistently greater or lesser than those from a second test by a constant amount, whereas proportional bias occurs when one test produces values that are greater or lesser than those from a second test by an amount proportional to the level of the variable assessed (Ludbrook, 1997).

2.2.7 Statistical Analysis

The effect of condition (baseline vs. apnea; baseline vs. LBNP) was assessed using two-tailed, paired *t*-tests. Cohen's *d* values are provided as an estimate of effect size (Cohen, 1988). For test-retest repeatability analysis, fixed bias was tested using a one-sample *t*-test, where the mean difference between test dates was tested against a value of "0". Proportional bias was determined to exist if the Pearson product-moment correlation coefficient was significantly different than $r = 0$. Statistical significance was set at $P < 0.05$ and all data are presented as means ± SD. All statistical analyses were performed using SigmaPlot 12.0 (Systat Software Inc., San Jose, CA).

2.3 Results

Baseline versus End-Inspiratory Apnea. Data were obtained and analyzed for 297 ± 6 seconds at baseline and during 23 ± 10 seconds of a maximal end-inspiratory apnea. A representative sample of data collected for one subject at baseline and during chemoreflex conditions is shown in Figure 2.2. The rebreathe protocol and subsequent apnea elicited severe chemoreflex stress, as evident by the significant end-apnea decrease in $P_{ET}O_2$ and increase in $P_{ET}CO_2$ compared with baseline (all $P < 0.0001$; Table 2.1). Results from the integrated MSNA analyses at baseline and during apnea are presented in Table 2.2. Specifically, compared with baseline, burst frequency, burst incidence, mean normalized burst amplitude, and total MSNA were significantly increased during apnea (all $P < 0.0001$). The elevated sympathetic nerve activity during apnea was concomitant with significant increases in mean arterial blood pressure and total peripheral resistance (both $P < 0.05$; Table 2.1).

When compared with baseline, both action potential frequency and action potential incidence were elevated during apnea, yielding an increase in the mean action potential content per burst during apnea (all $P < 0.01$; Table 2.2). When detected action potentials were binned according to peak-to-peak amplitude, the number of total clusters of action potentials detected (13 ± 4 to 20 ± 8 total clusters; $P = 0.0009$; $d = 1.14$; Figure 2.3*a*) increased during apnea. Moreover, the increased number of total clusters was associated with a significant increase in the number of active clusters per sympathetic burst (5 ± 2 to 8 ± 2 clusters/burst; $P < 0.0001$; $d = 1.44$; Figure 2.3*b*) during apnea. When histogram analysis was conducted to represent action potential content as a function of normalized cluster number (Figure 2.4), a shift in the median occurred during apnea compared with baseline ($P < 0.0001$), indicating preferential recruitment of larger-amplitude action potentials during apnea.

At baseline and during apnea, a pattern emerged whereby action potential cluster latency decreased in each subject as cluster number increased (i.e., as peak-to-peak cluster amplitude increased). The mean responses (Figure 2.5) were fitted using an exponential function model at baseline ($R^2 = 0.91$; $P < 0.001$) and during apnea ($R^2 = 0.98$; $P < 0.0001$). Interestingly, the cluster latency profile was shifted downwards for every corresponding cluster number during apnea versus baseline (range −15 to −99 ms; mean = −53 ± 27 ms), indicating that all action potentials with similar peak-to-peak amplitudes were detected approximately 53 ms earlier during apnea versus baseline.

Baseline versus −80 mmHg LBNP. Data were obtained and analyzed for 274 ± 39 seconds at baseline and for 188 ± 15 seconds at −80 mmHg LBNP. A representative sample of data collected for one subject at baseline and LBNP is shown in Figure 2.6.

Hemodynamic parameters at baseline and during LBNP are displayed in Table 2.3. Results from the integrated MSNA analyses during baseline and LBNP are presented in Table 2.4. Specifically, compared with baseline, burst frequency, burst incidence, mean normalized burst amplitude, and total MSNA were increased during LBNP (all $P < 0.001$). The increase in MSNA during LBNP was associated with a pronounced tachycardia and reduction in stroke volume, as well as a significant increase in total peripheral resistance (all $P < 0.05$; Table 2.3).

Action potential frequency, action potential incidence, and the mean action potential content per burst were increased during LBNP versus baseline (all $P < 0.01$; Table 2.4). When detected action potentials were binned according to their peak-to-peak amplitude, the number of total action potential clusters increased from 15 ± 5 at baseline to 26 ± 8 during LBNP ($P = 0.0012$, $d = 1.66$; Figure 2.7*a*), indicating recruitment of approximately 11 additional, larger amplitude clusters of action potentials during LBNP. This was associated with an increase in the number of active clusters per sympathetic burst during LBNP (5 ± 1 to 8 ± 3 clusters/burst; $P = 0.0076$, $d = 1.44$; Figure 2.7*b*). Histogram analysis representing action potential content as a function of normalized cluster number (Figure 2.8) revealed a shift in the median value during LBNP compared with the baseline period ($P = 0.0011$), indicating preferential recruitment of larger amplitude action potentials during LBNP.

As with the apnea outcomes, action potential cluster latency decreased in each participant as an inverse function of cluster number (i.e., as peak-to-peak amplitude increased) at both baseline and LBNP. Mean responses (Figure 2.9) were fitted using an exponential model at baseline ($R^2 = 0.97$; $P < 0.0001$) and LBNP ($R^2 = 0.95$; $P <$

0.0001). However, in contrast to apnea, the cluster latency-size profile during LBNP was shifted upwards relative to baseline for every corresponding cluster number (range +2 to +45 ms; mean = +31 ± 12 ms), indicating that action potentials with similar peak-to-peak amplitudes were detected approximately 31 ms later during LBNP.

Test-Retest Repeatability of Action Potential Detection. Results obtained from the Bland-Altman method of differences for action potential detection at baseline and during apnea and LBNP are summarized in Table 2.5. Specifically, action potential frequency and the number of active clusters per burst were without significant proportional or fixed bias during baseline, apnea, or LBNP in repeated test dates. Furthermore, all hemodynamic, integrated MSNA, and action potential indices assessed were without significant day-to-day variation (all $P > 0.05$).

Table 2.1: Hemodynamic parameters at baseline and during maximal end-inspiratory apnea

	Baseline	**Apnea**
MAP (mmHg)	86 ± 8	97 ± 16†
SBP (mmHg)	120 ± 13	134 ± 25*****
DBP (mmHg)	69 ± 8	78 ± 15†
HR (beats min^{-1})	55 ± 4	62 ± 6†
SV (mL)	86 ± 12	81 ± 11*****
CO (L min^{-1})	4.7 ± 0.6	5.0 ± 0.7
TPR (mmHg L^{-1} min^{-1})	19 ± 2	21 ± 3*****
$P_{ET}O_2$ (Torr)	103 ± 3	56 ± 3†
$P_{ET}CO_2$ (Torr)	39 ± 3	56 ± 4†

Values are mean ± SD. MAP, mean arterial pressure; SBP, systolic blood pressure; DBP, diastolic blood pressure; HR, heart rate; SV, stroke volume; CO, cardiac output; TPR, total peripheral resistance; $P_{ET}O_2$, end-tidal partial pressure of oxygen; $P_{ET}CO_2$, end-tidal partial pressure of carbon dioxide. *****Significantly different from baseline, $P \leq 0.05$; †Significantly different from baseline, $P \leq 0.01$.

Table 2.2: Integrated MSNA and action potential indices at baseline and during maximal end-inspiratory apnea

	Baseline	Apnea
Integrated MSNA		
Burst Frequency (bursts/min)	15 ± 8	48 ± 7†
Burst Incidence (bursts/100 heart beats)	28 ± 16	77 ± 9†
Normalized Burst Amplitude (AU)	24 ± 6	58 ± 9†
Total MSNA (AU)	366 ± 220	2745 ± 478†
Action Potential Indices		
AP Frequency (spikes/min)	174 ± 151	1083 ± 487†
AP Incidence (spikes/100 heart beats)	325 ± 293	1766 ± 829†
APs/Burst (spikes/burst)	11 ± 4	24 ± 12†

Values are mean ± SD. MSNA, muscle sympathetic nerve activity; AU, arbitrary units; AP, action potential. †Significantly different from baseline, $P \leq 0.01$.

Table 2.3: Hemodynamic parameters at baseline and during −80 mmHg lower body negative pressure

	Baseline	**LBNP**
MAP (mmHg)	88 ± 8	88 ± 9
SBP (mmHg)	121 ± 14	113 ± 14*****
DBP (mmHg)	71 ± 9	75 ± 8*****
HR (beats min^{-1})	56 ± 6	79 ± 14*****
SV (mL)	89 ± 19	59 ± 19†
CO (L min^{-1})	4.9 ± 1.0	4.4 ± 1.0†
TPR (mmHg L^{-1} min^{-1})	20 ± 4	21 ± 4*****

Values are mean ± SD. LBNP, lower body negative pressure; MAP, mean arterial pressure; SBP, systolic blood pressure; DBP, diastolic blood pressure; HR, heart rate; SV, stroke volume; CO, cardiac output; TPR, total peripheral resistance. *****Significantly different from baseline, $P \leq 0.05$; †Significantly different from baseline, $P \leq 0.01$.

Table 2.4: Integrated MSNA and action potential indices at baseline and during −80 mmHg lower body negative pressure

	Baseline	LBNP
Integrated MSNA		
Burst Frequency (bursts/min)	15 ± 7	41 ± 15†
Burst Incidence (bursts/100 heart beats)	26 ± 13	52 ± 12†
Normalized Burst Amplitude (AU)	31 ± 12	52 ± 4†
Total MSNA (AU)	472 ± 302	2138 ± 769†
Action Potential Indices		
AP Frequency (spikes/min)	165 ± 83	839 ± 709†
AP Incidence (spikes/100 heart beats)	296 ± 140	1027 ± 703†
APs/Burst (spikes/burst)	11 ± 2	19 ± 9†

Values are mean ± SD. MSNA, muscle sympathetic nerve activity; LBNP, lower body negative pressure; AU, arbitrary units; AP, action potential. †Significantly different from baseline, $P \leq 0.01$.

Table 2.5: Proportional and fixed bias outcomes for action potential detection determined from the Bland-Altman method of differences during baseline, maximal end-inspiratory apnea, and −80 mmHg lower body negative pressure protocols

Variable	*r*	P_{PB}	Proportional Bias	Mean Difference ± SE	95% CI for Mean Difference	P_{FB}	Fixed Bias
Baseline							
AP Frequency	0.18	0.78	NO	7.0 ± 176.6	−555.0, 569.0	0.97	NO
Clusters/Burst	0.04	0.95	NO	−0.8 ± 1.8	−6.4, 4.8	0.68	NO
Apnea							
AP Frequency	0.37	0.63	NO	−3.0 ± 309.2	−1333.6, 1327.6	0.99	NO
Clusters/Burst	0.02	0.98	NO	0.8 ± 2.6	−11.8, 10.3	0.79	NO
LBNP							
AP Frequency	0.02	0.98	NO	−102.2 ± 179.6	−673.7, 469.3	0.60	NO
Clusters/Burst	−0.65	0.23	NO	−1.6 ± 0.8	−4.0, 0.9	0.16	NO

N = 5 males; *r*, Pearson product-moment correlation coefficient for the Bland-Altman method of differences plots; P_{PB}, *P* value for the Pearson product-moment correlation coefficient for the determination of proportional bias; SE, standard error; CI, confidence interval; P_{FB}, *P* value for the one sample *t*-test on the mean differences versus 0 for the determination of fixed bias; AP, action potential.

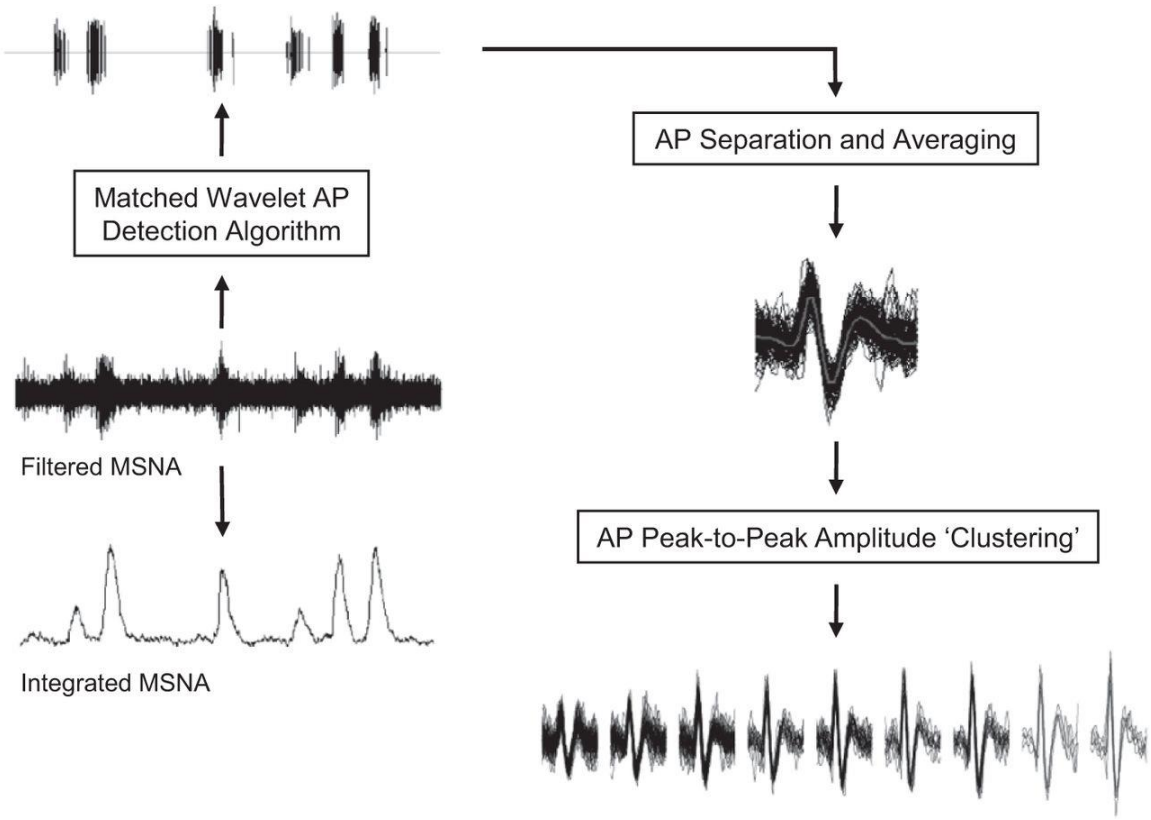

Figure 2.1: Schematic representation of action potential (AP) detection and classification.

MSNA, muscle sympathetic nerve activity.

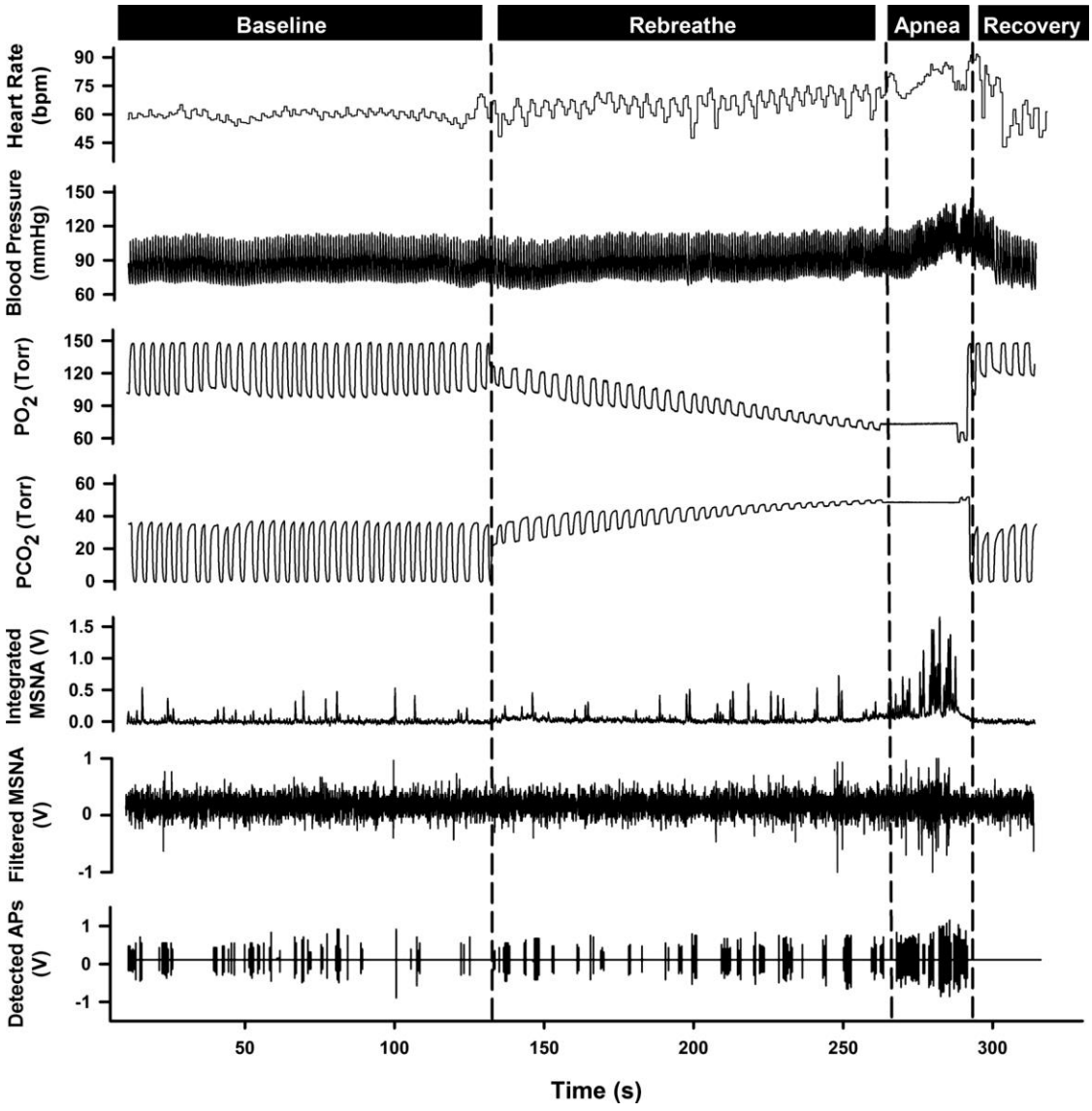

Figure 2.2: Representative sample of data from one subject collected at baseline, during rebreathe, maximal end-inspiratory apnea, and recovery.

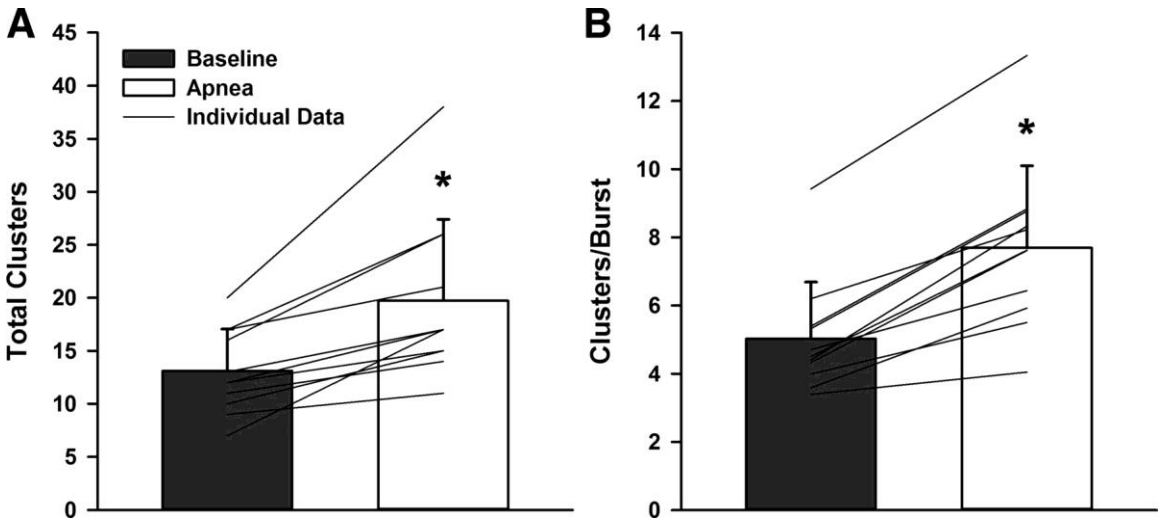

Figure 2.3: Total detected clusters (A) and active clusters/burst (B) at baseline and during maximal end-inspiratory apnea.

*Significantly different from baseline, $P < 0.001$.

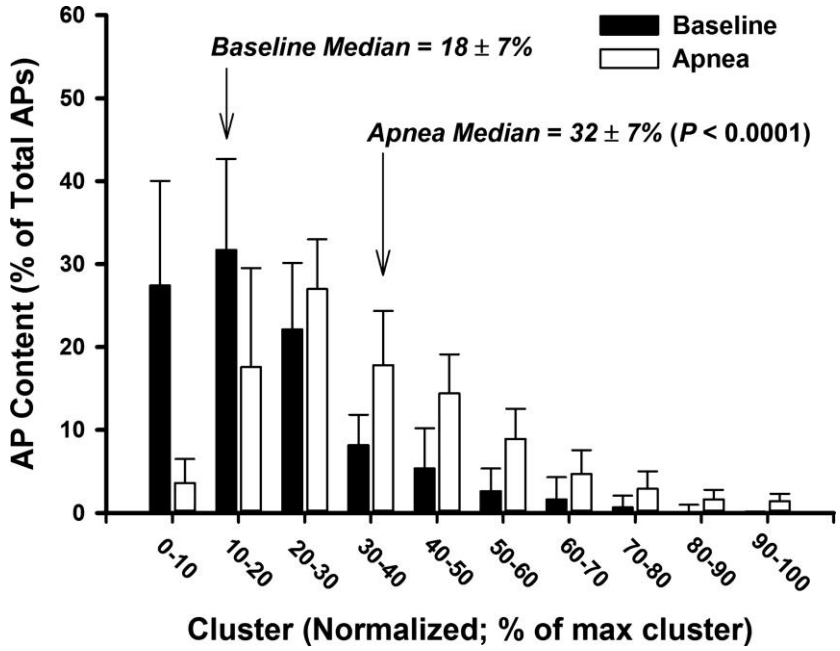

Figure 2.4: Histogram representing action potential (AP) content as a function of normalized cluster number at baseline and during maximal end-inspiratory apnea.

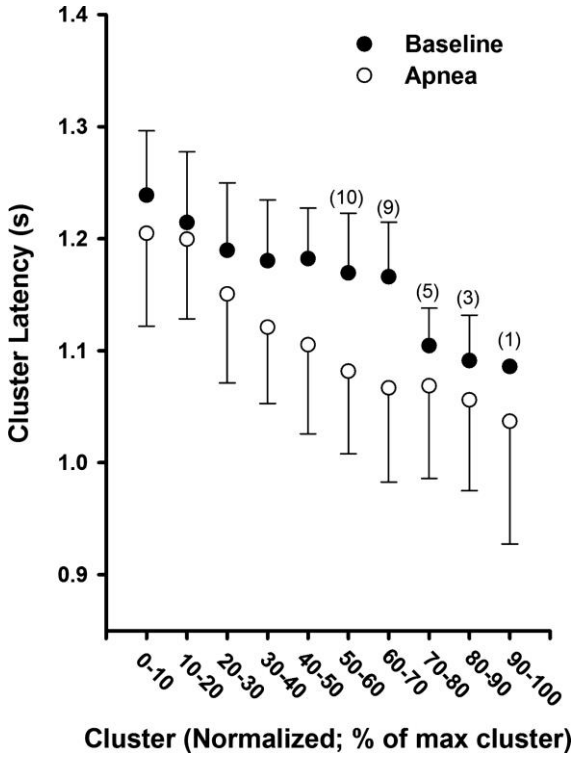

Figure 2.5: Mean action potential cluster latency across participants as a function of normalized cluster number at baseline and during maximal end-inspiratory apnea.

Sample size for clusters in which not all 11 subjects are included are indicated in parentheses. Sample sizes <11 at baseline represent subjects in whom these clusters were not present at baseline but were recruited during apnea.

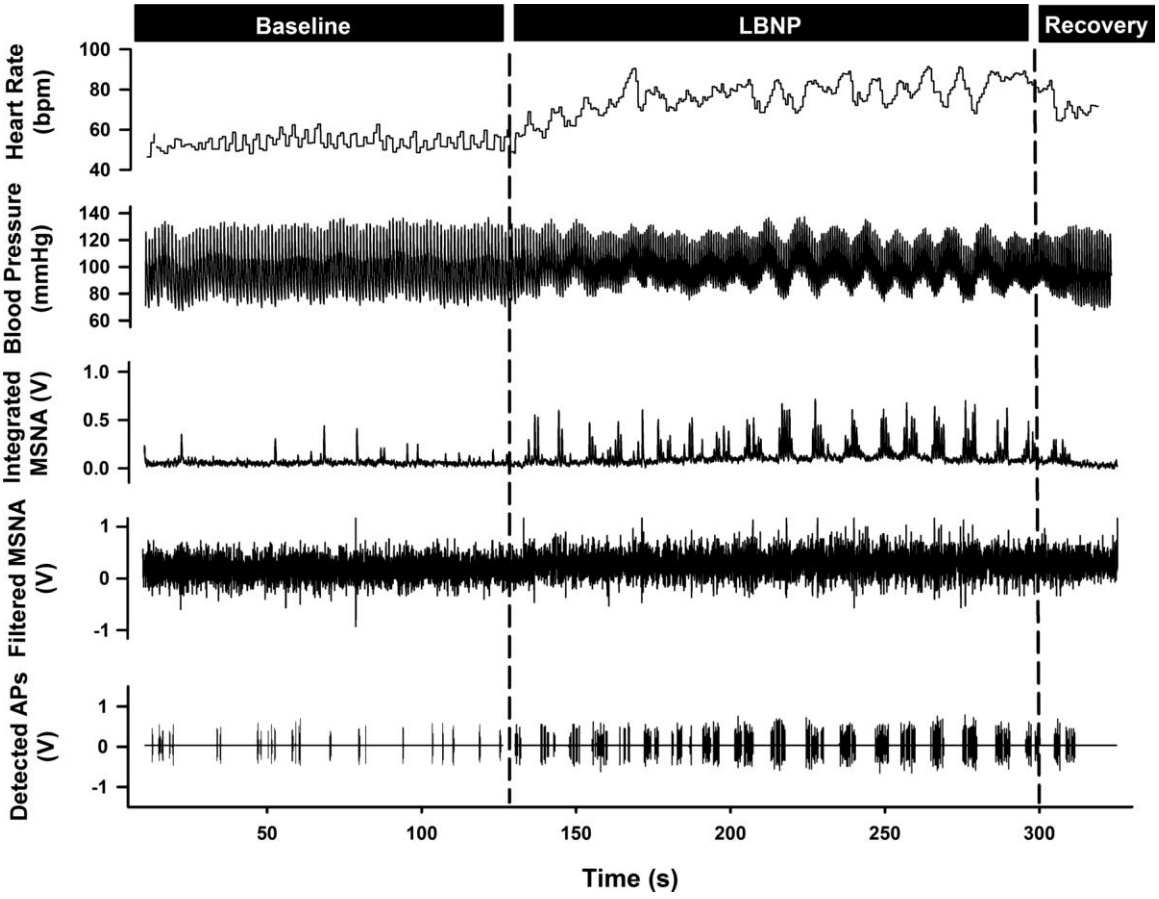

Figure 2.6: Representative sample of data from one subject collected at baseline and during −80 mmHg lower body negative pressure (LBNP) and recovery.

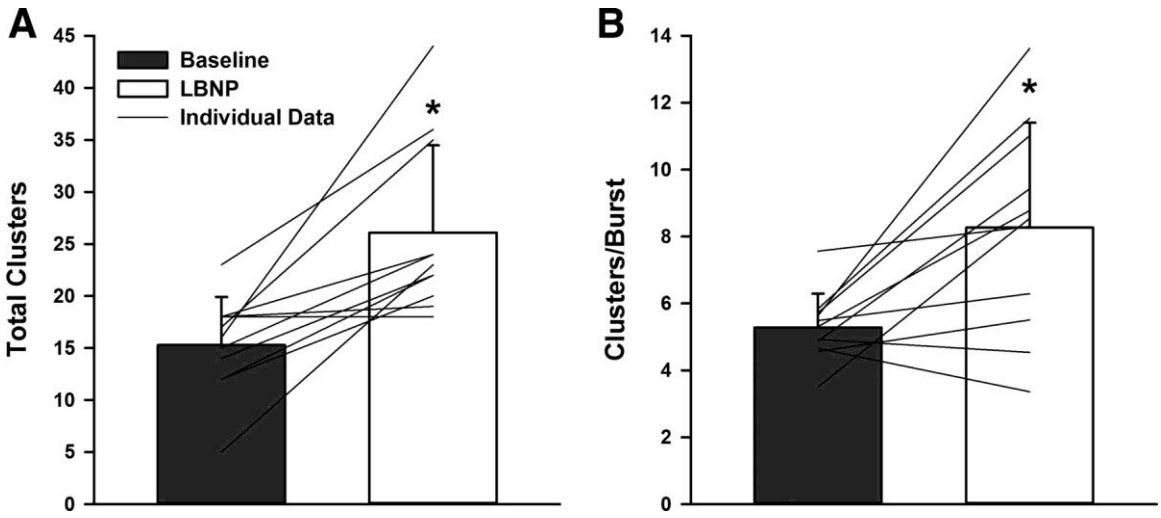

Figure 2.7: Total detected clusters (A) and active clusters/burst (B) at baseline and during −80 mmHg lower body negative pressure (LBNP).

*Significantly different from baseline, $P < 0.01$.

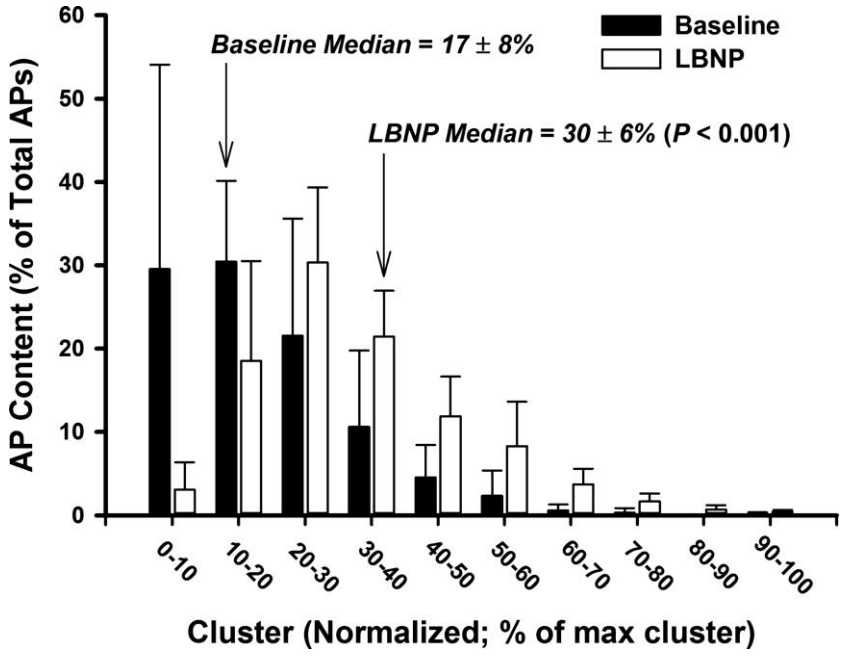

Figure 2.8: Histogram representing action potential (AP) content as a function of normalized cluster number at baseline and −80 mmHg lower body negative pressure (LBNP).

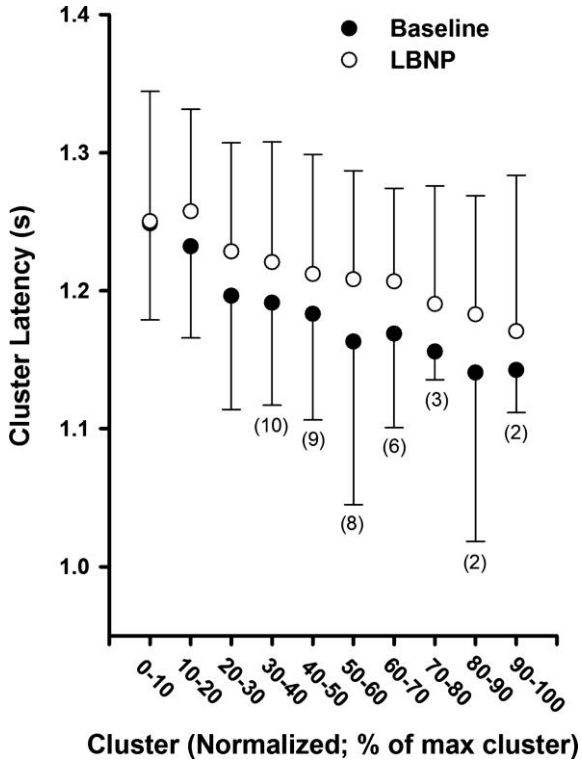

Figure 2.9: Mean action potential cluster latency across participants as a function of normalized cluster number at baseline and −80 mmHg lower body negative pressure (LBNP).

Sample size for clusters in which not all 11 subjects are included are indicated in parentheses. Sample sizes <11 at baseline represent subjects in whom these clusters were not present at baseline but were recruited during LBNP.

2.4 Discussion

The results of the current investigation reveal two novel findings which advance our understanding of the neural coding patterns employed within the sympathetic nervous system. First, we demonstrate the ability to recruit sub-populations of previously silent (i.e., not present at baseline), larger amplitude, and faster conducting sympathetic axons during periods of severe chemoreflex- and baroreflex-mediated sympathoexcitation. We interpret this to be reflective of a reflex-independent sympathetic neural recruitment strategy involving a latent sub-population of recruitable neurons that are reserved for periods of severe stress. Second, our results demonstrate the potential for reflex-specific changes in neural activation latency during periods of severe sympathetic stress. Specifically, the action potential cluster latency profile was shifted downwards during severe chemoreflex stress and upwards during severe baroreceptor unloading. Of note, the deflections in the cluster latency response curve were observed equally across all clusters, suggesting that this recruitment strategy was applied to all action potentials and does not reflect slower axonal conduction. Rather, this finding suggests variable synaptic delays as a second strategy to modify post-ganglionic sympathetic nerve activity. The combined data, observed in the same individuals, supports the idea that both synaptic delay variations and high-threshold sub-populations exist as recruitment strategies for post-ganglionic efferent sympathetic outflow.

To date, available information on neural recruitment strategies within the sympathetic nervous system has been largely inferred from the integrated neurogram. For example, an early observation that larger integrated bursts exhibit shorter reflex

latency led Wallin and colleagues to hypothesize that reductions in central synaptic delays or variations in central pathways may occur and/or that there may exist populations of latent sympathetic neurons with faster conduction velocities (Wallin *et al.* 1994). More specific positioning of higher impedance electrodes enabled Macefield and colleagues to isolate action potential discharge patterns of single sympathetic axons within human peripheral nerves (Macefield *et al.* 1994). This approach revealed that, when active, individual neurons generally fire only once per integrated burst (Macefield *et al.* 1994), with the probability of multiple within-burst firing increasing during periods of high sympathetic drive (Macefield & Wallin, 1999; Elam *et al.* 2002). Results from these studies led to the idea that increased firing of already-active neurons was an important mechanism by which burst strength is elevated during periods of sympathetic stress (Macefield & Wallin, 1999).

Results from the current investigation, which studied action potential recruitment from the multi-unit signal in both chemoreflex and baroreflex scenarios in the same individuals, validate and extend these previous observations and provide further insight into sympathetic neuronal recruitment strategies. First, evidence was provided that sub-populations of previously dormant, larger amplitude, and faster conducting sympathetic neurons are recruited during periods of high stress. Importantly, the present data suggest that this appears to be a reflex-independent strategy used within the sympathetic nervous system. These observations support the earlier report that, in addition to higher firing rates of axons already recruited during baseline, severe chemoreflex stress elicits activation of latent, higher-threshold, and faster conducting (therefore, larger diameter) axons (Steinback *et al.* 2010). This

discharge pattern was not observed during preliminary results using modest levels of simulated orthostatic stress (i.e., −60 mmHg LBNP), whereby higher frequency firing of action potential clusters already recruited at baseline was the primary determinant of elevated efferent activity, with about 30% of participants demonstrating recruitment of new, larger action potentials (Salmanpour *et al.* 2011*a*). Whereas orthostatic tolerance or reserve varies across individuals, it remains likely that the threshold for recruitment of this sub-population will also vary across individuals and with the level of stress. Our current data indicate that more severe baroreceptor unloading (−80 mmHg LBNP) can elicit recruitment of these latent axons. As such, it appears that during moderate levels of stress, sympathetic activity is elevated through the multiple firing of already-active neurons as previously hypothesized (Macefield & Wallin, 1999), whereas severe stress stimulates the recruitment of latent sub-populations of larger axons to achieve the high levels of sympathetic activity necessary. We therefore suggest that there may exist a type of sympathetic reserve, whereby latent sub-populations of larger diameter, faster conducting sympathetic neurons are reserved for severe sympathetic stress.

As previously established (Steinback *et al.* 2010; Salmanpour *et al.* 2011*a*), and in support of observations from integrated MSNA analyses (Wallin *et al.* 1994), action potential cluster latency was inversely related to action potential cluster amplitude, whereby larger amplitude neurons exhibited shorter reflex latencies. This pattern was observed both at baseline and during subsequent chemoreflex- and baroreflex-induced sympathoexcitation. Interestingly, during severe chemoreflex stimulation, there was an acute downward shift in the latency-size profile of all corresponding action potential clusters (~ 53 ms; see Figure 2.5), such that the latency of all action potentials with

similar peak-to-peak amplitudes was reduced during severe chemoreflex activation. This systemic downward shift in the cluster latency profile was also demonstrated during the Valsalva maneuver (Salmanpour *et al.* 2011*b*), and is consistent with observed changes in mean reflex burst latency seen during several sympathoexcitatory maneuvers (Fagius *et al.* 1987). The common pattern of this downward shift in latency during both end-inspiratory apnea and Valsalva maneuver suggests a common mechanism may be operating. Specifically, each maneuver elevates intrathoracic pressure, thereby reducing venous return. Each also expresses a particular perceptual stress related to individual volitional tolerance for the maneuver. While these two observations are from different studies, they suggest a cardiac stimulus may have contributed to the apneic outcomes of the current study. Alternatively, variations in action potential latency during chemoreflex stress may be due to direct glutaminergic activation of the rostral ventrolateral medulla from the nucleus tractus solitarius (Koshiya *et al.* 1993), and/or faster conduction velocities within spinal descending pathways specific to chemoreflex stimulation (Jänig & Szulczyk, 1979).

Conversely, we demonstrate that during −80 mmHg LBNP, the latency-size profile of all corresponding action potential clusters was shifted upward (~31 ms; see Figure 2.9), indicating that similarly sized post-ganglionic neurons were recruited with a slightly slower latency during severe baroreceptor unloading, a pattern consistent with that seen previously in a preliminary manner during −60 mmHg LBNP (Salmanpour *et al.* 2011*a*). These data indicate that the sympathetic nervous system displays a unique ability to modify acutely the reflex latency of all action potentials during severe orthostatic stress. In as much as the conduction velocity of given axon is relatively

fixed, these modifications in latency indicate malleability in the synaptic delays between the brainstem and the recording electrode. One limitation of the multi-unit recording approach is the inability to ensure that action potentials of the same size are the same neurons with varying latencies during severe sympathoexcitation. However, given the anatomical bundled distribution of axons in peripheral nerves (Tompkins *et al.* 2013), it is unlikely that the recordings reflect completely different populations of neurons. Regardless, all that can be concluded is that action potentials with similar peak-to-peak amplitudes exhibit altered reflex latencies during chemoreflex- and baroreflex-mediated sympathetic stress.

A potential limitation of the present study is that larger amplitude action potentials observed during periods of severe sympathetic stress could theoretically be the result of summation of two smaller-sized neurons firing concurrently, thereby eliciting an artificially large action potential (Spickler & Kezdi, 1969; Andresen & Yang, 1989). However, the likelihood for action potential summation is very low [~ 0.3%; (Salmanpour *et al.* 2010)]. Further, such occurrences can be detected if the resulting action potential is large and does not fit the latency-size pattern (Clamann & Henneman, 1976) so that it is automatically removed from the analysis. Furthermore, the mean signal-to-noise ratio of 4.15 ± 0.5 in the current data sets are expected to produce a correct detection rate of >90% and false detection rate of <3% (Salmanpour *et al.* 2010). Another consideration is that larger amplitude action potentials could be the result of firing of neurons in close proximity to the recording electrode tip. However, the consistent pattern that these larger action potentials reflect shorter latencies argues against that possibility. Finally, results from our test-retest repeatability

analysis, although completed in a small sample of men (n = 5), suggest that indices of action potential detection are reproducible across test dates. If larger amplitude action potentials were the result of summation or proximity to the recording electrode, one would expect action potential indices to differ in repeated test dates, when the physical relationship between the microelectrode placement and sympathetic axons is likely to differ.

Perspectives and Significance

The current data indicate the existence of neural coding patterns within the autonomic nervous system and enhances our understanding of how the sympathetic nervous system is activated during reflex-mediated stress. Specifically, there appears a fixed reflex-independent recruitment strategy, whereby the large increases in sympathetic outflow during severe chemoreflex and baroreflex stress are the result of recruitment of latent sub-populations of larger, faster conducting sympathetic neurons. In addition, it appears as though the sympathetic nervous system is able to acutely modify synaptic delays or central processing times and/or pathways, such that reflex latency of all action potentials are altered during severe sympathetic stress. Taken together, the data provide a new perspective on sympathetic stress responses. This new understanding opens opportunity to study how such axonal recruitment strategies may affect neurotransmitter discharge and overall vascular responses, as well as the effect of age and disease on the patterning of efferent sympathetic outflow.

2.5 References

Altman DG & Bland JM (1983). Measurement in medicine: the analysis of method comparison studies. *Statistician* **32,** 307-317.

Andresen MC & Yang M (1989). Interaction among unitary spike trains: implications for whole nerve measurements. *Am J Physiol Regul Integr Comp Physiol* **256,** R997-R1004.

Barman SM & Gebber GL (2000). "Rapid" rhythmic discharges of sympathetic nerves: sources, mechanisms of generation, and physiological relevance. *J Biol Rhythms* **15,** 365-379.

Bland JM & Altman DG (1986). Statistical methods for assessing agreement between two methods of clinical measurement. *Lancet* **327,** 307-310.

Clamann HP & Henneman E (1976). Electrical measurement of axon diameter and its use in relating motoneuron size to critical firing level. *J Neurophysiol* **39,** 844-851.

Cohen J (1988). Statistical power analysis for the behavioural sciences. Lawrence Erlbaum Associates, New Jersey.

Delius W, Hagbarth KE, Hongell A & Wallin BG (1972*a*). Manoeuvres affecting sympathetic outflow in human muscle nerves. *Acta Physiol Scand* **84,** 82-94.

Delius W, Hagbarth KE, Hongell A & Wallin BG (1972*b*). General characteristics of sympathetic activity in human muscle nerves. *Acta Physiol Scand* **84,** 65-81.

Elam M, McKenzie D & Macefield VG (2002). Mechanisms of sympathoexcitation: single-unit analysis of muscle vasoconstrictor neurons in awake OSAS subjects. *J Appl Physiol* **93,** 297-303.

Fagius J & Karhuvaara S (1989). Sympathetic activity and blood pressure increases with bladder distension in humans. *Hypertension* **14,** 511-517.

Fagius J, Sundlöf G & Wallin BG (1987). Variation of sympathetic reflex latency in man. *J Auton Nerv Syst* **21,** 157-165.

Hagbarth KE & Vallbo AB (1968). Pulse and respiratory grouping of sympathetic impulses in human muscle nerves. *Acta Physiol Scand* **74,** 96-108.

Henneman E, Somjen G & Carpenter DO (1965). Excitability and inhibitibility of motoneurons of different sizes. *J Neurophysiol* **28,** 599-620.

Jänig W & McLachlan EM (1992). Characteristics of function-specific pathways in the sympathetic nervous system. *Trends Neurosci* **15,** 475-481.

Jänig W & Szulczyk P (1979). Conduction velocity in spinal descending pathways of baro- and chemoreceptor reflex. *J Auton Nerv Syst* **1,** 149-160.

Johnstone IM & Silverman BW (1997). Wavelet threshold estimators for data with correlated noise. *J R Statist Soc* **59,** 319-351.

Koshiya N, Huangfu D & Guyenet PG (1993). Ventrolateral medulla and sympathetic chemoreflex in the rat. *Brain Res* **609,** 174-184.

Ludbrook J (1997). Special article comparing methods of measurement. *Clin Exp Pharmacol Physiol* **24,** 193-203.

Macefield VG & Wallin BG (1999). Firing properties of single vasoconstrictor neurones in human subjects with high levels of muscle sympathetic activity. *J Physiol* **516,** 293-301.

Macefield VG, Wallin BG & Vallbo AB (1994). The discharge behaviour of single vasoconstrictor motoneurones in human muscle nerves. *J Physiol* **481,** 799-809.

McAllen R & Trevaks D (2003). Are pre-ganglionic neurones recruited in a set order? *Acta Physiol Scand* **177,** 219-225.

Ninomiya I, Malpas SC, Matsukawa K, Shindo T & Akiyama T (1993). The amplitude of synchronized cardiac sympathetic nerve activity reflects the number of activated pre- and postganglionic fibers in anesthetized cats. *J Auton Nerv Syst* **45,** 139-147.

Salmanpour A, Brown LJ & Shoemaker JK (2010). Spike detection in human muscle sympathetic nerve activity using a matched wavelet approach. *J Neurosci Methods* **193,** 343-355.

Salmanpour A, Brown LJ, Steinback CD, Usselman CW, Goswami R & Shoemaker JK (2011*a*). Relationship between size and latency of action potentials in human muscle sympathetic nerve activity. *J Neurophysiol* **105,** 2830-2842.

Salmanpour A, Frances MF, Goswami R & Shoemaker JK (2011*b*). Sympathetic neural recruitment patterns during the Valsalva maneuver. *Conf Proc IEEE Eng Med Biol Soc* **2011,** 6951-6954.

Scott DW (1979). On optimal and data-based histograms. *Biometrika* **66,** 605-610.

Spickler JW & Kezdi P (1969). Probability of spike summations in baroreceptor electroneurograms. *J Appl Physiol* **27,** 919-922.

Steinback CD, Salmanpour A, Breskovic T, Dujic Z & Shoemaker JK (2010). Sympathetic neural activation: an ordered affair. *J Physiol* **588,** 4825-4836.

Tompkins RP, Melling CW, Wilson TD, Bates BD & Shoemaker JK (2013). Arrangement of sympathetic fibers within the human common peroneal nerve: implications for microneurography. *J Appl Physiol* **115,** 1553-1561.

Usselman CW, Gimon TI, Nielson CA, Luchyshyn TA, Coverdale NS, Van Uum SHM & Shoemaker JK (2015). Menstrual cycle and sex effects on sympathetic responses to acute chemoreflex stress. *Am J Physiol Heart Circ Physiol* **308,** H664-H671.

Wallin BG, Burke D & Gandevia S (1994). Coupling between variations in strength and baroreflex latency of sympathetic discharges in human muscle nerves. *J Physiol* **474,** 331-338.

Chapter 3

3 Central vs. peripheral determinants of sympathetic neural recruitment: insights from static handgrip exercise and postexercise circulatory occlusion

(Published in Am J Physiol Integr Comp Physiol 311: R1013-R1021, 2016)

3.1 Introduction

Neural coding patterns represent a fundamental feature in the exchange and processing of neural information. Recently, we have confirmed that neural coding principals operate within the sympathetic nervous system (Steinback *et al.* 2010; Breskovic *et al.* 2011; Salmanpour *et al.* 2011*a*,*b*; Badrov *et al.* 2015; Badrov *et al.* 2016). Specifically, increases in muscle sympathetic nerve traffic in response to acute physiological stress are the result of increased firing of low-threshold axons (i.e., rate coding), as well as the recruitment of latent sub-populations of larger-sized axons that are otherwise silent at baseline (i.e., population coding) (Steinback *et al.* 2010; Breskovic *et al.* 2011; Salmanpour *et al.* 2011*a*; Badrov *et al.* 2015; Badrov *et al.* 2016). Furthermore, it appears that synaptic delay variations exist as a third strategy to alter autonomic outflow (Salmanpour *et al.* 2011*b*; Badrov *et al.* 2015; Badrov *et al.* 2016). These strategies have been confirmed in two fundamental reflexes; that is, the arterial baroreflex, studied during −80 mmHg lower body negative pressure (LBNP) (Salmanpour *et al.* 2011*a*; Badrov *et al.* 2015) and the Valsalva maneuver (Salmanpour *et al.* 2011*b*), as well as the arterial chemoreflex, as inferred during maximal voluntary apnea (Steinback *et al.* 2010; Breskovic *et al.* 2011; Badrov *et al.* 2015; Badrov *et al.* 2016). However, a persistent question remains, particularly with the apnea response, as to whether or not these recruitment strategies are restricted to the perception of effort

during severe stress scenarios (i.e., a central command phenomenon), or to the severe reflex stress alone (i.e., a peripheral-reflex mechanism). Evidence from the Valsalva maneuver and voluntary apnea data do not exclude a role for a central perception of effort determinant, whereas the LBNP data suggest a dominant role for peripheral-reflex mechanisms. Additionally, one feature that may especially relate to central versus peripheral features is the ability to acutely modify reflex latency. That is, compared to resting levels, neural activation latency was reduced during voluntary apnea (Badrov *et al.* 2015; Badrov *et al.* 2016) and the Valsalva maneuver (Salmanpour *et al.* 2011*b*), but increased during LBNP-induced baroreceptor unloading (Badrov *et al.* 2015). As such, the exact central versus peripheral mechanisms of these sympathetic neural recruitment strategies remain to be fully elucidated.

The homeostatic response to fatiguing exercise represents a unique reflex in which the central and peripheral elements of the reflex can be studied separately as they develop over time. Specifically, alterations in efferent neural outflow during exercise are mediated through a highly coordinated and integrative system of reflexes involving feed-forward signals emanating from higher brain centres (i.e., central command) (Johansson, 1895; Krogh & Lindhard, 1913; Goodwin *et al.* 1972), as well as peripheral feedback from type III and IV muscle sensory afferents within active skeletal muscle (i.e., exercise pressor reflex) (Alam & Smirk, 1937; McCloskey & Mitchell, 1972; Kaufman *et al.* 1983; Mitchell *et al.* 1983). The exercise pressor reflex elicits large increases in muscle sympathetic nerve activity (MSNA) (Mark *et al.* 1985; Seals *et al.* 1988; Victor *et al.* 1988; Wallin *et al.* 1989; Saito *et al.* 1990; Seals & Victor, 1991; Shoemaker *et al.* 2007), albeit after a workload-dependent delay of approximately 30 to

60 seconds (Mark *et al.* 1985). Sympathetic activity remains elevated during post-exercise circulatory occlusion (PECO), which suggests that the mechanism of activation relates to muscle metabolism and a dominant metaboreflex component. Furthermore, a marked increase in integrated sympathetic burst size characterizes this reflex, most likely reflective of increases in the number (Ninomiya *et al.* 1993) and/or size (Salmanpour *et al.* 2011*a*) of action potentials (AP) firing more or less at the same time. Recently, Murai et al. (2006) examined the firing patterns of a single axon that was present at baseline and sustained during static handgrip (SHG) exercise and found elevations in total sympathetic activity, but no change in the probability of multiple within-burst firing of that axon. Combined, the observations of no change in the probability of a single axon firing, but the need for additional and/or larger axons to account for larger bursts, suggests that latent axons are recruited in the large sympathetic response to fatiguing exercise. Thus, fatiguing exercise and the muscle metaboreflex represents a unique model to study the central versus peripheral features of sympathetic neural recruitment, as it allows the opportunity to isolate the peripheral-reflex component from the central component (Alam & Smirk, 1937).

Therefore, to study the varying roles played by central versus peripheral elements in the neural coding strategies used by the sympathetic nervous system during acute physiological stress, we used a multi-unit AP approach to examine sympathetic outflow patterns during fatiguing SHG exercise and a period of PECO. The latter was designed to maintain and isolate the muscle metaboreflex (i.e., peripheral-reflex component) from the central command features of the reflex (Alam & Smirk, 1937).

3.2 Methods

3.2.1 Participants

Six young healthy, normotensive males (25 ± 3 yrs, 179 ± 7 cm, 82 ± 6 kg; body mass index = 26 ± 2 kg/m^2) were studied after providing informed written consent. Participants were recreationally active, non-smokers, and otherwise healthy with no history of cardiovascular or respiratory disease. The study was approved by the Health Sciences Research Ethics Board at Western University in London, Canada.

3.2.2 Experimental Protocol

Participants were tested following a 3-hour fast, a 12-hour abstinence from caffeinated products and alcohol, and a 24-hour abstinence from strenuous exercise. Testing was completed in the supine position. Participants performed two maximal voluntary contractions (MVCs) with their non-dominant hand (left hand in all participants), and the largest of the two was used to calculate relative handgrip intensity for the ensuing SHG protocol. Following a 3-minute baseline rest period, participants performed SHG exercise for five minutes at 20% MVC, which was followed immediately by PECO for three minutes. PECO was initiated approximately five seconds prior to exercise completion by rapidly inflating a pneumatic cuff (Hokanson SC12D, D.E. Hokanson, Bellevue, WA) on the upper exercised arm to suprasystolic levels (~200 mmHg). Throughout SHG, visual feedback of exercise intensity was provided to aid participants in the maintenance of target force. Upon exercise completion, and before PECO onset, participants assessed their level of perceived exertion using the 20-point Borg Rating of Perceived Exertion Scale (Borg, 1970).

3.2.3 Experimental Measures

Sympathetic neural recordings were obtained in the right peroneal nerve using microneurography (Hagbarth & Vallbo, 1968) (662C-3; Bioengineering of University of Iowa, Iowa City, IA). The methodology used in our laboratory have been described previously in detail (Steinback *et al.* 2010; Salmanpour *et al.* 2011*a*; Badrov *et al.* 2015). Heart rate (HR) was determined throughout the study protocol from a standard three-lead electrocardiogram. Mean arterial pressure (MAP) was obtained on a beat-to-beat basis using finger photoplethysmography (Finometer; Finapres Medical Systems, Amsterdam, The Netherlands) on the nonexercised hand, which was calibrated to manual sphygmomanometry values. The Finometer Modelflow algorithm was used to calculate stroke volume (SV) and cardiac output (CO), and total peripheral resistance (TPR) was calculated as MAP divided by CO. Data were collected using LabChart7 and PowerLab (ADInstruments, Colorado Springs, CO).

3.2.4 Data Analysis

Data were analyzed for the 3-minute baseline period, each minute of the 5-minute SHG exercise, and for the 3-minute PECO period. Sympathetic bursts were identified from the integrated MSNA neurogram if: 1) they exhibited pulse-synchrony; 2) they had a signal-to-noise ratio of at least 2:1 with respect to the previous period of neural silence between bursts; 3) they presented with characteristic rising and falling slopes; and 4) APs were visible in the corresponding raw and filtered neurograms. The level of integrated sympathetic activity was assessed using burst frequency (bursts/min) and burst incidence (bursts/100 heart beats; hb). Furthermore, burst amplitude, which reflects both the size (Salmanpour *et al.* 2011*a*) and number (Ninomiya *et al.* 1993) of

APs recruited within each burst, was assessed. However, due to the potential influence of microelectrode placement on the amplitude of the integrated signal (Vallbo *et al.* 1979; Tompkins *et al.* 2013), burst amplitude was normalized within each individual to the largest burst at baseline, which was assigned a value of 100 arbitrary units (AU). Finally, total MSNA (product of burst frequency and normalized burst amplitude) was determined.

Sympathetic APs were extracted from the filtered raw MSNA signal using wavelet-based methodology, as first used by others (Diedrich *et al.* 2003; Brychta *et al.* 2007), and modified in our laboratory (Salmanpour *et al.* 2010). Briefly, a continuous wavelet transform with a 'mother wavelet' (adapted from actual physiological recordings of post-ganglionic sympathetic APs) was applied to the filtered raw MSNA signal to extract sympathetic APs at their point of incidence. Extracted APs were ordered based on their peak-to-peak amplitude, and histogram analysis was conducted to separate APs into 'clusters' (i.e., bins of similarly-sized APs) (Scott, 1979). The AP detection, extraction, and classification process, as well as the reliability and repeatability of our AP detection technique has been described previously in detail, and readers are directed to this previous work (Salmanpour *et al.* 2010; Steinback *et al.* 2010; Badrov *et al.* 2015). Next, within participants, cluster characteristics were normalized to ensure that bin width, maximum bin center, and the total number of bins would be identical across conditions (i.e., baseline to SHG to PECO). This normalization procedure ensured that corresponding clusters across conditions contain APs with similar peak-to-peak amplitudes. Therefore, an increase in total clusters during SHG or PECO represents recruitment of sub-populations of previously silent,

larger-sized AP families that were not present at baseline. Finally, the average signal-to-noise ratio in the current study was 4.4 ± 0.6, and based on previous validation analysis of our analytical technique (Salmanpour *et al.* 2010), this is expected to produce a correct detection rate of >90% and a false positive rate of <3%.

Patterns of AP activity were expressed using AP frequency (APs/min). Recruitment of sympathetic APs was quantified using the mean AP content per integrated sympathetic burst (APs/burst), the number of total AP clusters, and the number of active AP clusters per integrated sympathetic burst (clusters/burst). AP cluster latency was calculated as the mean AP latency of all APs present within that respective cluster, which was measured as the time delay between the R-wave of the preceding cardiac cycle and the negative peak of the AP waveform. As the number of total AP clusters varied between participants, the number of total clusters was normalized to 10 clusters, each containing 10% ranges of the largest detected cluster, which was given a value of 100% (i.e., 0-10%, 10-20%, etc.), when assessing the AP cluster size-latency relationship (Badrov *et al.* 2015; Badrov *et al.* 2016).

3.2.5 Statistical Analysis

One-way repeated measures ANOVAs assessed the effect of time (i.e., baseline to SHG to PECO) on each hemodynamic, integrated MSNA, and AP variable (SigmaPlot 12.0; Systat Software Inc., San Jose, CA). Data were tested for normal distribution using Shapiro-Wilk tests. Non-normally distributed data were assessed using Friedman repeated measures ANOVAs on ranks. Significant main effects were assessed using Tukey's post-hoc analysis. Statistical significance was set at $P < 0.05$ and all data are presented as mean ± SD.

3.3 Results

Figure 3.1 displays original recordings of HR, MAP, integrated MSNA, filtered raw MSNA, and detected APs from one participant. On average, SHG exercise was completed at 20 ± 1% MVC and participants reported a Borg scale rating of 17 ± 2 at end exercise.

Figure 3.2 displays the mean and individual hemodynamic responses to SHG and PECO and Table 2.1 provides the delta values on going from baseline to each period of the SHG and PECO protocol. At baseline, MAP was 94 ± 7 mmHg, HR was 62 ± 5 beats/min, SV was 106 ± 17 mL, CO was 6.7 ± 1.4 L/min, and TPR was 15 ± 3 mmHg/L/min. When compared with baseline, MAP was increased by minute two of SHG, and remained elevated throughout the duration of exercise and PECO (all $P < 0.01$). HR was elevated during the entire SHG period and remained elevated during PECO (all $P < 0.001$), but at levels that were less than those observed during minutes three to five of SHG (all $P < 0.05$). When compared with baseline, SV was unchanged during SHG and PECO (all $P > 0.05$). CO was elevated throughout SHG and PECO (all $P < 0.05$). Finally, compared with baseline, TPR was reduced throughout SHG and PECO (all $P < 0.05$).

Figure 3.3 illustrates the mean and individual integrated MSNA responses to SHG and PECO and Table 3.2 provides the delta values. At baseline, burst frequency was 18 ± 13 bursts/min, burst incidence was 28 ± 20 bursts/100 hb, burst amplitude was 46 ± 13 AU, and total MSNA was 742 ± 519 AU/min. When compared with baseline, burst frequency and burst incidence were increased by minute three of SHG exercise and remained elevated for the duration of exercise and PECO (all $P < 0.05$).

Furthermore, burst amplitude increased above baseline by minute four of SHG and remained elevated at minute five and during PECO (all $P < 0.01$). Finally, total MSNA increased by minute three of SHG, remaining elevated above baseline levels for the duration of exercise and PECO (all $P < 0.05$).

Figure 3.4 outlines the mean and individual AP responses to SHG and PECO and Table 3.2 provides the delta values. At baseline, AP frequency was 223 ± 271 APs/min, the mean AP content per burst was 10 ± 5 APs/burst, the number of active clusters per burst was 5 ± 2, and the number of total clusters was 14 ± 6. When compared with baseline, AP frequency increased by minute three of SHG and remained elevated throughout SHG and PECO (all $P < 0.05$). The mean AP content per integrated sympathetic burst increased by minute four of SHG and remained elevated at minute five and PECO (all $P < 0.05$). Similarly, the number of active clusters per integrated burst was elevated by minute four and stayed elevated throughout the remainder of SHG and PECO (all $P < 0.01$). Finally, compared to baseline, the number of total AP clusters was increased at minutes four and five of SHG, and remained elevated during PECO (all $P < 0.01$).

At baseline, AP cluster latency decreased as a function of normalized cluster number (i.e., as the peak-to-peak AP cluster amplitude increased), such that larger-sized APs exhibited shorter reflex latency. The mean response was fitted using an exponential function model ($R^2 = 0.73$; $P < 0.001$). The same pattern was observed throughout SHG exercise (HG1: $R^2 = 0.92$; HG2: $R^2 = 0.93$; HG3: $R^2 = 0.83$; HG4: $R^2 = 0.69$; HG5: $R^2 = 0.91$; all $P < 0.01$) and PECO ($R^2 = 0.65$; $P < 0.01$). When compared with baseline, the AP cluster size-latency profile for corresponding clusters was not shifted significantly

upward or downward during the first three minutes of SHG exercise (HG1: mean = 8 ± 16 ms, range −12 to 28 ms; HG2: mean = 4 ± 17 ms, range −17 to 27 ms; HG3: mean = −11 ± 18 ms, range −38 to 12 ms; all $P > 0.05$). However, compared with baseline, the AP cluster-size latency profile was shifted downward for every corresponding cluster during minutes four (mean = −32 ± 22 ms, range −5 to −61 ms; $P < 0.05$) and five (mean = −49 ± 17 ms, range −27 to −77 ms; $P < 0.05$; Figure 3.5) of SHG exercise, such that all similarly sized APs were recruited earlier during SHG. During PECO, the AP cluster size-latency profile was not different than baseline levels (mean = −9 ± 12 ms, range −25 to 9 ms; $P > 0.05$).

Table 3.1: Hemodynamic responses to SHG and PECO

	Static Handgrip					PECO
	HG1	HG2	HG3	HG4	HG5	
Δ **MAP** (mmHg)	2±1	5±2*	7±4*	10±5*	13±7*	7±4*
Δ **HR** (beats/min)	6±3*	10±4*	13±3*	16±3*	19±6*	7±2*
Δ **SV** (mL)	−1±2	−1±2	−1±4	0±6	−1±9	7±6
Δ **CO** (L/min)	0.6±0.5*	1.0±0.5*	1.3±0.5*	1.7±0.8*	1.9±1.2*	1.2±0.6*
Δ **TPR** (mmHg/L/min)	−0.8±0.7*	−1.2±0.5*	−1.4±0.5*	−1.5±0.5*	−1.2±1.4*	−1.3±0.6*

Values are mean ± SD. SHG, static handgrip; PECO, post-exercise circulatory occlusion; HG, handgrip; MAP, mean arterial pressure; HR, heart rate; SV, stroke volume; CO, cardiac output; TPR, total peripheral resistance. *Significantly different from baseline, $P < 0.05$.

Table 3.2: Integrated MSNA and action potential responses to SHG and PECO

	Static Handgrip					PECO
	HG1	HG2	HG3	HG4	HG5	
Integrated MSNA						
Δ **BF** (bursts/min)	0±5	5±6	9±5*	12±6*	14±8*	8±9*
Δ **BI** (bursts/100 hb)	−3±6	2±6	7±5*	9±7*	10±10*	9±12*
Δ **BA** (AU)	1±7	8±3	9±7	12±8*	23±8*	15±8*
Δ **Total MSNA** (AU/min)	64±248	412±407*	724±496*	948±489*	1407±786*	814±646*
AP Indices						
Δ **APs/min**	44±92	139±187*	197±201*	252±203*	318±215*	195±296*
Δ **APs/Burst**	1±1	2±2	3±3	4±2*	6±4*	4±4*
Δ **Clusters/Burst**	0.7±0.4	0.8±0.7	1.2±0.8	1.4±0.7*	1.9±1.3*	1.3±1.0*
Δ **Total Clusters**	0±3	1±3	2±4	5±5*	6±3*	7±5*

Values are mean ± SD. MSNA, muscle sympathetic nerve activity; SHG, static handgrip; PECO, post-exercise circulatory occlusion; HG, handgrip; BF, burst frequency; BI, burst incidence; BA, burst amplitude; AU, arbitrary units; AP, action potential. *Significantly different from baseline, $P < 0.05$.

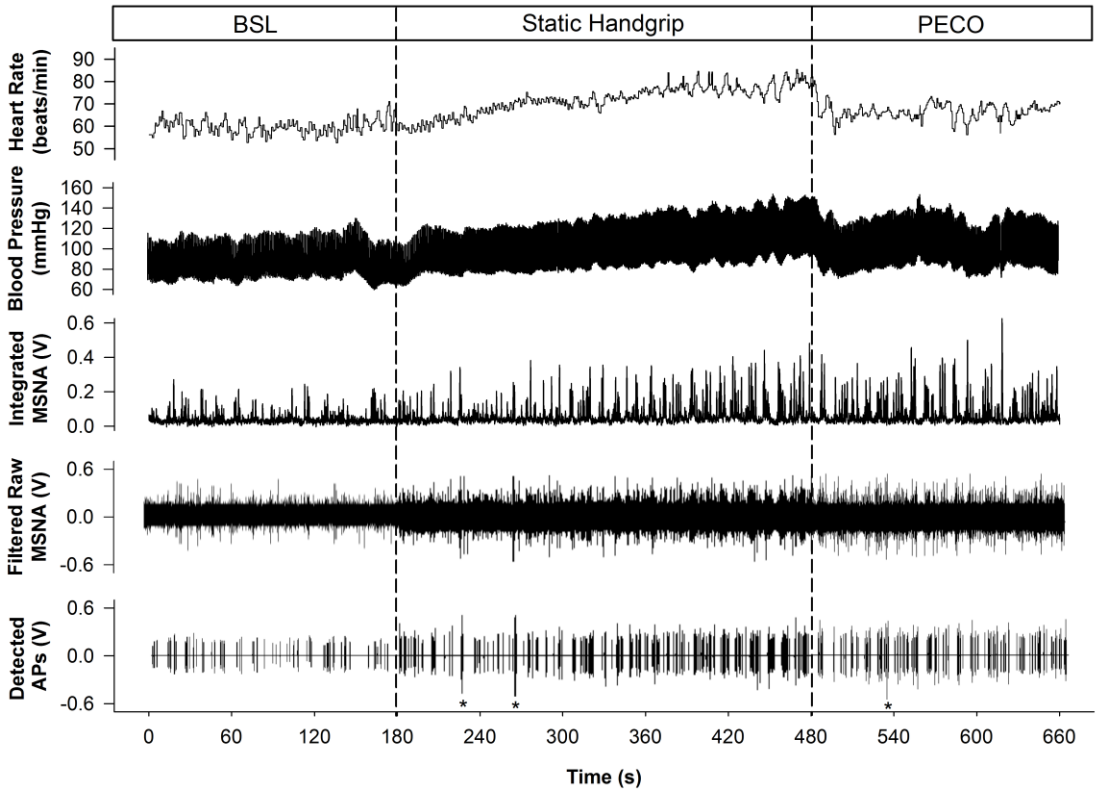

Figure 3.1: Representative sample of data collected from one subject at baseline (BSL) and during static handgrip and postexercise circulatory occlusion (PECO).

HR, heart rate; BP, blood pressure; MSNA, muscle sympathetic nerve activity; AP, action potential. *Denotes noise spikes not included in analysis.

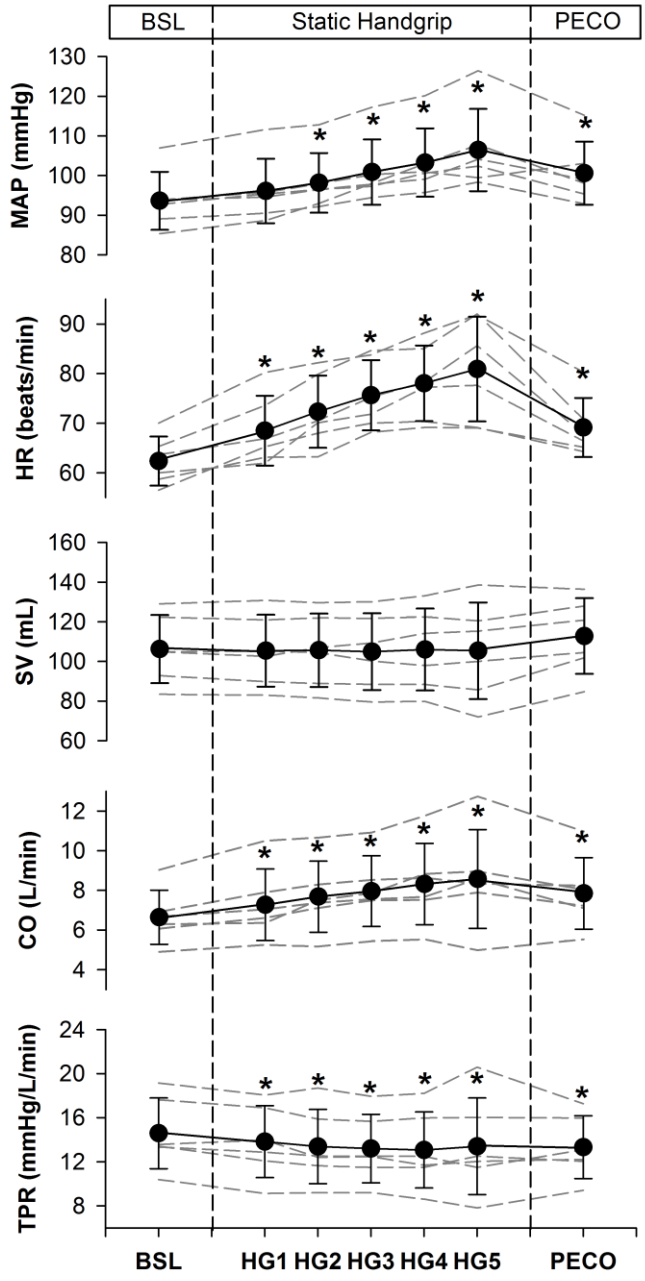

Figure 3.2: Hemodynamic responses to static handgrip (HG) and postexercise circulatory occlusion (PECO).

Dashed lines represent individual data. Values are mean ± SD. MAP, mean arterial pressure; HR, heart rate; SV, stroke volume; CO, cardiac output; TPR, total peripheral resistance. *$P < 0.05$, significantly different from baseline (BSL).

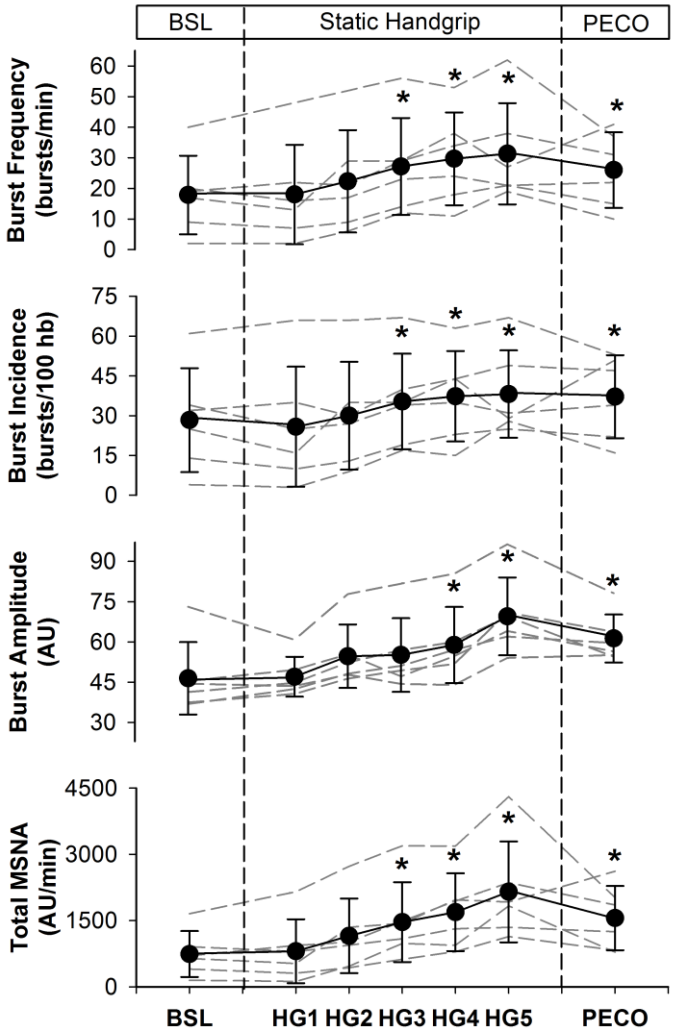

Figure 3.3: Integrated muscle sympathetic nerve activity (MSNA) responses to static handgrip (HG) exercise and postexercise circulatory occlusion (PECO).

Dashed lines represent individual data. Values are mean ± SD. AU, arbitrary units; hb, heartbeats. *$P < 0.05$, significantly different from baseline (BSL).

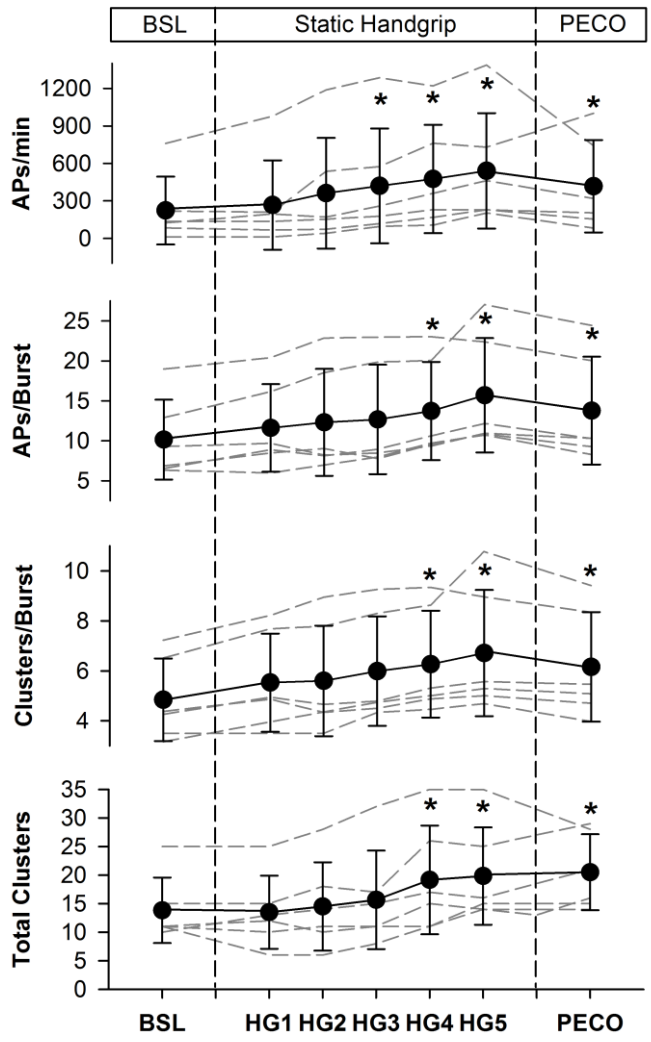

Figure 3.4: Sympathetic action potential (AP) responses to static handgrip (HG) exercise and postexercise circulatory occlusion (PECO).

Dashed lines represent individual data. Values are means ± SD. **P* < 0.05, significantly different from baseline (BSL).

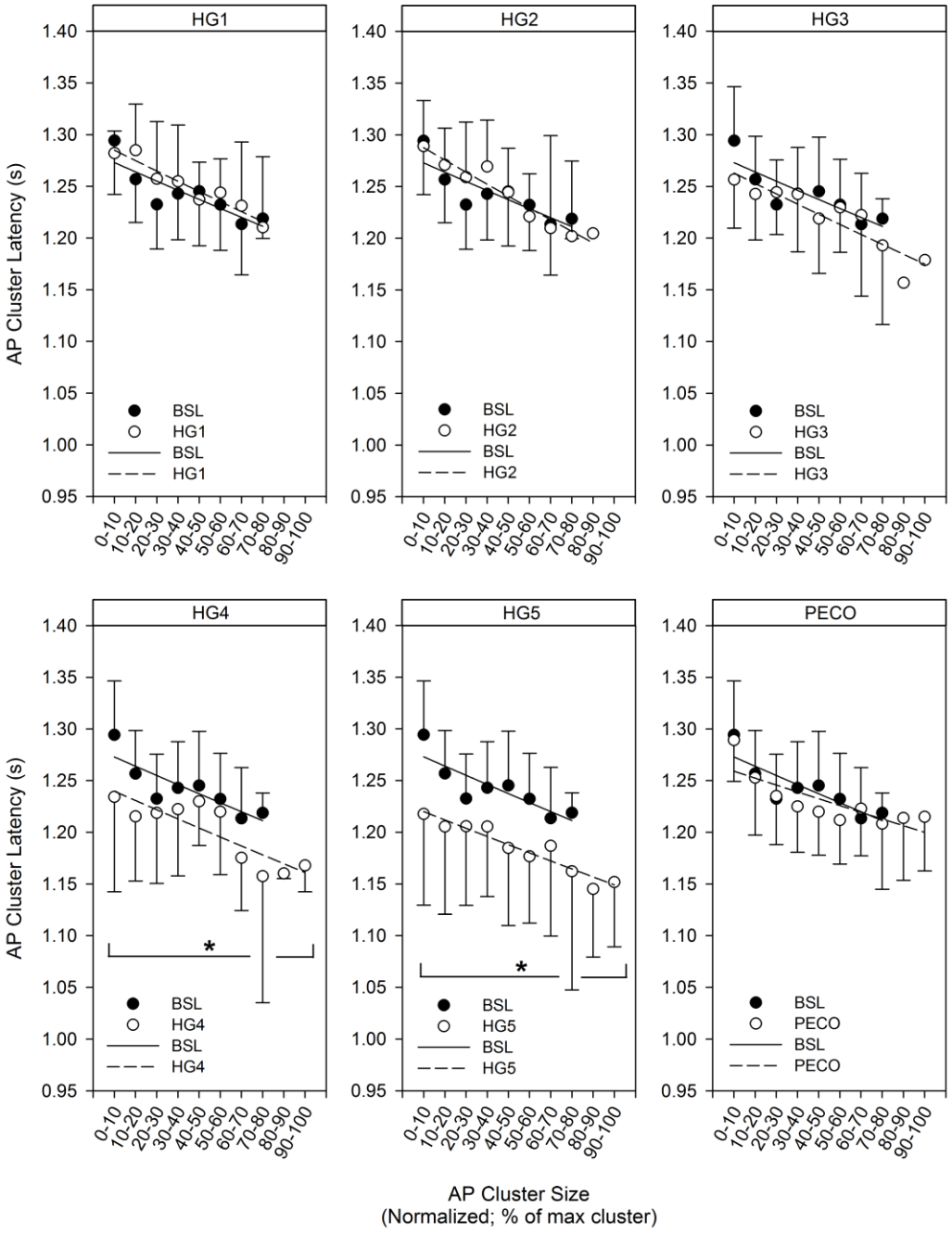

Figure 3.5: Action potential (AP) cluster latency as a function of AP cluster size at baseline (BSL), minutes one to five of static handgrip (HG), and post-exercise circulatory occlusion (PECO).

No significant upward or downward shift was seen in the AP cluster size-latency profile during HG1 (range −14 to 36 ms; range represents individual data), HG2 (range −18 to

35 ms), or HG3 (range −53 to 10 ms), whereas a significant downward shift in the profile was observed during HG4 (range 4 to −136 ms) and HG5 (range −9 to −198 ms). Finally, no significant upward or downward shift was seen during PECO (range −28 to 22 ms). *Significantly different from BSL, $P < 0.05$.

3.4 Discussion

This study examined AP recruitment patterns during the SHG and PECO phases of the exercise pressor response maneuver to gain insight into the role that central command elements versus peripheral-reflex mechanisms have in AP recruitment and sympathetic outflow patterns in humans. The major findings of the current study are as follows: 1) In response to exercise pressor reflex activation, the sympathetic nervous system increases efferent nerve discharge through increased firing of previously recruited axons, and also through the recruitment of latent sub-populations of larger-sized, faster conducting axons. These larger and faster APs were present at the end of the SHG period and persisted throughout the PECO phase. 2) The latency of all APs was reduced towards the end of fatiguing SHG exercise, but not during the PECO phase. The results suggest that central command features may play a specific role in modifying the synaptic delay aspect of efferent sympathetic discharge timing, whereas peripheral muscle chemoreflex mechanisms affect the recruitment of latent high-threshold APs.

Fatiguing SHG exercise elicits robust increases in muscle sympathetic outflow through activation of mechanically- and metabolically-sensitive Type III and IV sensory afferents (Kaufman *et al.* 1983; Mitchell *et al.* 1983), and perhaps modulatory input from higher brain sites during more intense contraction (Victor *et al.* 1995). To date, quantification of the integrated MSNA neurogram has formed the basis of determining the sympathetic response to this reflex, with the finding that MSNA is increased after an initial delay (Mark *et al.* 1985), the timing of which is most likely influenced inversely by contraction intensity (Hashimoto *et al.* 1998). Indeed, in the

current study, MSNA burst frequency and incidence were elevated after approximately two minutes of SHG exercise completed at the relatively modest intensity of 20% MVC.

Presently, using a multi-unit AP approach, we show for the first time that the sympathetic nervous system responds to fatiguing SHG exercise by increasing the firing of already recruited lower-threshold axons, and through the recruitment of sub-populations of previously silent (i.e., not present at baseline), higher-threshold and faster conducting (and therefore, larger) axons. This is similar to patterns observed previously during both baroreflex (Salmanpour *et al.* 2011*a*; Badrov *et al.* 2015) and arterial chemoreflex (Steinback *et al.* 2010; Breskovic *et al.* 2011; Badrov *et al.* 2015; Badrov *et al.* 2016) stimuli, and is supported by the concept that C-fiber diameter variations (~0.5 to 2.0 μm) exist within the human peroneal nerve (Tompkins *et al.* 2013). Since these larger and faster APs became evident after three minutes of exercise, and persisted throughout the PECO period, their recruitment appears to be related to peripheral events within the muscle and, therefore, related to the metaboreflex. These observations discount a role for central factors in eliciting the recruitment of these latent fibres, at least in this reflex model. Interestingly, the different time-course of change between integrated MSNA indices (i.e., increased after two minutes) and AP recruitment (i.e., increased after three minutes) may lend important information as to the order of discharge options used by the sympathetic nervous system. Specifically, MSNA burst frequency increased before the number of APs per burst or total AP clusters increased, which suggests that the first option for the sympathetic nervous system is to increase firing frequency and the second option is recruitment of additional

fibres, as previously hypothesized (Macefield & Wallin, 1999), and similar to the ordered recruitment observed in the motor system (i.e., Henneman's Size Principle) (Henneman *et al.* 1965). This also supports the conjecture that these axons are reserved for periods of high or severe physiological stress (Salmanpour *et al.* 2011*a*; Badrov *et al.* 2015). In line with this, recruitment of new, larger axons was observed in all individuals during −80 mmHg LBNP, but in only approximately 30% of these same individuals during −60 mmHg LBNP (Salmanpour *et al.* 2011*a*). Taken together, it appears as though a fixed, reflex-independent recruitment strategy exists within the sympathetic nervous system, whereby sub-populations of larger neurons are recruited during severe stress scenarios requiring high sympathetic outflow, albeit with some interindividual variations. Furthermore, the current results suggest that peripheral-reflex mechanisms play a dominant role in mediating this recruitment response. Whether this conclusion applies across all reflexes will require additional study. However, central command likely has a small role in LBNP, lending further support to the reflexive role played by peripheral sensory mechanisms in AP recruitment.

In addition to the above described recruitment options, the sympathetic nervous system also modifies efferent firing of lower-threshold axons through acute variations of reflex activation latency (Salmanpour *et al.* 2011*b*; Badrov *et al.* 2015; Badrov *et al.* 2016). In further support of this, we show here that the AP cluster size-latency profile was shifted downwards towards the end of fatiguing SHG exercise, such that during minutes four and five of SHG, all APs expressed a shorter latency. Similar observations have been made during the Valsalva maneuver (Salmanpour *et al.* 2011*b*) and during maximal voluntary apnea (Badrov *et al.* 2015; Badrov *et al.* 2016). That this downward

shift occurred during both peripheral chemoreflex activation (i.e., during volitional apnea) (Badrov *et al.* 2015; Badrov *et al.* 2016) and muscle chemoreflex activation (i.e., during SHG) suggests perhaps that chemoreflex stress may be involved. However, during isolation of the metaboreflex with PECO in the current study, the AP cluster size-latency profile was shifted back toward baseline resting levels, indicating that the muscle chemosensitive sensory afferents are unlikely to play a role in our observed findings. Rather, the common pattern of a downward shift in the AP cluster size-latency profile during the Valsalva maneuver (Salmanpour *et al.* 2011*b*), during maximal voluntary apnea (Badrov *et al.* 2015; Badrov *et al.* 2016), and toward the end of fatiguing SHG exercise here, suggests that a perceptual component (i.e., central command) may be involved in this outcome. Specifically, each maneuver exhibits a certain level of volitional stress that is related to individual tolerance and perception of the maneuver. The exact mechanism(s)/source(s) for this change in AP latency cannot be discerned from the current analysis and requires additional study. However, in as much as conduction velocity of a given axon is relatively stable, our observations suggest the possibility of variations in synaptic delays somewhere within the neural pathway. Indeed, Macefield *et al.* (1994) noted that the AP latency of a single axon can vary rather significantly (i.e., 358 ± 33 ms), demonstrating the potential for considerable modification of synaptic delays and/or central processing times. The functional significance of this systemic and coordinated shift to shorter reflex latency remains unknown. However, the consistent observation of this downward shift in latency during several sympathoexcitatory maneuvers suggests it may be a response reserved for severe stress scenarios requiring high, and perhaps faster occurring,

sympathetic outflow. Nonetheless, it appears that acute malleability of synaptic delays and/or central processing times may represent a unique option available to alter efferent sympathetic outflow during fatiguing SHG exercise, and this is perhaps mediated through a central command phenomenon.

While the use of fatiguing SHG exercise and PECO offers a unique model to study the central versus peripheral features of sympathetic neural recruitment, we cannot conclude with certainty that the PECO phase represents solely peripheral (i.e., metaboreflex) feedback to the central nervous system, without any lingering central, or perceptual, component. Indeed, the discomfort experienced during this period, and retained pressor response, may sustain and/or modify residual centrally-determined sympathetic patterns. In this sense, the lack of a control exercise recovery (i.e., no PECO phase following SHG exercise) period, as performed by other groups (Crisafulli *et al.* 2003; Mulliri *et al.* 2016), may represent a limitation of the current study. However, data from these groups using a handgrip model without PECO supports the concept that the occlusion phase represents selectively peripheral, metaboreflex-mediated input, as the exercise pressor response is maintained during PECO, but absent during the control recovery phase (Crisafulli *et al.* 2003). Furthermore, a 'resting' circulatory occlusion period (i.e., not preceded by exercise) had no effect on baseline resting cardiovascular parameters, further discounting a role for central, or perceptual, elements during our PECO phase in the current study.

In summary, alterations in efferent sympathetic neural outflow during fatiguing exercise occur as a result of increased firing frequency and probability of lower-threshold axons, as a result of recruitment of previously silent sub-populations of

larger-sized, faster conducting axons, and perhaps through acute changes of synaptic delays and/or central processing times. Taken together, it appears as though this represents a generalized central neural coding response to severe stress within the sympathetic nervous system. Our findings here, although in one reflex model, suggest a role for central command features in mediating the synaptic delay aspect of sympathetic discharge patterning, whereas peripheral-reflex mechanisms appear largely responsible for recruitment of latent sympathetic fibres.

Perspectives and Significance

The current work and analytical technique complements traditional integrated methodology, but provides a novel perspective on sympathetic discharge patterns during exercise pressor reflex activation and, therefore, may offer new insights into important unanswered concepts, such as 1) the influence of these neural coding patterns on neurotransmitter release and end-organ vascular responses; 2) the apparent decoupling between elevated sympathetic outflow and vascular resistance in the inactive limb during metaboreflex activation (i.e., neurovascular transduction) (Shoemaker *et al.* 2016); 3) the complex interplay between and neurocircuitry involved in central command and perception of effort during exercise and the potential for feedback-related central control (Williamson, 2010; Basnayake *et al.* 2012); and 4) the exaggerated sympathetic responses to exercise (and in turn, limited exercise capacity) observed in certain clinical pathologies (i.e., congestive heart failure) (Notarius *et al.* 2001; Murai *et al.* 2009).

3.5 References

Alam M & Smirk FH (1937). Observations in man upon a blood pressure raising reflex arising from the voluntary muscles. *J Physiol* **89,** 372-383.

Badrov MB, Lalande S, Olver TD, Suskin N & Shoemaker JK (2016). Effects of aging and coronary artery disease on sympathetic neural recruitment strategies during end-inspiratory and end-expiratory apnea. *Am J Physiol Heart Circ Physiol* **311**, H1040-H1050.

Badrov MB, Usselman CW & Shoemaker JK (2015). Sympathetic neural recruitment strategies: responses to severe chemoreflex and baroreflex stress. *Am J Physiol Regul Integr Comp Physiol* **309,** R160-R168.

Basnayake SD, Green AL & Paterson DJ (2012). Mapping the central neurocircuitry that integrates the cardiovascular response to exercise in humans. *Exp Physiol* **97,** 29-38.

Borg G (1970). Perceived exertion as an indicator of somatic stress. *Scand J Rehabil Med* **2,** 92-98.

Breskovic T, Steinback CD, Salmanpour A, Shoemaker JK & Dujic Z (2011). Recruitment pattern of sympathetic neurons during breath-holding at different lung volumes in apnea divers and controls. *Auton Neurosci* **164,** 74-81.

Brychta RJ, Shiavi R, Robertson D & Diedrich A (2007). Spike detection in human muscle sympathetic nerve activity using the kurtosis of stationary wavelet transform coefficients. *J Neurosci Methods* **160,** 359-367.

Crisafulli A, Scott AC, Wensel R, Davos CH, Francis DP, Pagliaro P, Coasts AJ, Concu A & Piepoli MF (2003). Muscle metaboreflex-induced increases in stroke volume. *Med Sci Sports Exerc* **35,** 221-228.

Diedrich A, Charoensuk W, Brychta RJ, Ertl AC & Shiavi R (2003). Analysis of raw microneurographic recordings based on wavelet de-noising technique and classification algorithm: wavelet analysis in microneurography. *IEEE Trans Biomed Eng* **50,** 41-50.

Goodwin GM, McCloskey DI & Mitchell JH (1972). Cardiovascular and respiratory responses to changes in central command during isometric exercise at constant muscle tension. *J Physiol* **226,** 173-190.

Hagbarth KE & Vallbo AB (1968). Pulse and respiratory grouping of sympathetic impulses in human muscle nerves. *Acta Physiol Scand* **74,** 96-108.

Hashimoto I, Miyamura M & Saito M (1998). Initiation of increase in muscle sympathetic nerve activity delay during maximal voluntary contraction. *Acta Physiol Scand* **164,** 293-297.

Henneman E, Somjen G & Carpenter DO (1965). Functional significance of cell size in spinal motoneurons. *J Neurophysiol* **28,** 560-580.

Johansson J (1895). Ueber die einwirkung der muskelthltigkeit auf die athmung und die hertzhiitigkeit. *Skand Arch Physiol* **5,** 20-66.

Kaufman MP, Longhurst JC, Rybicki KJ, Wallach JH & Mitchell JH (1983). Effects of static muscular contraction on impulse activity of groups III and IV afferents in cats. *J Appl Physiol* **55,** 105-112.

Krogh A & Lindhard J (1913). The regulation of respiration and circulation during the initial stages of muscular work. *J Physiol* **47,** 112-136.

Macefield VG & Wallin BG (1999). Firing properties of single vasoconstrictor neurones in human subjects with high levels of muscle sympathetic activity. *J Physiol* **516,** 293-301.

Macefield VG, Wallin BG & Vallbo AB (1994). The discharge behaviour of single vasoconstrictor motoneurones in human muscle nerves. *J Physiol* **481,** 799-809.

Mark AL, Victor RG, Nerhed C & Wallin BG (1985). Microneurographic studies of the mechanisms of sympathetic nerve responses to static exercise in humans. *Circ Res* **57,** 461-469.

McCloskey DI & Mitchell JH (1972). Reflex cardiovascular and respiratory responses originating in exercising muscle. *J Physiol* **224,** 173-186.

Mitchell JH, Kaufman MP & Iwamoto GA (1983). The exercise pressor reflex: its cardiovascular effects, afferent mechanisms, and central pathways. *Annu Rev Physiol* **45,** 229-242.

Mulliri G, Sainas G, Magnani S, Palazzolo G, Milia N, Orrù A, Roberto S, Marongiu E, Milia R & Crisafulli A (2016). Ischemic preconditioning reduces hemodynamic

response during metaboreflex activation. *Am J Physiol Regul Integr Comp Physiol* **310,** R777-R787.

Murai H, Takamura M, Maruyama M, Nakano M, Ikeda T, Kobayashi D, Otowa K, Ootsuji H, Okajima M, Furusho H, Takata S & Kaneko S (2009). Altered firing pattern of single-unit muscle sympathetic nerve activity during handgrip exercise in chronic heart failure. *J Physiol* **587,** 2613-2622.

Murai H, Takata S, Maruyama M, Nakano M, Kobayashi D, Otowa K, Takamura M, Yuasa T, Sakagami S & Kaneko S (2006). The activity of a single muscle sympathetic vasoconstrictor nerve unit is affected by physiological stress in humans. *Am J Physiol Heart Circ Physiol* **290,** H853-H860.

Ninomiya I, Malpas SC, Matsukawa K, Shindo T & Akiyama T (1993). The amplitude of synchronized cardiac sympathetic nerve activity reflects the number of activated pre- and postganglionic fibers in anesthetized cats. *J Auton Nerv Syst* **45,** 139-147.

Notarius CF, Atchison DJ & Floras JS (2001). Impact of heart failure and exercise capacity on sympathetic response to handgrip exercise. *Am J Physiol Heart Circ Physiol* **280,** H969-H976.

Saito M, Mano T & Iwase S (1990). Changes in muscle sympathetic nerve activity and calf blood flow during static handgrip exercise. *Eur J Appl Physiol Occup Physiol* **60,** 277-281.

Salmanpour A, Brown LJ & Shoemaker JK (2010). Spike detection in human muscle sympathetic nerve activity using a matched wavelet approach. *J Neurosci Methods* **193,** 343-355.

Salmanpour A, Brown LJ, Steinback CD, Usselman CW, Goswami R & Shoemaker JK (2011*a*). Relationship between size and latency of action potentials in human muscle sympathetic nerve activity. *J Neurophysiol* **105,** 2830-2842.

Salmanpour A, Frances MF, Goswami R & Shoemaker JK (2011*b*). Sympathetic neural recruitment patterns during the Valsalva maneuver. *Conf Proc IEEE Eng Med Biol Soc* **2011,** 6951-6954.

Scott DW (1979). On optimal and data-based histograms. *Biometrika* **66,** 605-610.

Seals DR, Chase PB & Taylor JA (1988). Autonomic mediation of the pressor responses to isometric exercise in humans. *J Appl Physiol* **64,** 2190-2196.

Seals DR & Victor RG (1991). Regulation of muscle sympathetic nerve activity during exercise in humans. *Exerc Sport Sci Rev* **19,** 313-350.

Shoemaker JK, Badrov MB, Al-Khazraji BK & Jackson DN (2016). Neural control of vascular function in skeletal muscle. *Compr Physiol* **6,** 303-329.

Shoemaker JK, Mattar L, Kerbeci P, Trotter S, Arbeille P & Hughson RL (2007). WISE 2005: stroke volume changes contribute to the pressor response during ischemic handgrip exercise in women. *J Appl Physiol* **103,** 228-233.

Steinback CD, Salmanpour A, Breskovic T, Dujic Z & Shoemaker JK (2010). Sympathetic neural activation: an ordered affair. *J Physiol* **588,** 4825-4836.

Tompkins RP, Melling CW, Wilson TD, Bates BD & Shoemaker JK (2013). Arrangement of sympathetic fibers within the human common peroneal nerve: implications for microneurography. *J Appl Physiol* **115,** 1553-1561.

Vallbo AB, Hagbarth KE, Torebjork HE & Wallin BG (1979). Somatosensory, proprioceptive, and sympathetic activity in human peripheral nerves. *Physiol Rev* **59,** 919-957.

Victor RG, Bertocci LA, Pryor SL & Nunnally RL (1988). Sympathetic nerve discharge is coupled to muscle cell pH during exercise in humans. *J Clin Invest* **82,** 1301-1305.

Victor RG, Secher NH, Lyson T & Mitchell JH (1995). Central command increases muscle sympathetic nerve activity during intense intermittent isometric exercise in humans. *Circ Res* **76,** 127-131.

Wallin BG, Victor RG & Mark AL (1989). Sympathetic outflow to resting muscles during static handgrip and postcontraction muscle ischemia. *Am J Physiol Heart Circ Physiol* **256,** H105-H110.

Williamson JW (2010). The relevance of central command for the neural cardiovascular control of exercise. *Exp Physiol* **95,** 1043-1048.

Chapter 4

4 Effects of aging and coronary artery disease on sympathetic neural recruitment strategies during end-inspiratory and end-expiratory apnea

(Published in Am J Physiol Heart Circ Physiol 311: H1040-H1050, 2016)

4.1 Introduction

Sympathetic nervous system dysregulation represents a hallmark of increasing age and cardiovascular disease. This dysregulation has been well-studied at rest, where aging and cardiovascular disease are characterized by a net elevation in baseline sympathetic outflow (Seals & Esler, 2000; Grassi *et al.* 2015), which contributes to numerous deleterious consequences, including cardiac and vascular damage and remodeling, cardiac dysrhythmias, and an elevated risk of mortality (Pauletto *et al.* 1991; Barretto *et al.* 2009; Grassi *et al.* 2011). However, the mechanisms involved in aberrant sympathetic control with aging and cardiovascular disease, such as the distinct features of central recruitment strategies, are not known.

Normally, sympathetic neural control involves central integration of sensory and cortical/sub-cortical signals within the brain stem and spinal cord (Barman & Gebber, 2000), synapses at the sympathetic ganglia (Jänig & McLachlan, 1992), efferent post-ganglionic nerve traffic, neurotransmitter release, and the subsequent vascular effect at the end-organ (Shoemaker *et al.* 2016). These elements introduce multiple sites of control in which sympathetic outflow can be coded and modified in response to acute physiological perturbation. Data from direct single- and multi-fibre recordings of central sympathetic outflow in young healthy individuals indicate that the sympathetic

nervous system has options to increase the firing frequency and probability of low-threshold axons (Macefield & Wallin, 1999; Salmanpour *et al.* 2011*a*), recruit latent sub-populations of higher-threshold and faster conducting axons (Steinback *et al.* 2010*b*; Badrov *et al.* 2015), as well as acutely modify synaptic delays and/or central processing times (Salmanpour *et al.* 2011*b*; Badrov *et al.* 2015). These patterns illustrate unique properties of the central nervous system to fine-tune autonomic homeostatic control.

Whether these neural coding strategies are affected by increasing age and cardiovascular pathology normally associated with advancing age remains uncertain. While recordings from single muscle vasoconstrictor axons reveal an increased firing probability and frequency of single-units in cardiovascular disease (Greenwood *et al.* 1999; Macefield *et al.* 1999), the typical observation that a given neuron will fire usually only once per sympathetic burst at rest appears unchanged in congestive heart failure with reduced left ventricular ejection fraction (LVEF) (Macefield *et al.* 1994; Macefield *et al.* 1999). Conversely, within-burst firing frequency of single axons at baseline is increased in other states of chronic sympathetic arousal, such as obstructive sleep apnea (Elam *et al.* 2002) and chronic obstructive pulmonary disease (Ashley *et al.* 2010), as well as in response to an acute physiological challenge (Macefield & Wallin, 1999; Elam & Macefield, 2001; Murai *et al.* 2006). However, information regarding the several recruitment strategies available (i.e., recruitment of new axons) to the sympathetic nervous system cannot be extracted from single-unit recordings, but requires a multi-unit analysis model. Using multi-fibre recordings, we have documented recruitment of new sub-populations of larger axons (Steinback *et al.* 2010*b*; Breskovic

et al. 2011; Badrov *et al.* 2015), as well as modifiable synaptic delays (Badrov *et al.* 2015), in response to voluntary apnea-induced sympathoexcitation in young healthy individuals. However, the ability to recruit latent neuronal sub-populations may be diminished with healthy aging and cardiovascular disease (Maslov *et al.* 2012; Maslov *et al.* 2014).

Therefore, the current study examined the hypothesis that cardiovascular disease impairs sympathetic neural recruitment. Coronary artery disease (CAD) patients with preserved LVEF completed maximal voluntary apneas, which served as a stimulus for sympathoexcitation, and the response was compared to that of young healthy and older healthy individuals to account for the concurrent effect of age.

4.2 Methods

4.2.1 Participants

Forty-two individuals participated in the current investigation after providing informed written consent. Participants comprised three groups: 1) young healthy individuals (YH; n = 14, 5 females), 2) older healthy individuals (OH; n = 14; 6 females), and 3) CAD patients (CAD; n = 14, 3 females). Participant characteristics are summarized in Table 4.1. YH and OH participants were non-smokers, free of overt disease, and non-medicated. CAD patients included those who were discharged from hospital following an acute ST elevation (n = 7) or non-ST elevation (n = 7) myocardial infarction (MI) as documented by their attending physician. In all instances, patients presented with their first MI. Eleven patients underwent percutaneous coronary intervention and four underwent coronary artery bypass grafting surgery. No CAD

patients had a history of congestive heart failure, renal insufficiency, or diabetes mellitus, and all had preserved LVEF at the time of study. Although all patients were on anti-hypertensive medications, all presented with resting blood pressures within the normal range (i.e., <140/90 mmHg). Six patients were former or current smokers at the time of study. On average, testing took place 67 ± 37 days following hospital discharge. Medication use in the CAD patients included beta-blockers (n = 13; 93%), angiotensin converting enzyme inhibitors (n = 13; 93%), calcium channel blockers (n = 3; 21%), diuretics (n = 1; 8%), statins (n = 13; 93%), and anti-platelets, including aspirin (n = 14; 100%). All experimental protocols were approved by the Health Sciences Research Ethics Board at Western University.

4.2.2 Experimental Protocols

Participants arrived for testing having fasted and abstained from caffeine and alcohol for 12 hours, and vigorous exercise for 24 hours. Data were collected in the supine position during 1) a 1-minute baseline period and a subsequent end-inspiratory (EI) apnea of maximal voluntary duration, and 2) a 1-minute baseline period and a subsequent end-expiratory (EE) apnea of maximal voluntary duration. Both EI- and EE-apnea were repeated twice, with each trial separated by three minutes of rest. EI- and EE-apnea were used as stimuli to increase muscle sympathetic nerve activity (MSNA) in order to study the neural recruitment strategies employed by the sympathetic nervous system during reflex-mediated sympathoexcitation. Both EI- and EE-apnea elicit marked increases in sympathetic outflow, albeit through different mechanisms. Voluntary EI-apnea increases MSNA through a variety of factors including unloading of the baroreceptors, chemoreflex activation, and an increased central drive-to-breathe

(Ferrigno *et al.* 1986; Somers *et al.* 1989; Hardy *et al.* 1994; Steinback *et al.* 2010*a*). On the other hand, EE-apnea increases MSNA predominantly through chemoreflex stimulation, as well as a lack of ventilatory restraint on sympathetic outflow, and increased central drive-to-breathe (Somers *et al.* 1989; Hardy *et al.* 1994; Steinback *et al.* 2010*a*).

4.2.3 Experimental Measures

Sympathetic neural recordings were obtained in the right peroneal nerve by microneurography, using standard procedures originally defined by Hagbarth and Vallbo (1968) and used frequently in our hands (Steinback *et al.* 2010*b*; Salmanpour *et al.* 2011*a*; Badrov *et al.* 2015) (662C-3; Bioengineering of University of Iowa, Iowa City, IA). Blood pressure was obtained throughout the experimental protocol using finger photoplethysmography (Finometer; Finapres Medical Systems, Amsterdam, The Netherlands), which was calibrated to manual sphygmomanometry. Heart rate (HR) was calculated from a standard three-lead electrocardiogram. Stroke volume (SV) and cardiac output (CO) were acquired using the Finometer Modelflow algorithm and total peripheral resistance (TPR) was calculated as the quotient of mean arterial pressure (MAP) and CO. All data were collected and analyzed offline using LabChart6 and PowerLab (ADInstruments, Colorado Springs, CO).

4.2.4 Data Analysis

For both the EI- and EE-apnea protocols, data were analyzed for the 1-minute baseline period and during the second half of maximal voluntary apnea. MSNA was analyzed from the integrated neurogram and from our technique to detect and extract action potentials (APs) from the filtered raw MSNA signal (Salmanpour *et al.* 2010).

Integrated MSNA was quantified using burst frequency and burst incidence [bursts per minute and bursts per 100 heart beats (hb), respectively]. Furthermore, burst amplitude (normalized to the largest burst at baseline, which was given a value of 100) and total MSNA (product of normalized burst amplitude and burst frequency) were determined.

Individual APs were extracted from the filtered raw MSNA signal using wavelet-based methodology, as first reported by others (Diedrich *et al.* 2003; Brychta *et al.* 2007), and modified in our hands (Salmanpour *et al.* 2010). Our approach, described in detail elsewhere (Salmanpour *et al.* 2010; Badrov *et al.* 2015), uses a continuous wavelet transform constructed from real post-ganglionic sympathetic APs (Salmanpour *et al.* 2010), that extracts APs at their point of occurrence, and classifies them according to their peak-to-peak amplitude into clusters (i.e., bins) of similarly-sized APs using Scott's rule (Scott, 1979). To enable investigation into whether recruitment of new, larger AP clusters occurred during apnea, a secondary analysis stage was introduced whereby cluster characteristics were manipulated within each participant so that minimum bin width, maximum bin center, and the total number of bins would be identical across conditions. Therefore, corresponding clusters at baseline and apnea contain APs with similar peak-to-peak amplitudes, while additional clusters during apnea represent recruitment of latent sub-populations of larger-sized axons (i.e., not present at baseline).

AP variables were quantified using AP frequency and AP incidence (APs per minute and APs per 100 hb, respectively), as well as the mean AP content per integrated sympathetic burst. Furthermore, the number of total AP clusters and the number of active clusters per burst are presented. AP cluster latency was calculated as

the average latency of all APs present within that cluster (as measured by the time delay between the R-wave of the electrocardiogram of the preceding cardiac cycle and the negative peak of the AP waveform). To adjust for the impact of interindividual variations in total cluster number on calculations of changes in AP cluster latency, the number of total clusters was normalized to 10 bins (i.e., 10% ranges of the largest detected cluster, which was given a value of 100%) for this analysis step, as described previously (Badrov *et al.* 2015).

4.2.5 Statistical Analysis

Mixed model ANOVAs (SigmaPlot 12.0; Systat Software Inc., San Jose, CA) assessed the effect of group versus time (baseline vs. EI-apnea; baseline vs. EE-apnea) on MSNA and hemodynamic variables. Bonferroni-corrected post hoc procedures were used to evaluate specific differences between means. Regression analyses were used to determine specific relationships between variables when applicable. For the EE-apnea protocol, six participants (YH, n = 2; OH, n = 2; CAD, n = 2) were excluded as their MSNA signal was obscured by motor-unit activation and/or a signal-to-noise ratio (SNR) that was too poor to allow for adequate AP analysis. Statistical significance was set at $P < 0.05$ and all data are means ± SD, unless otherwise stated.

4.3 Results

As noted above, some MSNA recordings lacked appropriate SNR or were contaminated by motor-unit activation. Also, variations exist between individuals in the duration of apnea, as well as within individuals in terms of the response and duration to repeated apneas. To address these issues, Bland-Altman analyses assessed the

agreement between the first and second EI- and EE-apneas for all MSNA and AP variables. Participants with SNR >3.7 (i.e., to allow for adequate AP detection) for both apneas were included in the analysis (EI-apnea, n = 33; EE-apnea, n = 21). Briefly, while the second EI- and EE-apnea were of longer duration (EI-apnea: 41 ± 17 vs. 36 ± 17 s; EE-apnea: 21 ± 10 vs. 19 ± 10 s; both $P < 0.05$), no differences existed between the first and second sympathetic response to either EI- or EE-apnea (all P = NS), and all MSNA and AP variables were without significant fixed or proportional bias (EI-apnea: Total MSNA: 127 ± 139, mean difference ± SE; APs/burst: 0.6 ± 0.5; Clusters/burst: 0.1 ± 0.1; Total Clusters: 0.2 ± 0.5; EE-apnea: Total MSNA: −474 ± 315; APs/burst: 0.6 ± 0.7; Clusters/burst: 0.3 ± 0.2; Total Clusters: −0.5 ± 0.6). With no within-individual differences between the first and second apnea, the average of the two EI- and two EE-apneas were used in the final analysis. Re-examination of results with removal of statistical outliers (i.e., those individuals with data points that were more than 1.5 interquartile ranges below the first quartile or above the third quartile) did not significantly alter the results; therefore, data from these individuals were retained in the final analysis (Tukey, 1977). Finally, the mean SNR in the current study was 4.1 ± 0.5, which is expected to produce a correct detection rate of >90% and a false positive rate of <3% (Salmanpour *et al.* 2010).

Figure 4.1 displays representative recordings of the integrated MSNA neurogram and detected APs from one YH individual, one OH individual, and one CAD patient at baseline and during EI-apnea and EE-apnea.

Baseline versus End-Inspiratory Apnea. The duration of the second half of EI-apnea was 46 ± 17 s (range 27 to 78 s) in YH, 35 ± 15 s (range 15 to 70 s) in OH, and

28 ± 6 s (range 19 to 44 s) in CAD patients. In a pointwise contrast, CAD patients had a lower EI-apnea duration compared to YH ($P < 0.01$). MAP, HR, and TPR exhibited effects of time, whereby each increased during EI-apnea, while reductions in SV and CO occurred (all $P < 0.05$; Table 4.2); however, no group differences existed in the hemodynamic response to EI-apnea (all P = NS).

Table 4.3 outlines the integrated MSNA and AP indexes during EI-apnea and their relative baseline values. Compared to YH, baseline burst frequency and burst incidence were higher in OH and CAD (all $P < 0.01$), but no differences were observed between OH and CAD (P = NS). Compared with baseline, all integrated MSNA variables increased during EI-apnea in all groups (all $P < 0.01$). However, compared to YH, the change in integrated MSNA was blunted in OH and CAD (all $P < 0.01$), with no differences between OH and CAD (P = NS). Whereas EI-apnea resulted in increased AP frequency and AP incidence in all groups (all $P < 0.01$), CAD patients had a reduced ability to increase AP frequency and AP incidence compared to YH (both $P < 0.01$). No differences in the AP frequency and AP incidence response existed between YH and OH (P = NS) or OH and CAD (P = NS).

Compared with baseline, the mean AP content per burst increased during EI-apnea in YH (11 ± 8 to 17 ± 11 APs/burst; $P < 0.01$) and OH (10 ± 5 to 13 ± 7 APs/burst; $P < 0.01$), while no change occurred in CAD patients (10 ± 4 to 11 ± 5 APs/burst; P = NS; Figure 4.2*a*). The magnitude of response was reduced in both OH and CAD compared to YH ($P < 0.01$), and further reduced in CAD versus OH ($P < 0.01$). When APs were binned according to their peak-to-peak amplitude, the number of total clusters of APs increased in YH (9 ± 3 to 14 ± 4 total clusters; $P < 0.01$) and OH

(13 ± 3 to 14 ± 3 total clusters; $P < 0.01$) during EI-apnea, but not in CAD patients (14 ± 3 to 12 ± 3 total clusters; P = NS; Figure 4.2*b*). The ability to recruit new clusters of APs was diminished in OH and CAD patients compared to YH ($P < 0.01$), and further decreased in CAD versus OH ($P < 0.01$). Finally, the number of active clusters per burst increased during EI-apnea in YH (4 ± 2 to 6 ± 2 clusters/burst; $P < 0.01$) and OH (5 ± 1 to 6 ± 2 clusters/burst; $P < 0.01$), but not in CAD patients (5 ± 1 to 5 ± 1 clusters/burst; P = NS; Figure 4.2*c*). The magnitude of change was lower in OH and CAD compared with YH (both $P < 0.01$), and further lowered in CAD compared with OH ($P < 0.01$). When all subjects were pooled, EI-apnea duration correlated poorly with the mean AP content per burst response (r = 0.207; P = NS) and the active clusters per burst response (r = 0.277; P = NS) to apnea. EI-apnea duration correlated moderately well with the total clusters response (r = 0.553; $P < 0.01$) to apnea; however, when accounting for age and incidence of CAD, EI-apnea duration no longer predicted the total cluster response to apnea (P = NS).

In all groups, at baseline (YH: $R^2 = 0.93$; OH: $R^2 = 0.90$; CAD: $R^2 = 0.77$; all $P < 0.01$) and during EI-apnea (YH: $R^2 = 0.97$; OH: $R^2 = 0.94$; CAD: $R^2 = 0.91$; all $P < 0.01$), a pattern emerged whereby AP cluster latency decreased as a function of normalized cluster number (i.e., as peak-to-peak AP cluster amplitude increased). The mean responses (Figure 4.3) were fitted using an exponential function model at baseline and during EI-apnea. Interestingly, the cluster size-latency profile shifted downward for every corresponding cluster during apnea in YH (range −8 to −48 ms; mean: −28 ± 15 ms; $P < 0.01$), OH (range −15 to −38 ms; mean: −32 ± 7 ms; $P < 0.01$), and CAD

patients (range −5 to −58 ms; mean: −21 ± 17 ms; $P < 0.01$). No differences were found in the magnitude of change between groups (all P = NS).

Baseline versus End-Expiratory Apnea. The duration of the second half of EE-apnea was 20 ± 10 s (range 12 to 47 s) in YH, 22 ± 11 s (range 8 to 45 s) in OH, and 16 ± 5 s (range 10 to 27 s) in CAD patients. No differences in duration were observed for EE-apnea between groups (P = NS). Both MAP and TPR exhibited effects of time, whereby values increased during EE-apnea; in contrast, reductions occurred in SV and CO (all $P < 0.05$; Table 4.2). However, no group differences existed in the hemodynamic response to EE-apnea (all P = NS).

Table 4.4 outlines the integrated MSNA and AP indexes during EE-apnea and their relative baseline values. Once again, compared with YH, baseline burst frequency and burst incidence were higher in OH and CAD (all $P < 0.01$), but no differences were observed between OH and CAD (P = NS). Compared with baseline, all integrated MSNA variables increased during EE-apnea in all groups (all $P < 0.01$). However, compared with YH, the changes in burst frequency, burst amplitude, and total MSNA were blunted in OH and CAD (all $P < 0.01$), while the change in burst incidence was lower in CAD versus YH ($P < 0.01$). No differences were found between OH and CAD for any integrated MSNA variable (all P = NS). Additionally, compared to baseline, EE-apnea resulted in increased AP frequency and AP incidence in all groups ($P < 0.05$); however, CAD patients had a decreased ability to increase AP frequency and AP incidence compared with YH ($P < 0.01$), while no differences existed between OH and CAD (P = NS).

Compared to baseline, the mean AP content per burst increased in YH (11 ± 6 to 20 ± 9 APs/burst; $P < 0.01$) and OH (11 ± 4 to 15 ± 8 APs/burst; $P < 0.01$) in response to EE-apnea, but was unchanged in CAD patients (11 ± 6 to 13 ± 6 APs/burst; P = NS; Figure 4.4*a*). The change in the mean AP content per burst was lower in OH and CAD than in YH (both $P < 0.01$); however, no difference existed between OH and CAD (P = NS). When APs were binned according to their peak-to-peak amplitude, the number of total clusters of APs increased in YH (8 ± 4 to 14 ± 5 total clusters; $P < 0.01$), but was unchanged in both OH (12 ± 3 to 13 ± 4 total clusters; P = NS) and CAD patients (13 ± 4 to 12 ± 2 total clusters; P = NS; Figure 4.4*b*). As such, the ability to recruit new clusters of APs was diminished in OH and CAD compared with YH (both $P < 0.01$). Finally, compared with baseline, the number of active clusters per burst increased during EE-apnea in YH (4 ± 2 to 6 ± 2 clusters/burst; $P < 0.01$) and OH (5 ± 1 to 6 ± 2 clusters/burst; $P < 0.01$), but not in CAD patients (5 ± 1 to 6 ± 1 clusters/burst; P = NS; Figure 4.4*c*). The magnitude of change was lower in OH and CAD compared with YH ($P < 0.01$). When all subjects were pooled, EE-apnea duration correlated poorly with the mean AP content per burst response (r = 0.029; P = NS), the active clusters per burst response (r = 0.117; P = NS), as well as the total clusters response (r = 0.297; P = NS) to apnea.

Similar to EI-apnea, a pattern emerged during baseline (YH: $R^2 = 0.76$; OH: $R^2 = 0.85$; CAD: $R^2 = 0.88$; all $P < 0.01$) and EE-apnea (YH: $R^2 = 0.95$; OH: $R^2 = 0.97$; CAD: $R^2 = 0.87$; all $P < 0.05$), whereby AP cluster latency decreased as a function of normalized cluster number (i.e., as peak-to-peak AP cluster amplitude increased). The mean responses (Figure 4.5) were fitted using an exponential function model at baseline

and during EE-apnea. Once again, the cluster size-latency profile shifted downward for every corresponding cluster during apnea in YH (range −12 to −74 ms; mean: −35 ± 23 ms; $P < 0.01$), OH (range 0 to −47 ms; mean: −30 ± 14 ms; $P < 0.01$), and CAD patients (range −31 to −87 ms; mean: −59 ± 17 ms; $P < 0.01$). No differences were found in the magnitude of change between groups (all P = NS).

Table 4.1: Participant characteristics

	YH	OH	CAD
Age (y)	25±3	59±9*	61±10*
Height (cm)	173±8	168±7	169±9
Weight (kg)	74±13	68±11	86±15*†
Body Mass Index (kg/m^2)	25±4	25±2	30±5*†
Systolic BP (mmHg)	113±13	121±16	120±21
Diastolic BP (mmHg)	69±10	74±10	66±9
HR (beats/min)	63±6	58±8	60±8
CO (L/min)	6.2±1.3	5.4±1.4	6.2±1.2
TPR (mmHg/L/min)	14±4	18±7	14±4
LVEF (%)	68±4	68±4	61±9
Burst Frequency (bursts/min)	18±8	34±9*	41±7*
Burst Incidence (bursts/100 hb)	29±13	58±14*	69±11*
Total MSNA (AU)	989±380	1916±540*	2331±372*
Glucose (mmol/L)	5.1±0.6	5.2±0.4	5.6±0.7
Total Cholesterol (mmol/L)	3.6±1.0	4.3±0.6	3.2±0.6†
HDL Cholesterol (mmol/L)	1.2±0.2	1.5±0.3	1.0±0.1†
LDL Cholesterol (mmol/L)	2.0±1.0	2.4±0.6	1.7±0.5
Triglycerides (mmol/L)	0.9±0.3	0.9±0.4	1.0±0.3
HbA1C (%)	5.4±0.2	5.7±0.2*	5.8±0.3*

Values are the mean of the two baseline periods (mean ± SD). YH, young healthy; OH, older healthy; CAD, coronary artery disease; BP, blood pressure; HR, heart rate; CO, cardiac output; TPR, total peripheral resistance; LVEF, left ventricular ejection fraction; hb, heart beats; MSNA, muscle sympathetic nerve activity; AU, arbitrary units. HDL, high density lipoprotein; LDL, low density lipoprotein; HbA1C, hemoglobin A1C. *Significantly different from YH, $P < 0.01$; †Significantly different from OH, $P < 0.01$.

Table 4.2: Hemodynamic responses to end-inspiratory and end-expiratory apnea

	YH	OH	CAD
End-Inspiratory Apnea			
Δ MAP (mmHg)	9±5	6±8	8±8
Δ HR (beats/min)	2±9	3±10	2±4
Δ SV (mL)	−20±13	−22±12	−17±17
Δ CO (L/min)	−1.1±1.0	−1.2±0.9	−1.0±0.9
Δ TPR (mmHg/L/min)	5±3	7±5	5±3
End-Expiratory Apnea			
Δ MAP (mmHg)	11±4	8±6	7±5
Δ HR (beats/min)	4±11	0±9	0±3
Δ SV (mL)	−4±10	−12±8	−7±10
Δ CO (L/min)	0.1±0.5	−0.6±0.6	−0.5±0.5
Δ TPR (mmHg/L/min)	2±2	5±4	3±2

Values are mean ± SD. YH, young healthy; OH, older healthy; CAD, coronary artery disease; MAP, mean arterial pressure; HR, heart rate; SV, stroke volume; CO, cardiac output; TPR, total peripheral resistance.

Table 4.3: Integrated MSNA and action potential indexes at baseline and during maximal end-inspiratory apnea

	Baseline	EI-Apnea	Δ
Integrated MSNA Indices			
Burst Frequency (bursts/min)			
YH	17±8	41±8†	25±10
OH	35±9*	51±11†	16±7‡
CAD	41±7*	53±8†	11±8‡
Burst Incidence (bursts/100 hb)			
YH	27±14	65±15†	38±18
OH	60±14*	82±13†	22±14‡
CAD	70±10*	88±6†	18±10‡
Burst Amplitude (AU)			
YH	57±8	100±25†	43±20
OH	57±6	80±16†	24±15‡
CAD	57±5	69±13†	12±12‡
Total MSNA (AU)			
YH	908±389	4144±1379†	3236±1476
OH	2002±614*	4077±1211†	2075±1113‡
CAD	2357±415*	3624±811†	1267±700‡
Action Potential Indices			
AP Frequency (spikes/min)			
YH	189±222	691±480†	502±356
OH	372±226	698±402†	326±223
CAD	410±180	584±279†	174±196‡
AP Incidence (spikes/100 hb)			
YH	307±353	1081±757†	774±581
OH	614±343	1136±681†	522±461
CAD	694±302	968±465†	274±305‡

Values are mean ± SD. EI, end-inspiratory; MSNA, muscle sympathetic nerve activity; YH, young healthy; OH, older healthy; CAD, coronary artery disease; hb, heart beats; AU, arbitrary units; AP, action potential. *Significantly different from

YH baseline value, $P < 0.01$; †Significantly different from baseline, $P < 0.01$; ‡Significantly different from YH delta value, $P < 0.01$.

Table 4.4: Integrated MSNA and action potential indexes at baseline and during maximal end-expiratory apnea

	Baseline	EE-Apnea	Δ
Integrated MSNA Indices			
Burst Frequency (bursts/min)			
YH	19±7	42±12†	24±13
OH	33±9*	49±11†	16±6‡
CAD	41±8*	51±5†	10±7‡
Burst Incidence (bursts/100 hb)			
YH	29±11	64±17†	34±20
OH	56±16*	83±13†	27±14
CAD	70±11*	89±5†	18±13‡
Burst Amplitude (AU)			
YH	57±7	124±55†	67±51
OH	56±9	79±25†	22±22‡
CAD	58±5	81±19†	23±16‡
Total MSNA (AU)			
YH	1006±381	5147±2379†	4141±2523
OH	1839±557	3793±1170†	1953±1165‡
CAD	2372±425*	4103±996†	1731±762‡
Action Potential Indices			
AP Frequency (spikes/min)			
YH	216±207	852±491†	636±351
OH	370±191	731±430†	361±303
CAD	447±262	662±301†	215±155‡
AP Incidence (spikes/100 hb)			
YH	347±340	1278±669†	931±499
OH	609±298	1219±738†	610±589
CAD	760±418	1162±531†	402±312‡

Values are mean ± SD. EE, end-expiratory; MSNA, muscle sympathetic nerve activity; YH, young healthy; OH, older healthy; CAD, coronary artery disease; hb, heart beats; AU, arbitrary units; AP, action potential. *Significantly different from

YH baseline value, $P < 0.01$; †Significantly different from baseline, $P < 0.01$; ‡Significantly different from YH delta value, $P < 0.01$.

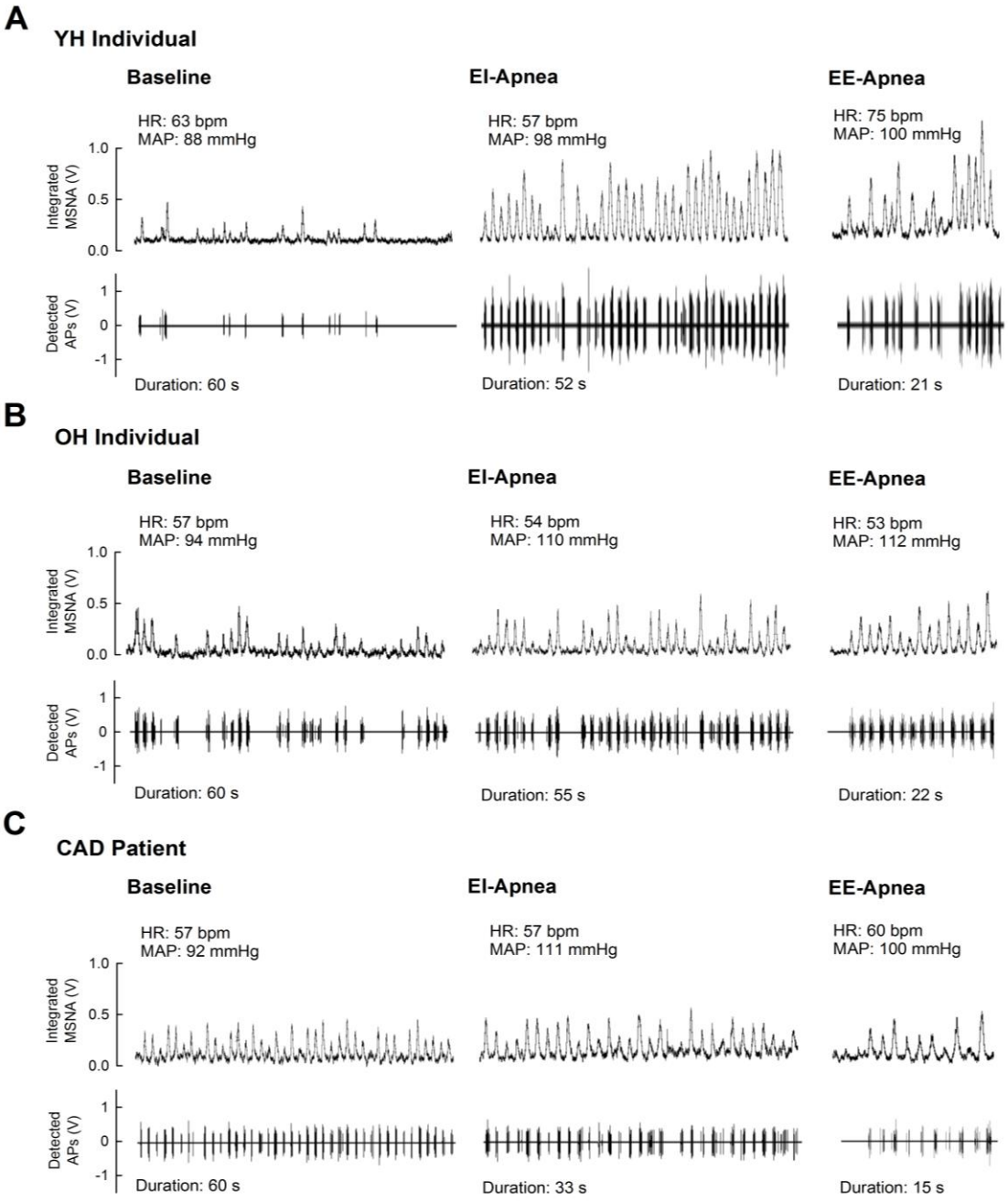

Figure 4.1: Representative recordings of the integrated muscle sympathetic nerve activity (MSNA) neurogram and detected action potentials (APs) from one young healthy (YH) individual (A), one older healthy (OH) individual (B), and one coronary artery disease (CAD) patient (C) at baseline and during end-inspiratory (EI) and end-expiratory (EE) apnea.

HR, heart rate; MAP, mean arterial pressure; bpm, beats per minute.

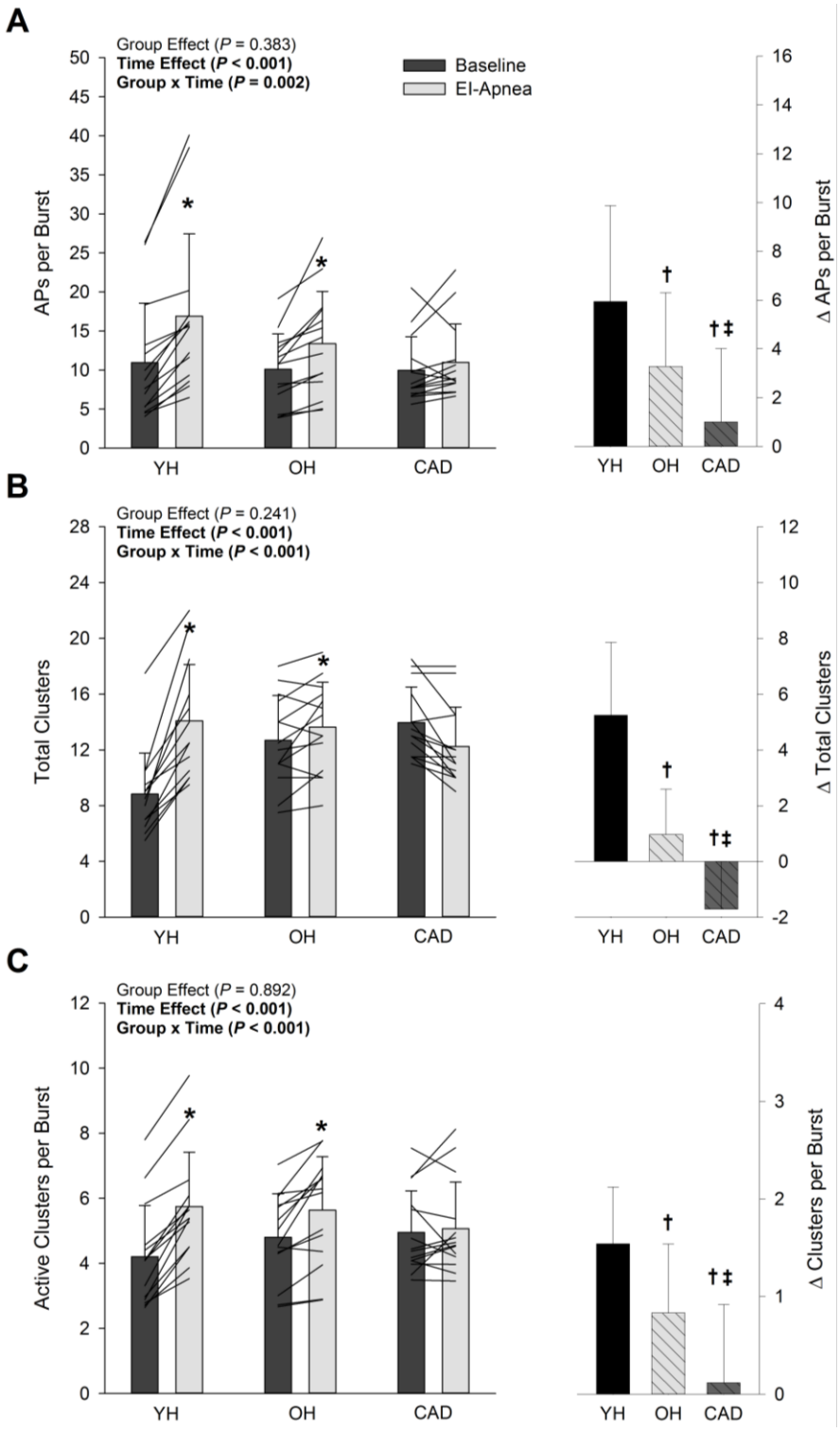

Figure 4.2: Action potential (AP) content per burst (A), total clusters (B), and active clusters per burst (C) in young healthy (YH), older healthy (OH), and

coronary artery disease (CAD) patients at baseline and during end-inspiratory (EI) apnea.

Left panel; individual lines represent individual data. Right panel represents the absolute delta change from baseline to EI-apnea. *Significantly different from baseline, $P < 0.01$. †Significantly different from YH, $P < 0.01$. ‡Significantly different from OH, $P < 0.01$.

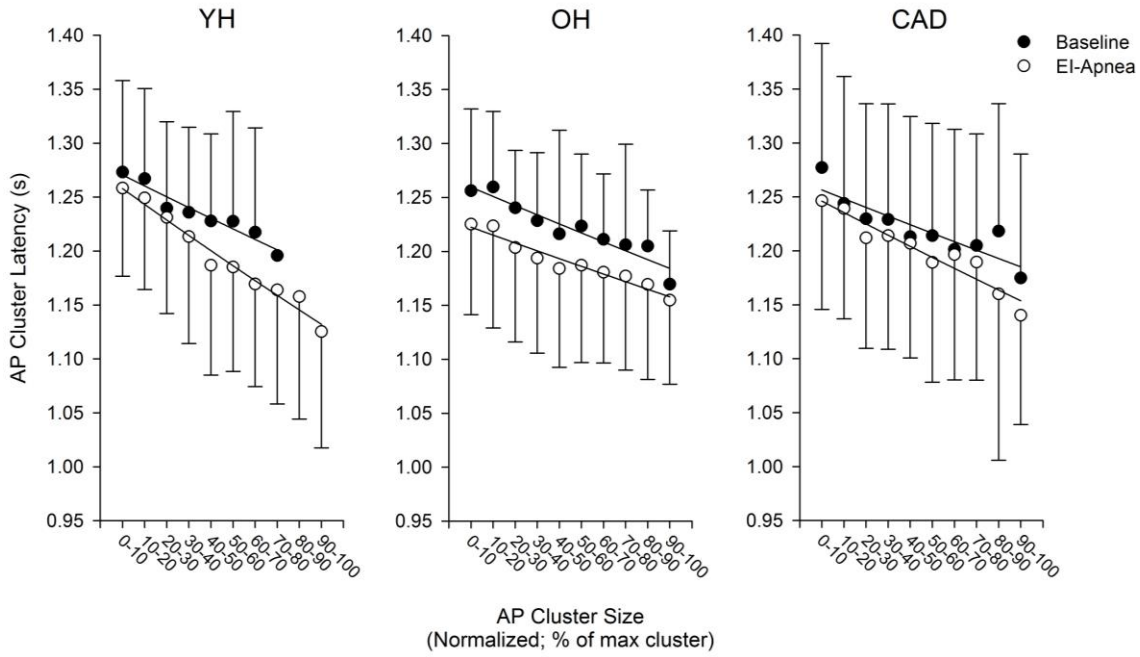

Figure 4.3: Action potential (AP) cluster latency as a function of normalized cluster number (i.e., size) at baseline and during end-inspiratory (EI) apnea in young healthy (YH; left panel), older healthy (OH; middle panel), and coronary artery disease patients (CAD; right panel).

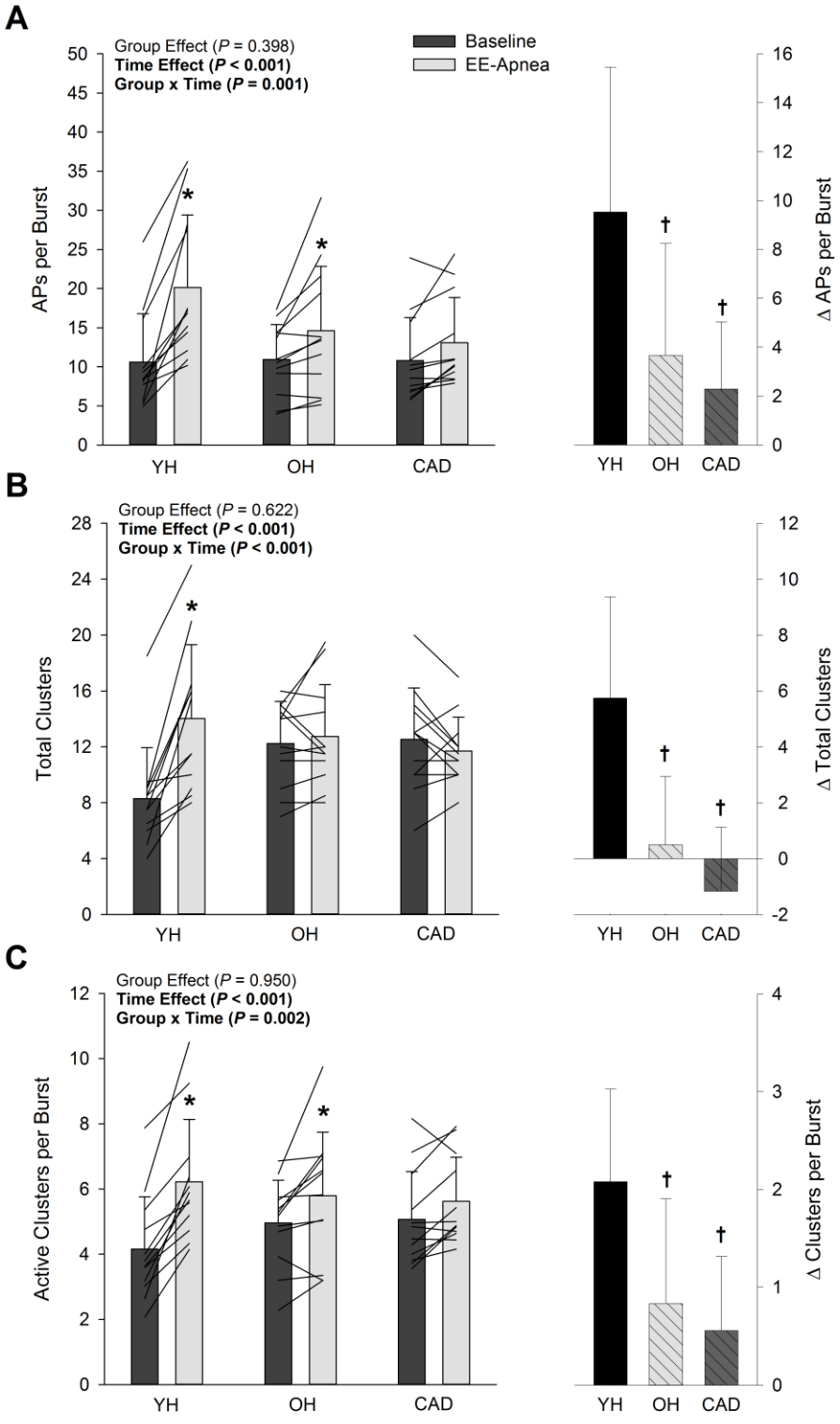

Figure 4.4: Action potential (AP) content per burst (A), total clusters (B), and active clusters per burst (C) in young healthy (YH), older healthy (OH), and

coronary artery disease (CAD) patients at baseline and during end-expiratory (EE) apnea.

Left panel; individual lines represent individual data. Right panel represents the absolute delta change from baseline to EE-apnea. *Significantly different from baseline, $P < 0.01$. †Significantly different from YH, $P < 0.01$.

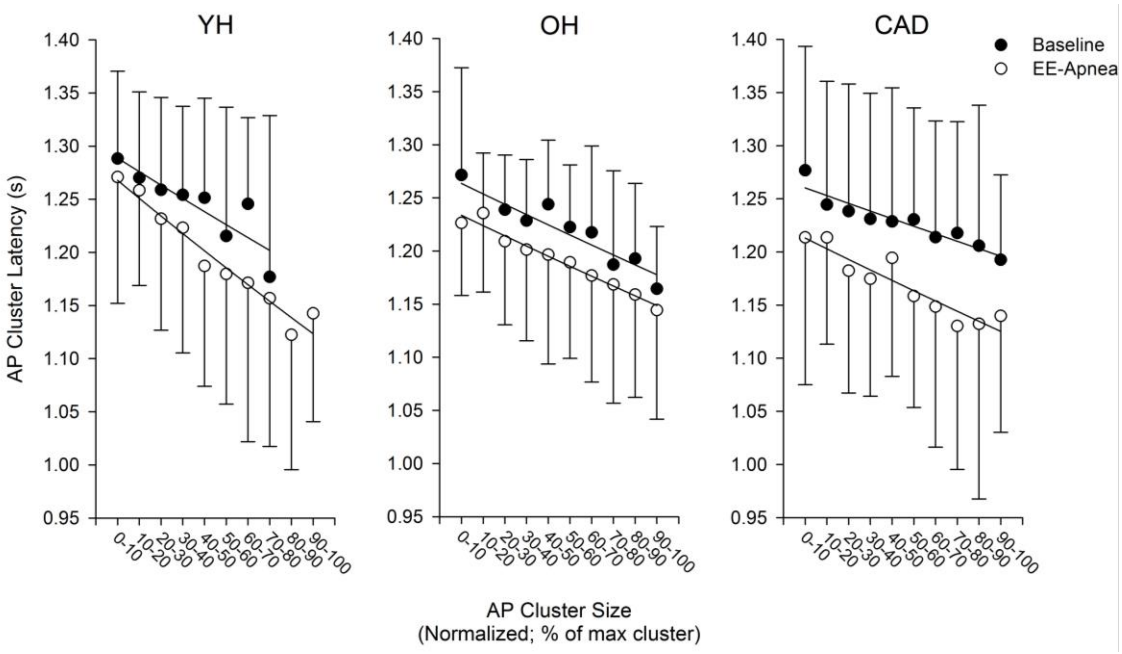

Figure 4.5: Action potential (AP) cluster latency as a function of normalized cluster number (i.e., size) at baseline and during end-expiratory (EE) apnea in young healthy (YH; left panel), older healthy (OH; middle panel), and coronary artery disease patients (CAD; right panel).

4.4 Discussion

The novel findings of the current work are: 1) compared with young individuals, the ability to increase within-burst firing frequency of already recruited sympathetic fibres was reduced with aging and CAD; 2) the capacity of the sympathetic nervous system to recruit sub-populations of previously silent and faster conducting fibres was reduced with aging and lost in CAD; and 3) the ability to acutely modify synaptic delays and/or central processing times appears preserved with aging and CAD. Taken together, this work supports the hypothesis that cardiovascular disease impairs sympathetic recruitment during apneic stress.

Voluntary apnea represents a robust stimulus for efferent sympathetic outflow through various mechanisms including hypoxia and hypercapnia-induced chemoreceptor activation, removal of the inhibitory influence of lung-stretch receptors, and an increased central drive-to-breathe (Somers *et al.* 1989; Hardy *et al.* 1994; Steinback *et al.* 2010*a*). Early work from single-unit recordings demonstrated that the homeostatic adjustment to apnea involves an increased neural firing frequency and probability, as well as an increase in the incidence of multiple within-burst firing of single axons (Macefield & Wallin, 1999). Our previous work (Steinback *et al.* 2010*b*; Breskovic *et al.* 2011; Badrov *et al.* 2015), and the results from the current study using a multi-unit approach, are in agreement with this finding, at least in YH individuals. Although both OH individuals and CAD patients achieved an elevation in total sympathetic outflow through increased frequency and incidence of AP firing during apnea, the ability to increase the number of APs per sympathetic burst was reduced with

healthy aging and lost in CAD patients. Therefore, the impact of CAD appears to be additive to normal age-related changes in central autonomic integration.

Previously, we observed recruitment of latent sub-populations of larger and faster conducting sympathetic axons during periods of severe autonomic stress, elicited via voluntary apnea (Steinback *et al.*, 2010*b*; Breskovic *et al.* 2011; Badrov *et al.* 2015) and by −80 mmHg lower body negative pressure (Salmanpour *et al.* 2011*a*; Badrov *et al.* 2015). However, the current work extends this knowledge to pathological states with known sympathetic dysregulation. In accordance with previous work (Maslov *et al.* 2012; Maslov *et al.* 2014), we show here that older individuals have a reduced capacity to recruit these latent neural sub-populations compared with their young counterparts, while the ability to do so is further reduced and perhaps lost all together in CAD. The mechanism of this dysregulation is unknown. One possibility is that the elevation in efferent sympathetic outflow at rest observed with healthy aging and cardiovascular disease is, in part, mediated by the additional recruitment of these latent sub-populations, thereby reducing the residual capacity for further recruitment during acute physiological stress. However, the capacity for neural recruitment was not hindered in otherwise healthy, younger subjects with high baseline MSNA (~75 bursts/100 hb) (Macefield & Wallin, 1999), discounting the possibility that a ceiling effect impairs the ability to observe normal recruitment patterns. Furthermore, if these larger axons were already recruited at rest, one may presume that older individuals and CAD patients would have greater AP content per sympathetic burst during baseline resting conditions; however, this was not the case in our study. These observations point to abnormal central features of neural recruitment with healthy aging and perhaps more so with

cardiovascular disease, rather than a loss of sympathetic reserve due to elevated resting sympathetic outflow.

Synaptic delay variations and/or altered central processing times appear to exist as a third recruitment strategy used by the sympathetic nervous system to modify efferent sympathetic outflow in the face of physiological challenge (Salmanpour *et al.* 2011*b*; Badrov *et al.* 2015). The current observations replicate earlier observations (Badrov *et al.* 2015), in that voluntary apnea caused an acute downward shift in the AP cluster size-latency relationship in YH individuals, such that all APs with similar peak-to-peak amplitudes were recruited with a shorter latency during the reflex-mediated stress. Previous reports indicate that single axons display large latency variations at rest (Macefield *et al.* 1994), and that reflex latency can change acutely with stress (Coote & Macleod, 1974; Fagius *et al.* 1987). The multi-unit approach used here suggests that a systemic and coordinated change in synaptic delay can occur as well. Interestingly, this systemic downward shift in the AP cluster size-latency profile with apnea was preserved with aging, as well as CAD, suggesting that, in contrast to actual recruitment, the option for synaptic delay variations is preserved in these individuals. The location(s) or source of the change in synaptic delay during apnea-induced stress remains unknown, but may be due to the direct activation of the rostral ventrolateral medulla from the nucleus tractus solitarius (Koshiya *et al.* 1993) specific to chemoreceptor activation, and/or the presence of faster conduction velocities within spinal descending pathways specific to chemoreceptor stimulation (~5.5 m/s) versus baroreceptor activation (~3.3 m/s) (Jänig & Szulczyk, 1979).

Methodological Considerations

Whether the recruitment impairment in OH individuals and CAD patients was due to a smaller reflex stimulus, or to the pathology, cannot be determined specifically from the current analysis. In the context of stimulus strength, variations in the apnea stimulus may have influenced the between-group variations reported in the current study. As mentioned above, the determinants of the apnea autonomic response are not certain and may include the magnitude of chemoreflex stress, loss of lung-stretch afferent activity, or an emotional drive to breathe (Somers *et al.* 1989; Hardy *et al.* 1994; Steinback *et al.* 2010*a*), and various factors influence the breakpoint for voluntary apnea (Parkes, 2006). In this context, lack of arterial blood gas measures represents a potential limitation of the current study. Although the apnea duration varied within and amongst groups, they were each of maximal voluntary duration and elicited near-maximal levels of burst probability; therefore, these represent maximal sympathetic efforts. Furthermore, in the current study, EI- and EE-apnea duration correlated poorly with indexes of AP recruitment. While apnea duration related significantly to the total clusters response ($r = 0.554$) to EI-apnea (but not EE-apnea; $r = 0.297$), this was no longer the case when the effects of age and CAD were accounted for. Therefore, at least in our data set, variations in apnea duration are an unlikely determinant of the current observations.

Second, as is commonly practiced (Macefield *et al.* 1999; Murai *et al.* 2009; Maslov *et al.* 2014), CAD patients were studied during their standard pharmacological treatment, and no data exist regarding the effect of medications on sympathetic neural recruitment strategies. However, medication use is a ‘life-long’ therapy for CAD patients, increasing the relevance of studying these participants in the

pharmacologically treated state. In addition, all OH individuals studied currently were unmedicated and still displayed impaired central recruitment. If the pharmacological treatment in CAD was causing the further detriment in recruitment observed in CAD versus OH during EI-apnea, one would expect the same further detriment in recruitment during EE-apnea; however, this was not the case. Taken together, these observations provide evidence to the fact that anti-hypertensive medications are unlikely to be playing a role in our observed findings.

Furthermore, CAD patients had greater body mass index (BMI) than their YH and OH counterparts, and increased BMI has been known to alter baseline integrated MSNA (Scherrer *et al.* 1994). Whether elevated BMI affects AP recruitment patterns remains unknown; however, in the current study, BMI correlated poorly to all but one indice of sympathetic recruitment, suggesting it did not play a role in our observed findings. Nonetheless, when all subjects were pooled, BMI was correlated moderately to the total cluster response to EI- ($r = 0.441$, $P = 0.003$) and EE- ($r = 0.371$, $P = 0.026$) apnea. However, when accounting for age and incidence of CAD, BMI no longer predicted the total cluster response to either apnea. In addition, these aberrant AP recruitment patterns were observed within two to four months of the coronary event, and their persistence will require additional study.

Finally, we acknowledge that the use of only one sympathoexcitatory reflex limits the applicability of the apnea outcomes to other important reflexes, and therefore, future study should assess responses to additional reflex stimuli (i.e., baroreflex, metaboreflex, cold pressor test, etc.) to determine if the observed impairment in central

recruitment with aging and cardiovascular disease is specific to apneic stress or a generalized pattern across reflexes.

Summary

Autonomic nervous system dysregulation represents a hallmark of increasing age and cardiovascular disease. Studied primarily under resting conditions, healthy aging and cardiovascular disease are characterized by chronic sympathetic activation, and this state has deleterious consequences for overall health and prognosis. For the first time, the current data indicate that this sympathetic dysfunction extends to the neural coding strategies used by the sympathetic nervous system to respond to acute homeostatic challenge. Specifically, the sympathetic nervous system normally has options to increase the firing of already-recruited axons, recruit latent sub-populations of higher-threshold and faster conducting axons, and modify acutely synaptic delays in response to autonomic arousal. The ability to acutely modify synaptic delays and/or central processing times appears preserved with aging and CAD. However, the ability to increase firing frequency and probability of low-threshold axons is reduced with healthy aging and more so with CAD. Furthermore, the ability to recruit previously silent sub-populations is reduced with increasing age and perhaps lost altogether with CAD. As such, CAD augments the impact of age on recruitment strategies employed by the sympathetic nervous system.

4.5 References

Ashley C, Burton D, Sverrisdottir YB, Sander M, McKenzie DK & Macefield VG (2010). Firing probability and mean firing rates of human muscle vasoconstrictor neurones are elevated during chronic asphyxia. *J Physiol* **588,** 701-712.

Badrov MB, Usselman CW & Shoemaker JK (2015). Sympathetic neural recruitment strategies: responses to severe chemoreflex and baroreflex stress. *Am J Physiol Regul Integr Comp Physiol* **309,** R160-R168.

Barman SM & Gebber GL (2000). "Rapid" rhythmic discharges of sympathetic nerves: sources, mechanisms of generation, and physiological relevance. *J Biol Rhythms* **15,** 365-379.

Barretto AC, Santos AC, Munhoz R, Rondon MU, Franco FG, Trombetta IC, Roveda F, de Matos LN, Braga AM, Middlekauff HR & Negrão CE (2009). Increased muscle sympathetic nerve activity predicts mortality in heart failure patients. *Int J Cardiol* **135,** 302-307.

Breskovic T, Steinback CD, Salmanpour A, Shoemaker JK & Dujic Z (2011). Recruitment pattern of sympathetic neurons during breath-holding at different lung volumes in apnea divers and controls. *Auton Neurosci* **164,** 74-81.

Coote JH & Macleod VH (1974). Evidence for the involvement in the baroreceptor reflex of a descending inhibitory pathway. *J Physiol* **241,** 477-496.

Elam M & Macefield VG (2001). Multiple firing of single muscle vasoconstrictor neurons during cardiac dysrhythmias in human heart failure. *J Appl Physiol* **91,** 717-724.

Elam M, McKenzie D & Macefield VG (2002). Mechanisms of sympathoexcitation: single-unit analysis of muscle vasoconstrictor neurons in awake OSAS subjects. *J Appl Physiol* **93,** 297-303.

Fagius J, Sundlöf G & Wallin BG (1987). Variation of sympathetic reflex latency in man. *J Auton Nerv Syst* **21,** 157-165.

Ferrigno M, Hickey DD, Liner MH & Lundgren CE (1986). Cardiac performance in humans during breath holding. *J Appl Physiol* **60,** 1871-1877.

Grassi G, Seravalle G, Dell'Oro R & Mancia G (2011). Sympathetic mechanisms, organ damage, and antihypertensive treatment. *Curr Hypertens Rep* **13,** 303-308.

Grassi G, Seravalle G & Mancia G (2015). Sympathetic activation in cardiovascular disease: evidence, clinical impact and therapeutic implications. *Eur J Clin Invest* **45,** 1367-1375.

Greenwood JP, Stoker JB & Mary DA (1999). Single-unit sympathetic discharge: quantitative assessment in human hypertensive disease. *Circulation* **100,** 1305-1310.

Hagbarth KE & Vallbo AB (1968). Pulse and respiratory grouping of sympathetic impulses in human muscle nerves. *Acta Physiol Scand* **74,** 96-108.

Hardy JC, Gray K, Whisler S & Leuenberger U (1994). Sympathetic and blood pressure responses to voluntary apnea are augmented by hypoxemia. *J Appl Physiol* **77,** 2360-2365.

Jänig W & McLachlan EM (1992). Characteristics of function-specific pathways in the sympathetic nervous system. *Trends Neurosci* **15,** 475-481.

Jänig W & Szulczyk P (1979). Conduction velocity in spinal descending pathways of baro- and chemoreceptor reflex. *J Auton Nerv Syst* **1,** 149-160.

Koshiya N, Huangfu D & Guyenet PG (1993). Ventrolateral medulla and sympathetic chemoreflex in the rat. *Brain Res* **609,** 174-184.

Macefield VG, Rundqvist B, Sverrisdottir YB, Wallin BG & Elam M (1999). Firing properties of single muscle vasoconstrictor neurons in the sympathoexcitation associated with congestive heart failure. *Circulation* **100,** 1708-1713.

Macefield VG & Wallin BG (1999). Firing properties of single vasoconstrictor neurones in human subjects with high levels of muscle sympathetic activity. *J Physiol* **516,** 293-301.

Macefield VG, Wallin BG & Vallbo AB (1994). The discharge behaviour of single vasoconstrictor motoneurones in human muscle nerves. *J Physiol* **481,** 799-809.

Maslov P, Shoemaker JK & Dujic Z (2014). Firing patterns of muscle sympathetic neurons during apnea in chronic heart failure patients and healthy controls. *Auton Neurosci* **180,** 66-69.

Maslov PZ, Breskovic T, Brewer DN, Shoemaker JK & Dujic Z (2012). Recruitment pattern of sympathetic muscle neurons during premature ventricular contractions in heart failure patients and controls. *Am J Physiol Regul Integr Comp Physiol* **303,** R1157-R1164.

Murai H, Takamura M, Maruyama M, Nakano M, Ikeda T, Kobayashi D, Otowa K, Ootsuji H, Okajima M, Furusho H, Takata S & Kaneko S (2009). Altered firing pattern of single-unit muscle sympathetic nerve activity during handgrip exercise in chronic heart failure. *J Physiol* **587,** 2613-2622.

Murai H, Takata S, Maruyama M, Nakano M, Kobayashi D, Otowa K, Takamura M, Yuasa T, Sakagami S & Kaneko S (2006). The activity of a single muscle sympathetic vasoconstrictor nerve unit is affected by physiological stress in humans. *Am J Physiol Heart Circ Physiol* **290,** H853-H860.

Parkes MJ (2006). Breath-holding and its breakpoint. *Exp Physiol* **91,** 1-15.

Pauletto P, Scannapieco G & Pessina AC (1991). Sympathetic drive and vascular damage in hypertension and atherosclerosis. *Hypertension* **17,** III75-III81.

Salmanpour A, Brown LJ & Shoemaker JK (2010). Spike detection in human muscle sympathetic nerve activity using a matched wavelet approach. *J Neurosci Methods* **193,** 343-355.

Salmanpour A, Brown LJ, Steinback CD, Usselman CW, Goswami R & Shoemaker JK. (2011*a*) Relationship between size and latency of action potentials in human muscle sympathetic nerve activity. *J Neurophysiol* **105,** 2830-2842.

Salmanpour A, Frances MF, Goswami R & Shoemaker JK (2011*b*). Sympathetic neural recruitment patterns during the Valsalva maneuver. *Conf Proc IEEE Eng Med Biol Soc* **2011,** 6951-6954.

Scherrer U, Randin D, Tappy L, Vollenweider P, Jéquier E & Nicod P (1994). Body fat and sympathetic nerve activity in healthy subjects. *Circulation* **89,** 2634-2640.

Scott DW (1979). On optimal and data-based histograms. *Biometrika* **66,** 605-610.

Seals DR & Esler MD (2000). Human ageing and the sympathoadrenal system. *J Physiol* **528,** 407-417.

Shoemaker JK, Badrov MB, Al-Khazraji BK & Jackson DN (2016). Neural control of vascular function in skeletal muscle. *Compr Physiol* **6,** 303-329.

Somers VK, Mark AL, Zavala DC & Abboud FM (1989). Influence of ventilation and hypocapnia on sympathetic nerve responses to hypoxia in normal humans. *J Appl Physiol* **67,** 2095-2100.

Steinback CD, Breskovic T, Frances M, Dujic Z & Shoemaker JK (2010*a*). Ventilatory restraint of sympathetic activity during chemoreflex stress. *Am J Physiol Regul Integr Comp Physiol* **299,** R1407-R1414.

Steinback CD, Salmanpour A, Breskovic T, Dujic Z & Shoemaker JK (2010*b*). Sympathetic neural activation: an ordered affair. *J Physiol* **588,** 4825-4836.

Tukey J (1977). Exploratory Data Analysis. Addison-Wesley, Reading.

Chapter 5

5 Ventilation inhibits sympathetic action potential recruitment even during severe chemoreflex stress

5.1 Introduction

The chemoreflex represents a highly coordinated and integrative pattern of response to systemic hypoxia and/or hypercapnia that ultimately regulates and defends perfusion to critical organs and tissues within the body. As such, the homeostatic challenges presented by central and/or peripheral chemoreceptor stimulation are corrected through reflexive increases in ventilation, as well as autonomic circulatory arousal (Guyenet, 2014). Indeed, the compensatory response to chemoreflex activation involves large elevations in efferent sympathetic nerve outflow directed to skeletal muscle (i.e., muscle sympathetic nerve activity; MSNA) and other vascular beds (Saito *et al.* 1988; Malpas & Ninomiya, 1992*a*,*b*; Morgan *et al.* 1995; Leuenberger *et al.* 2005). Furthermore, the sympathetic response to voluntary apnea and/or pathological apnea (i.e., obstructive sleep apnea) is large (Morgan *et al.* 1993; Hardy *et al.* 1994; Leuenberger *et al.* 1995; Steinback *et al.* 2010*b*) and, in turn, has been linked to poor clinical outcomes (Kara *et al.* 2003).

The mechanisms mediating the robust sympathetic response to apnea remain uncertain and appear to be diverse. Indeed, one fundamental issue is the identification of the specific roles played by the ventilatory response (or the lack thereof in the case of volitional apnea) versus the chemoreflex activation itself. For example, voluntary apnea potentiated the sympathetic response to isocapnic hypoxia, indicating the sympathoinhibitory nature of ventilation (Somers *et al.* 1989*a*,*b*). Furthermore, the

chemoreflex stimulus to typical 20- to 30-second apneas in untrained breath-hold performers is rather unremarkable (Leuenberger *et al.* 2005; Heusser *et al.* 2009; Seitz *et al.* 2013), yet the MSNA response is large; therefore, factors other than chemoreflex stress must be involved in eliciting sympathetic activation. The possible factors affecting the sympathoinhibitory effect of ventilation during chemoreflex stimulation may include central pathways that coordinate respiratory drive with sympathetic inhibition. Evidence for such pathways has been difficult to find in humans (St. Croix *et al.* 1999), whereby MSNA is inhibited during inspiration (or at high lung volumes) and increases during expiration (or at low lung volumes) (Eckberg *et al.* 1985; Seals *et al.* 1993); however, current evidence in the intact human argues against a significant role played by central respiratory drive on the ventilatory modulation of MSNA (Seals *et al.* 1993; St. Croix *et al.* 1999). In contrast, such pathways can be induced in anesthetized rodents (Numao *et al.* 1987; Haselton & Guyenet, 1989; Darnall & Guyenet, 1990), leading Guyenet (Guyenet *et al.* 2010; Guyenet 2014) to speculate that species differences exist. Nonetheless, current evidence suggests that the sympathetic response to apnea has more to do with the lack of breathing rather than the chemoreflex stimulus *per se*.

Yet, much remains uncertain regarding the interactions between chemoreflex stress and ventilation on sympathetic neuro-circulatory control. For example, the degree of chemoreflex stress may be an important caveat in understanding the role of respiratory movements in sympathetic control. The central motor hypothesis has been studied in humans mainly under normoxic and normocapnic conditions (St. Croix *et al.* 1999) or low levels of hypercapnia (Seals *et al.* 1993), raising the possibility that

potentiation of central pathways associated with the drive-to-breathe and sympathetic inhibition with breathing may be augmented with concurrent chemoreflex activation. Observations arguing against this possibility are provided from our earlier study (Steinback *et al.* 2010*a*), in which the very large sympathetic responses occurring during prolonged apnea at functional residual capacity (FRC), performed by elite breath-hold divers, were acutely inhibited by a two-breath rebreathe protocol performed immediately following the apnea, despite a sustained chemoreflex stimulus. However, the acute versus chronic effects were not studied, nor was it determined whether this has to do with reduction of the emotional component of resisting the breathing movements, the absence of lung-stretch during apnea, or the actual degree of chemoreflex stimulus (Steinback *et al.* 2010*a*).

In addition, the mode of studying sympathetic nerve activity likely has an impact on determinations of chemoreflex versus ventilatory control over sympathetic nerve recruitment. Indeed, early work from single-unit action potential (AP) recordings demonstrated that the sympathetic adjustment to apnea involves not only an increase in neural firing probability, but also, a shift towards greater within-burst firing of single axons (Macefield & Wallin, 1999). Therefore, the content and variability of sympathetic APs within and between integrated bursts more accurately represents the neural signal, and ultimately, reflects the neural discharge and recruitment patterns used by the central nervous system to fine-tune sympathetic outflow. The need to study AP behaviour becomes especially relevant when one considers that burst frequency, reflecting the rate of discharge, and burst size, reflecting the number and/or size of recruited APs (Ninomiya *et al.* 1993; Salmanpour *et al.* 2011), may be differentially

regulated during chemoreflex stress, emphasizing increases in burst size (i.e., AP recruitment) (Malpas *et al.* 1996; Lim *et al.* 2015). Using a multi-unit AP approach, we have found that the central recruitment strategies used to alter sympathetic drive in response to apneic stress involve both an increased firing of previously-recruited axons and recruitment of sub-populations of larger, latent axons (Steinback *et al.* 2010*b*; Breskovic *et al.* 2011; Badrov *et al.* 2015; Badrov *et al.* 2016*a*). However, whether neural recruitment is restrained and/or inhibited in the presence of ventilation remains unknown.

Therefore, the objective of the current investigation was to determine the influence of ventilation on sympathetic AP recruitment during varying levels of high chemoreflex stress. To do so, we studied sympathetic AP discharge during apnea at FRC (i.e., absence of ventilation) and during asphyxic rebreathing (i.e., presence of ventilation) in trained breath-hold divers. Trained breath-hold divers were studied because of their unique ability to perform apneas for prolonged periods of time and their capacity to endure high levels of chemoreflex stress (Heusser *et al.* 2009). We tested the hypothesis that the sympathoinhibitory effect of ventilation on chemoreflex-induced sympathetic activation is limited to mild chemoreflex stress. If so, then it can be expected that for similar levels of chemoreflex stimuli, the presence of ventilation during rebreathing would restrain sympathetic AP recruitment as compared to apnea. However, during more severe rebreathe-induced chemoreflex levels, the inhibitory influence of ventilation would be overridden, such that AP recruitment would be similar to that observed during apnea.

5.2 Methods

5.2.1 Participants

Seven healthy individuals (1 female; 33±12 yr, 181±10 cm, 74±12 kg, body mass index = 22±2 kg/m^2) participated in the current investigation after providing informed written consent. Participants were non-smokers without any history of cardiovascular or respiratory disease. All studies were conducted at the University of Split, adhering to the standards set by the latest revision of the Declaration of Helsinki, and all experimental procedures were approved by the Research Ethics Board at the University of Split School of Medicine in Croatia.

5.2.2 Experimental Protocol

All experiments were conducted following a 3-hour fast and a 12-hour abstinence from caffeine, alcohol, and vigorous exercise. Participants voided their bladder immediately prior-to study. All testing was completed in the supine position. Participants were fitted with a mouthpiece (series 9060, Hans Rudolph, Kansas City, MO) connected to a three-way valve, allowing them to breathe either room air, or through a Y-connector (VacuMed, Ventura, CA) leading to two 3-litre breathing bags. An infrared probe connected to a pulse oximeter (Poet II, Criticare Systems, Waukesha, WI) was applied to the index finger to monitor arterial oxygen saturation (i.e., hemoglobin saturation; HbSat). Respiratory gases were analyzed using an infrared carbon dioxide sensor and optical oxygen detector fed from a damped micro-vacuum sampling pump (ML206 Gas Analyzer, ADInstruments, Colorado Springs, CO) and calibrated using ambient air pressure values, which were converted to online measurements of oxygen (PO_2) and carbon dioxide (PCO_2) partial pressures. End-tidal

values for PO_2 ($P_{ET}O_2$) and PCO_2 ($P_{ET}CO_2$) were acquired using peak parameters software (LabChart7; ADInstruments, Colorado Springs, CO).

Participants completed three protocols in random order, each separated by five minutes of recovery. Prior-to the onset of each protocol, participants expired into the breathing bags to fill them with air for an ensuing rebreathing period. The first protocol (i.e., apnea protocol) assessed the impact of high levels of chemoreflex stress on sympathetic axonal recruitment in the absence of ventilation. Specifically, following three minutes of baseline data collection, the three-way valve was turned at end-expiration to begin an initial period of rebreathing, in an attempt to maximize the severity of chemoreflex stimulation incurred during the ensuing apnea period (Usselman *et al.* 2013; Badrov *et al.* 2015). This initial rebreathe period continued until $P_{ET}O_2$ reached 70 Torr, at which point participants performed an end-expiratory apnea at FRC until they achieved ~85% of their self-perceived 'maximal' tolerance for the maneuver. Upon cessation, participants breathed twice into and out of the breathing bags for the measurement of end-apnea $P_{ET}O_2$ and $P_{ET}CO_2$. Average apnea duration in the current study was 89±18 seconds. The second protocol (i.e., rebreathing protocol) assessed the impact of chemoreflex stress on sympathetic axonal recruitment in the presence of ventilation. Specifically, following three minutes of baseline data collection, the three-way valve was turned to initiate rebreathing and participants were instructed to rebreathe until, once again, they achieved ~85% of their self-perceived 'maximal' tolerance for the maneuver. Finally, a third protocol (FRC-RBR_{ALT} protocol; n=6) was completed in which baseline data were collected for two minutes, followed by

alternating 30-second periods of FRC apnea and rebreathing until ~85% maximal tolerance.

5.2.3 Experimental Measures

Multi-unit recordings of MSNA were obtained from the right peroneal nerve by microneurography (Hagbarth & Vallbo, 1968) (662C-3; Bioengineering of University of Iowa, Iowa City, IA), using standard methodology described in detail elsewhere (Badrov *et al.* 2015). Heart rate (HR) was determined from a standard three-lead electrocardiogram. Continuous beat-to-beat blood pressure was obtained throughout all protocols using finger photoplethysmography (Finometer; Finapres Medical Systems, Amsterdam, The Netherlands), the values of which were calibrated to manual sphygmomanometry values taken at baseline. Stroke volume (SV) and cardiac output (CO) were determined using the Finometer Modelflow algorithm (Wesseling *et al.*, 1993) and total peripheral resistance (TPR) was calculated as the quotient of mean arterial pressure (MAP) and CO. All data were collected using LabChart7 and PowerLab data acquisition system (ADInstruments, Colorado Springs, CO).

5.2.4 Data Analysis

As a first aim, the study addressed the effect of the ‘absence or presence’ of ventilation on sympathetic neural recruitment during similar (i.e., matched) levels of chemoreflex stress. To address this aim, data were analyzed from the apnea protocol for the 3-minute baseline period, the rebreathe period (i.e., until 70 Torr $P_{ET}O_2$), and the second half of the FRC apnea maneuver (i.e., FRC_{Apnea}). For the rebreathe protocol, data were analyzed for the 3-minute baseline period, the initial rebreathe period (i.e., until 70 Torr $P_{ET}O_2$), and during the period of continued rebreathe that corresponded to

the same HbSat levels incurred during the second half of FRC_{Apnea} (i.e., $RBR_{Matched}$). Therefore, this represents the FRC_{Apnea} versus $RBR_{Matched}$ comparison at the same level of chemoreflex stress, as inferred from the HbSat values (i.e., because $P_{ET}CO_2$ could not be measured in the FRC_{Apnea} component).

The second aim determined the influence of ventilation on sympathetic neural recruitment at more severe levels of chemoreflex stress than that induced by FRC_{Apnea}. Therefore, we compared data from the second half of the FRC_{Apnea} protocol, as above, to data observed at the end of the continued rebreathe protocol (i.e., RBR_{End}). The duration of data studied in the RBR_{End} period was matched to that of the last half of the FRC_{Apnea}, used in the first aim. Therefore, this represents the FRC_{Apnea} versus RBR_{End} comparison.

A third aim addressed the issue that the apnea or continued rebreathe protocols always occurred at the end of each protocol, and therefore, this aim compared alternating periods of FRC apnea with rebreathe during progressively increasing chemoreflex stress. For the FRC-RBR_{ALT} protocol, as the number of alternating FRC apnea and rebreathe periods differed between participants, the 2-minute baseline and the final three FRC apnea and rebreathe periods for each participant were used for analysis.

MSNA data were analyzed in two manners. First, the integrated neurogram was quantified as per traditional methodology. Second, we studied the patterns of change in APs from the filtered raw MSNA signal as per our approach detailed previously (Salmanpour *et al.* 2010). Integrated sympathetic bursts were identified as exhibiting a

pulse-synchronous burst pattern, having a signal-to-noise ratio of at least 2:1 with respect to the previous period of neural silence, presenting with characteristic rising and falling slopes, and having APs visible in the corresponding raw and filtered neurograms. Integrated sympathetic activity was quantified using burst frequency (the number of bursts per minute), burst incidence (the number of bursts per 100 heartbeats; hb), burst amplitude (normalized to the largest burst recorded at baseline, which was given a value of 100), and total MSNA (the product of normalized burst amplitude and burst frequency).

For the analysis of sympathetic AP patterns, wavelet-based methodology was used to detect and extract APs from the filtered raw MSNA signal (Salmanpour *et al.* 2010). Specifically, as described in detail previously (Steinback *et al.* 2010*b*; Salmanpour *et al.* 2011; Badrov *et al.* 2015), a continuous wavelet transform was used, in which a "mother wavelet" (adapted from actual physiological recordings of postganglionic sympathetic APs) was applied to the filtered raw MSNA neurogram to identify and extract APs at their point of occurrence. Next, extracted APs were ordered based on their peak-to-peak amplitude into 'clusters' (i.e., bins of similarly-sized APs) (Scott, 1979). Within participants, cluster characteristics were normalized within (i.e., baseline to rebreathe to maneuver) and between (i.e., FRC_{Apnea} vs. $RBR_{Matched}$ vs. RBR_{End}) protocols to ensure that bin width, maximum bin center, and the total number bins would be identical across conditions. This procedure ensured that corresponding clusters within and between protocols contain APs with the same peak-to-peak amplitude. Therefore, within protocols (i.e., baseline to rebreathe to maneuver), an increase in the number of total clusters represents recruitment of latent sub-populations

of larger-sized axons not present at baseline, whereas between protocols (i.e., FRC_{Apnea} vs. $RBR_{Matched}$ vs. RBR_{End}), a greater number of total clusters represents further recruitment of these latent sub-populations as compared to other protocols. Sympathetic AP patterns were quantified using AP frequency (the number of APs per minute), while sympathetic AP recruitment was expressed using the mean AP content per integrated sympathetic burst (APs/burst), the number of active AP clusters per integrated sympathetic burst (clusters/burst), and the number of total AP clusters (total clusters). Based on previous validation analysis of our technique (Salmanpour *et al.* 2010), the average signal-to-noise ratio in the current study (i.e., 4.8±0.6) is expected to produce a correct AP detection rate of >90% and a false positive rate of <3%.

5.2.5 Statistical Analysis

All statistical analyses were performed using SigmaPlot 12.0 (Systat Software, San Jose, CA). All data were normally distributed as confirmed by Shapiro-Wilk tests. Two-way repeated measures ANOVAs assessed the effect of protocol (i.e., FRC_{Apnea} vs. $RBR_{Matched}$; FRC_{Apnea} vs. RBR_{End}) vs. time (i.e., baseline vs. rebreathe vs. maneuver). For the FRC-RBR_{ALT} protocol, one-way repeated measures ANOVAs assessed the effect of time (i.e., baseline vs. FRC vs. RBR). Bonferroni corrected post-hoc procedures were used to assess specific differences between means, when appropriate. Statistical significance was set at $P<0.05$ and all data are presented as means ± SD.

5.3 Results

Figure 5.1 displays representative recordings of the integrated MSNA neurogram and detected APs (and associated chemoreflex stimuli) from one individual during the FRC apnea and rebreathing protocols.

FRC_{Apnea} vs. $RBR_{Matched}$. Both FRC_{Apnea} and $RBR_{Matched}$ elicited large reductions in HbSat (Table 5.1; $P < 0.001$) at end-maneuver. By design, HbSat levels were similar (i.e., matched) between maneuvers (71 ± 6 vs. 71 ± 6%; P = NS). Compared to baseline, $P_{ET}CO_2$ (FRC_{Apnea}: +17 ± 2 Torr; $RBR_{Matched}$: +19 ± 2 Torr; both $P < 0.001$) increased, while $P_{ET}O_2$ (FRC_{Apnea}: −68 ± 7 Torr; $RBR_{Matched}$: −84 ± 7 Torr; both $P < 0.001$) decreased, during FRC_{Apnea} and $RBR_{Matched}$.

Integrated MSNA indexes during the baseline, rebreathe, and maneuver periods of the FRC_{Apnea} and $RBR_{Matched}$ protocols are outlined in Table 5.2. Specifically, compared to baseline, burst frequency (FRC_{Apnea}: +29 ± 7 bursts/min; $RBR_{Matched}$: +12 ± 9 bursts/min; both $P < 0.01$) and burst incidence (FRC_{Apnea}: +52 ± 16 bursts/100 hb; $RBR_{Matched}$: +14 ± 12 bursts/100 hb; both $P < 0.05$) increased during both maneuvers; however, values of burst frequency and burst incidence were greater during FRC_{Apnea} than $RBR_{Matched}$ (both $P < 0.001$). Similarly, burst amplitude (FRC_{Apnea}: +165 ± 85%; $RBR_{Matched}$: +69 ± 55%; both $P < 0.01$) increased above baseline levels during both maneuvers, though levels were greater during FRC_{Apnea} ($P < 0.001$). As such, compared to baseline, total MSNA was elevated during both maneuver periods (FRC_{Apnea}: +695 ± 397%; $RBR_{Matched}$: +336 ± 481%; both $P < 0.05$); yet, once again, levels of total MSNA were greater during FRC_{Apnea} ($P < 0.001$).

Figure 5.2 presents the sympathetic AP discharge indexes during the baseline, rebreathe, and maneuver periods of the FRC_{Apnea} and $RBR_{Matched}$ protocols. Specifically, compared to baseline, AP frequency (FRC_{Apnea}: +1122 ± 534 APs/min; $RBR_{Matched}$: +328 ± 172 APs/min; both $P < 0.05$) increased during both maneuvers; however, AP frequency was greater during FRC_{Apnea} compared to $RBR_{Matched}$ (1304 ± 534 vs. 511 ± 167 APs/min; $P < 0.001$). This increase in AP frequency was due to the elevated levels of burst frequency, but also, an increase in the AP content per integrated sympathetic burst (FRC_{Apnea}: +18 ± 7 APs/burst; $RBR_{Matched}$: +7 ± 3 APs/burst; both $P < 0.01$) during both maneuvers, as compared to baseline. The AP content per integrated sympathetic burst, however, was greater during FRC_{Apnea} than $RBR_{Matched}$ (28 ± 9 vs. 18 ± 4 APs/burst; $P < 0.001$). Furthermore, when APs were binned according to peak-to-peak amplitude (i.e., into clusters), the number of total AP clusters increased during FRC_{Apnea} (+10 ± 2 total clusters; $P < 0.001$), but not during $RBR_{Matched}$ (+1 ± 2 total clusters; P = NS). As such, the number of total AP clusters was greater during FRC_{Apnea} ($P < 0.001$). Finally, the number of active clusters per burst (FRC_{Apnea}: +4 ± 2 clusters/burst; $RBR_{Matched}$: +2 ± 1 clusters/burst; both $P < 0.01$) was elevated above baseline levels during both maneuvers, though levels were greater during FRC_{Apnea} than $RBR_{Matched}$ ($P < 0.01$).

The hemodynamic responses to both maneuvers were consistent with the sympathetic response patterns as shown in Table 5.1. Specifically, compared to baseline, MAP (FRC_{Apnea}: +18 ± 9 mmHg; $RBR_{Matched}$: +10 ± 7 mmHg; both $P < 0.01$) increased during both maneuvers; yet, the pressor response was greater during FRC_{Apnea} ($P < 0.001$). The greater pressor response was associated with a greater TPR during

FRC_{Apnea} ($P < 0.001$). HR decreased during FRC_{Apnea} and increased during $RBR_{Matched}$ (both $P < 0.05$), whereas reductions in SV were similar between maneuvers (P = NS). Subsequently, compared to baseline, CO decreased during FRC_{Apnea} ($P < 0.001$), but remained unchanged during $RBR_{Matched}$ (P = NS).

FRC_{Apnea} vs. RBR_{End}. By design, when rebreathing was allowed to continue and analyzed at the end (i.e., RBR_{End}), the RBR_{End} maneuver elicited a larger reduction in HbSat versus FRC_{Apnea} (56 ± 13 vs. 71 ± 6%; $P < 0.001$; Table 5.3). Similarly, larger increases in $P_{ET}CO_2$ (FRC_{Apnea}: +17 ± 2 Torr; RBR_{End}: +21 ± 3 Torr; both $P < 0.001$), and larger decreases in $P_{ET}O_2$ (FRC_{Apnea}: −68 ± 7 Torr; RBR_{End}: −94 ± 4 Torr; both $P < 0.001$), were observed during RBR_{End} compared to FRC_{Apnea} (Table 5.3; both $P < 0.001$).

Table 5.4 outlines the integrated MSNA indexes during the baseline, rebreathe, and maneuver periods of the FRC_{Apnea} and RBR_{End} protocols. Compared to baseline, burst frequency (FRC_{Apnea}: +29 ± 7 bursts/min; RBR_{End}: +32 ± 17 bursts/min; both $P < 0.001$) increased to similar levels during both maneuvers (P = NS), whereas burst incidence (FRC_{Apnea}: +52 ± 16 bursts/100 hb; $RBR_{Matched}$: +33 ± 17 bursts/100 hb; both $P < 0.001$) increased to a greater extent during FRC_{Apnea} than RBR_{End} ($P = 0.001$). Burst amplitude (FRC_{Apnea}: +165 ± 85%; RBR_{End}: +103 ± 46%; both $P < 0.01$) increased above baseline levels during both maneuvers, though levels were greater during FRC_{Apnea} than RBR_{End} ($P < 0.05$). Finally, compared to baseline, total MSNA was elevated during both maneuver periods (FRC_{Apnea}: +695 ± 397%; RBR_{End}: +785 ± 903%; both $P < 0.01$); however, levels of total MSNA were not different during FRC_{Apnea} and RBR_{End} (P = NS).

Sympathetic AP discharge indexes during the baseline, rebreathe, and maneuver periods of the FRC_{Apnea} and RBR_{End} protocols are displayed in Figure 5.3. Compared to baseline, AP frequency (FRC_{Apnea}: +1122 ± 534 APs/min; RBR_{End}: +912 ± 429 APs/min; $P < 0.001$) increased during both maneuvers; however, AP frequency was not different during FRC_{Apnea} and RBR_{End} (1304 ± 534 vs. 1095 ± 423 APs/min; *P* = NS). Once again, the increased AP frequency was due to the elevated burst frequency, but also, an increase in the AP content per integrated sympathetic burst (FRC_{Apnea}: +18 ± 7 APs/burst; RBR_{End}: +11 ± 5 APs/burst; both $P < 0.001$) during both maneuvers, as compared to baseline. However, the AP content per integrated sympathetic burst was greater during FRC_{Apnea} than RBR_{End} (28 ± 9 vs. 23 ± 5 APs/burst; $P < 0.05$). Furthermore, when APs were binned according to peak-to-peak amplitude (i.e., into clusters), the number of total AP clusters increased during FRC_{Apnea} (+10 ± 2 total clusters; $P < 0.001$) and RBR_{End} (+6 ± 4 total clusters; $P < 0.001$); yet, total AP clusters was greater during FRC_{Apnea} ($P < 0.01$). Finally, the number of active clusters per burst (FRC_{Apnea}: +4 ± 2 clusters/burst; RBR_{End}: +2 ± 1 clusters/burst; both $P < 0.001$) was elevated above baseline levels during both maneuvers, whereby no differences were observed during FRC_{Apnea} versus RBR_{End} (*P* = NS).

The hemodynamic responses to FRC_{Apnea} and RBR_{End} are shown in Table 5.3. Compared to baseline, MAP (FRC_{Apnea}: +18 ± 9 mmHg; $RBR_{Matched}$: +20 ± 12 mmHg; both $P < 0.001$) increased similarly during both maneuvers (*P* = NS). However, this pressor response was achieved differently for FRC_{Apnea} and RBR_{End}. Specifically, compared to baseline, TPR increased during FRC_{Apnea} ($P < 0.001$), but not during RBR_{End} (*P*=NS), whereas CO was increased during RBR_{End} ($P < 0.01$), but decreased

during FRC_{Apnea} ($P < 0.001$). The latter was due to an increase in HR ($P < 0.001$) during RBR_{End} versus no change during FRC_{Apnea} (P = NS), and a similar decrease in SV during both maneuvers (both $P < 0.001$).

FRC-RBR$_{ALT}$. Figure 5.4 displays representative recordings of the integrated MSNA neurogram and detected APs (and associated chemoreflex stimuli) from one individual during the FRC-RBR_{ALT} protocol. HbSat levels were decreased versus baseline during each of the final two FRC and RBR periods of the FRC-RBR_{ALT} protocol (Table 5.5; all $P < 0.001$). Compared to baseline, $P_{ET}CO_2$ was increased and $P_{ET}O_2$ decreased during each FRC and RBR period (Table 5.5; all $P < 0.001$). No differences existed between corresponding periods of FRC and RBR for HbSat or $P_{ET}CO_2$ and $P_{ET}O_2$ levels (all P = NS).

Table 5.6 displays the integrated MSNA indexes during baseline and FRC and RBR periods of the FRC-RBR_{ALT} protocol. Specifically, compared to baseline, all integrated MSNA variables were elevated during each FRC (all $P < 0.001$), but not during any of the three RBR periods (all P = NS). As such, every corresponding FRC-RBR period was associated with greater levels of integrated MSNA during FRC versus RBR (all $P < 0.001$).

Sympathetic AP discharge indexes at baseline and during the FRC and RBR periods of the FRC-RBR_{ALT} protocol are shown in Figure 5.5. Compared to baseline, all AP indices were increased during each FRC (all $P < 0.001$), but not during any RBR period (all P = NS). Therefore, every corresponding FRC-RBR period was associated with greater AP recruitment during FRC than RBR (all $P < 0.001$).

Finally, the hemodynamic responses to the FRC-RBR$_{ALT}$ protocol are provided in Table 5.5. Compared to baseline, MAP increased during the final FRC and RBR periods (both $P < 0.001$), whereas TPR increased during each FRC (all $P < 0.001$), but not during RBR (all P = NS). HR was reduced during the final FRC versus the final RBR ($P < 0.001$), whereas SV remained unchanged throughout the FRC-RBR$_{ALT}$ protocol (all P = NS). CO decreased during each FRC ($P < 0.001$), was above baseline levels during the first RBR period ($P < 0.001$), but not in each of the final two RBR periods (both P = NS).

Table 5.1: Hemodynamic responses to FRC_{Apnea} and $RBR_{Matched}$ protocols

	Baseline	Rebreathe	Maneuver
MAP (mmHg)			
FRC_{Apnea}	87±3	89±3	105±9*†
$RBR_{Matched}$	87±3	88±2	97±6*
HR (beats/min)			
FRC_{Apnea}	70±14	68±13	60±9*†
$RBR_{Matched}$	68±12	66±13	75±19*
SV (mL)			
FRC_{Apnea}	97±20	90±18	84±18
$RBR_{Matched}$	96±19	91±19	86±24
CO (L/min)			
FRC_{Apnea}	6.6±1.3	6.0±1.0	5.0±0.7*†
$RBR_{Matched}$	6.4±0.9	5.9±0.8	6.1±0.9
TPR (mmHg/L/min)			
FRC_{Apnea}	13.5±2.3	15.1±2.1	21.6±3.3*†
$RBR_{Matched}$	13.7±1.7	15.2±1.9	16.1±2.8*
HbSat (%)			
FRC_{Apnea}	99.5±0.3	97.2±1.5	71.3±6.3
$RBR_{Matched}$	99.5±0.4	97.5±1.8	71.3±6.3
$P_{ET}CO_2$ (Torr)			
FRC_{Apnea}	27±6	41±5*	44±4*†
$RBR_{Matched}$	28±6	40±6*	47±5*
$P_{ET}O_2$ (Torr)			
FRC_{Apnea}	118±5	66±5*	50±5*†
$RBR_{Matched}$	117±7	68±6*	33±3*

Values are mean ± SD. MAP, mean arterial pressure; HR, heart rate; SV, stroke volume; CO, cardiac output; TPR, total peripheral resistance; HbSat, hemoglobin saturation; $P_{ET}CO_2$, end-tidal partial pressure of carbon dioxide; $P_{ET}O_2$, end-tidal partial pressure of oxygen. *Significantly different from baseline, $P < 0.05$; †Significantly different from $RBR_{Matched}$, $P < 0.05$. Effects of time were found for SV and HbSat, whereby the maneuver periods were reduced versus baseline, both $P \leq 0.001$.

Table 5.2: Integrated MSNA responses to FRC_{Apnea} and $RBR_{Matched}$ protocols

	Baseline	Rebreathe	Maneuver
Burst Frequency (bursts/min)			
FRC_{Apnea}	17±5	17±6	46±8*†
$RBR_{Matched}$	16±7	17±6	28±7*
Burst Incidence (bursts/100 hb)			
FRC_{Apnea}	25±10	26±11	77±15*†
$RBR_{Matched}$	24±13	26±11	38±11*
Burst Amplitude (AU)			
FRC_{Apnea}	50±10	53±9	127±32*†
$RBR_{Matched}$	51±4	63±15	87±33*
Total MSNA (AU/min)			
FRC_{Apnea}	832±298	877±251	5774±1572*†
$RBR_{Matched}$	780±386	1019±307	2496±1434*

Values are mean ± SD. MSNA, muscle sympathetic nerve activity; hb, heart beats; AU, arbitrary units. *Significantly different from baseline, $P < 0.05$; †Significantly different from $RBR_{Matched}$, $P < 0.001$.

Table 5.3: Hemodynamic responses to FRC_{Apnea} and RBR_{End} protocols

	Baseline	Rebreathe	Maneuver
MAP (mmHg)			
FRC_{Apnea}	87±3	89±3	105±9
RBR_{End}	87±3	88±2	106±11
HR (beats/min)			
FRC_{Apnea}	70±14	68±13	60±9†
RBR_{End}	68±12	66±13	84±23*
SV (mL)			
FRC_{Apnea}	97±20	90±18	84±18
RBR_{End}	96±19	91±19	87±23
CO (L/min)			
FRC_{Apnea}	6.6±1.3	6.0±1.0	5.0±0.7*†
RBR_{End}	6.4±0.9	5.9±0.8	7.0±1.1
TPR (mmHg/L/min)			
FRC_{Apnea}	13.5±2.3	15.1±2.1	21.6±3.3*†
RBR_{End}	13.7±1.7	15.2±1.9	15.5±2.1
HbSat (%)			
FRC_{Apnea}	99.5±0.3	97.2±1.5	71.3±6.3*†
RBR_{End}	99.5±0.4	97.5±1.8	51.9±13.1*
$P_{ET}CO_2$ (Torr)			
FRC_{Apnea}	27±6	41±5*	44±4*†
RBR_{End}	28±6	40±6*	49±6*
$P_{ET}O_2$ (Torr)			
FRC_{Apnea}	118±5	66±5*	50±5*†
RBR_{End}	117±7	68±6*	23±5*

Values are mean ± SD. MAP, mean arterial pressure; HR, heart rate; SV, stroke volume; CO, cardiac output; TPR, total peripheral resistance; HbSat, hemoglobin saturation; $P_{ET}CO_2$, end-tidal partial pressure of carbon dioxide; $P_{ET}O_2$, end-tidal partial pressure of oxygen. *Significantly different from baseline, $P < 0.01$; †Significantly different from RBR_{End}, $P < 0.01$. An effect of time was found for MAP, whereby the rebreathe and maneuver period were greater than baseline, both $P < 0.001$. An effect of time was found for SV, whereby the maneuver period was reduced versus baseline, $P < 0.001$.

Table 5.4: Integrated MSNA responses to FRC_{Apnea} and RBR_{End} protocols

	Baseline	Rebreathe	Maneuver
Burst Frequency (bursts/min)			
FRC_{Apnea}	17±5	17±6	46±8
RBR_{End}	16±7	17±6	47±15
Burst Incidence (bursts/100 hb)			
FRC_{Apnea}	25±10	26±11	77±15*†
RBR_{End}	24±13	26±11	57±15*
Burst Amplitude (AU)			
FRC_{Apnea}	50±10	53±9	127±32*†
RBR_{End}	51±4	63±15	104±29*
Total MSNA (AU/min)			
FRC_{Apnea}	832±298	877±251	5774±1572
RBR_{End}	780±386	1019±307	5170±2745

Values are mean ± SD. MSNA, muscle sympathetic nerve activity; hb, heart beats; AU, arbitrary units. *Significantly different from baseline, $P < 0.05$; †Significantly different from RBR_{End}, $P < 0.001$. Effects of time were found for burst frequency and total MSNA, whereby the rebreathe and maneuver periods were greater than baseline, all $P < 0.001$.

Table 5.5: Hemodynamic responses to the FRC-RBR$_{ALT}$ protocol

	Baseline	FRC_1	RBR_1	FRC_2	RBR_2	FRC_3	RBR_3
MAP (mmHg)	88±3	92±3	88±3	96±7	96±6	105±11*	101±10*
HR (beats/min)	63±6	57±7	63±7	60±9	66±11	58±10†	69±12
SV (mL)	97±23	88±21	88±21	87±24	87±24	90±28	91±26
CO (L/min)	6.0±1.1	5.0±0.9*	5.4±0.9*	5.1±1.1*	5.6±0.8	5.1±1.0*†	6.1±0.8
TPR (mmHg/L/min)	15.1±2.6	19.2±3.9*	16.4±2.2	20.0±4.0*	17.6±3.0	21.5±5.6*†	17.0±3.2
HbSat (%)	99.5±0.5	95.3±2.3	95.3±3.5	88.6±5.5*	88.7±6.9*	75.9±2.9*	72.1±11.9*
$P_{ET}CO_2$ (Torr)	28±7	40±3*	41±4*	44±4*	44±5*	47±5*	48±7*
$P_{ET}O_2$ (Torr)	114±12	67±11*	69±11*	50±4*	50±10*	40±4*	36±8*

Values are mean ± SD. FRC, functional residual capacity apnea; RBR, rebreathe; MAP, mean arterial pressure; HR, heart rate; SV, stroke volume; CO, cardiac output; TPR, total peripheral resistance; HbSat, hemoglobin saturation; $P_{ET}CO_2$, end-tidal partial pressure of carbon dioxide; $P_{ET}O_2$, end-tidal partial pressure of oxygen. *Significantly different from baseline, $P<0.001$; †Significantly different from corresponding RBR period, $P<0.001$.

Table 5.6: Integrated MSNA responses to the FRC-RBR$_{ALT}$ protocol

	Baseline	FRC_1	RBR_1	FRC_2	RBR_2	FRC_3	RBR_3
BF (bursts/min)	18±7	40±7*†	14±7	41±6*†	20±7	53±8*†	19±8
BI (bursts/100 hb)	29±10	69±9*†	22±12	69±13*†	30±10	91±8*†	27±9
BA (AU)	54±12	75±18*	54±7	92±13*†	62±9	135±28*†	80±18*
Total MSNA (AU/min)	931±327	2997±969*†	726±339	3760±827*†	1262±515	7076±1498*†	1427±540

Values are mean ± SD. MSNA, muscle sympathetic nerve activity; FRC, functional residual capacity apnea; RBR, rebreathe; BF, burst frequency; BI, burst incidence; hb, heart beats; BA, burst amplitude; AU, arbitrary units. *Significantly different from baseline, $P < 0.001$; †Significantly different from corresponding RBR period, $P < 0.001$.

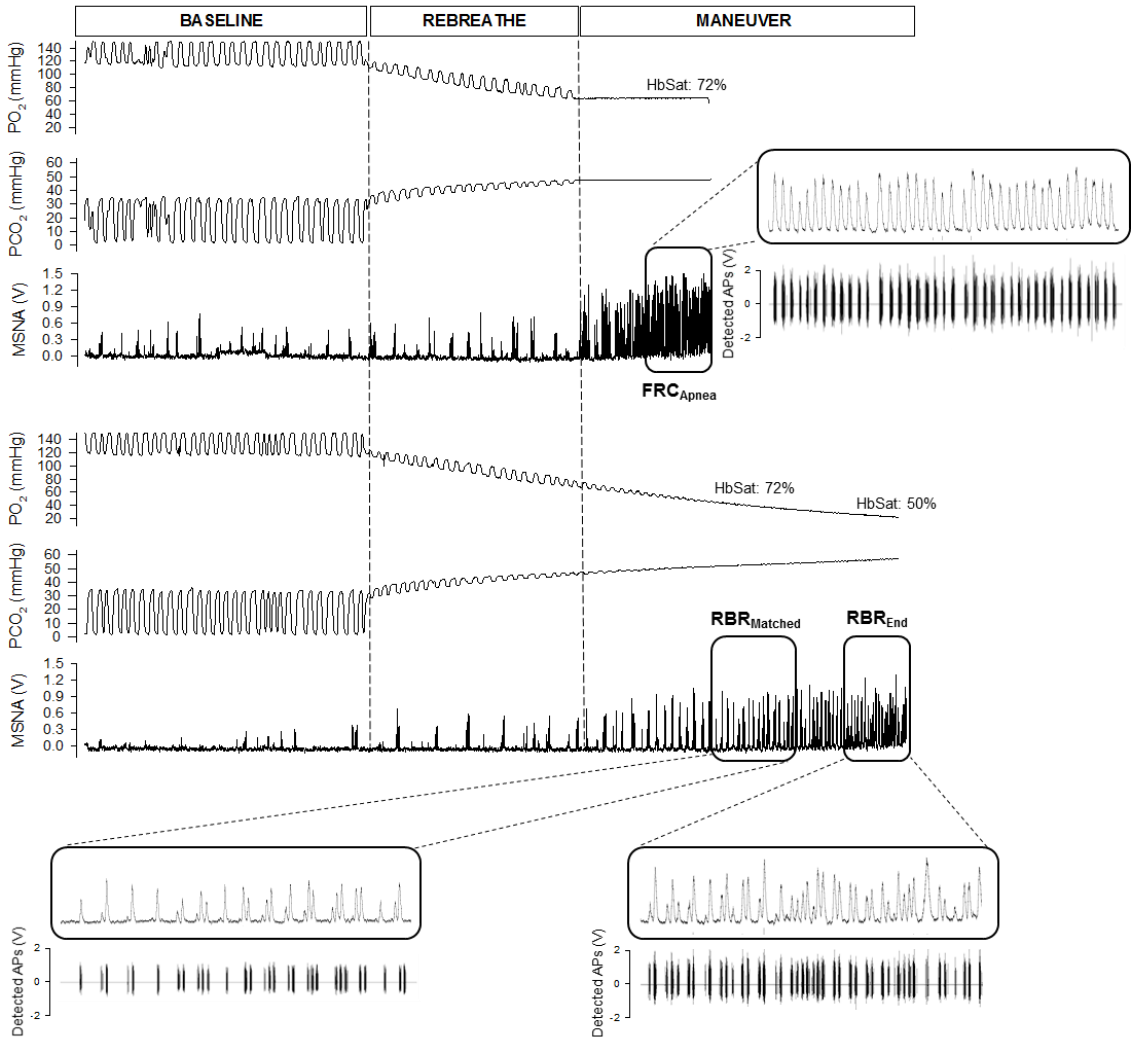

Figure 5.1: Representative recordings of the integrated muscle sympathetic nerve activity (MSNA) neurogram and detected action potentials (APs) (and associated chemoreflex stimuli) from one individual during the functional residual capacity (FRC) apnea and rebreathing protocols.

PO_2, partial pressure of oxygen; PCO_2, partial pressure of carbon dioxide; HbSat, hemoglobin saturation. Highlighted (i.e., boxed) areas represent portions of the maneuver used for analysis.

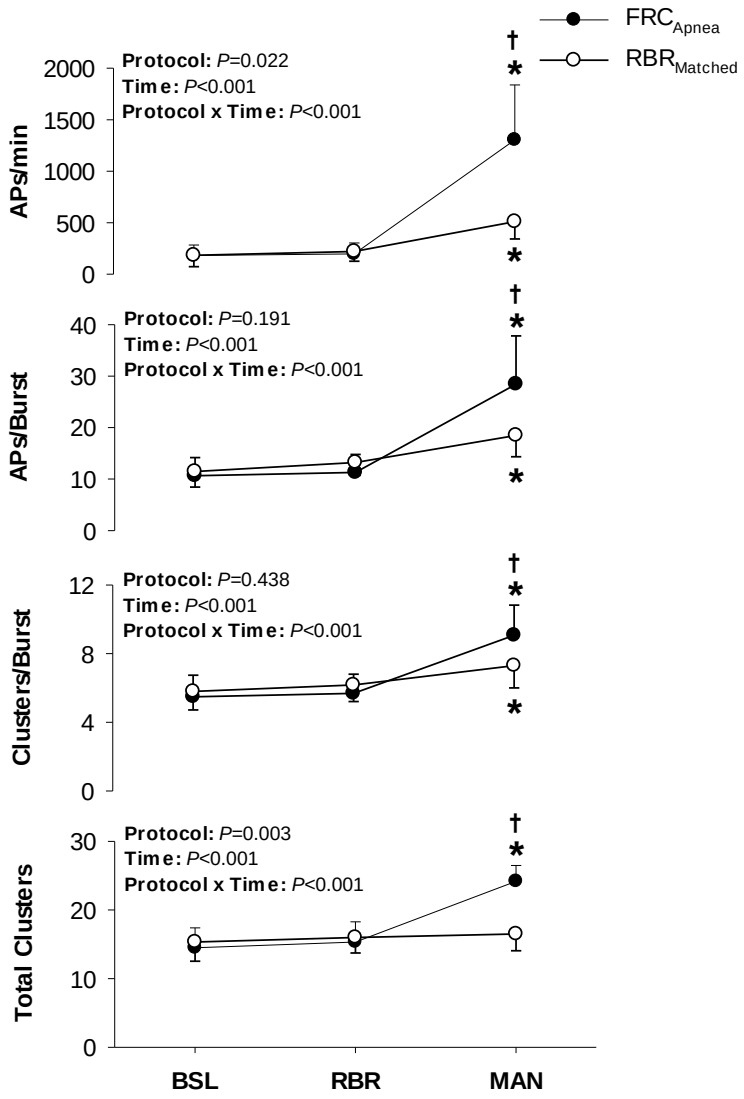

Figure 5.2: Sympathetic action potential (AP) recruitment during baseline (BSL), initial rebreathe (RBR), and maneuver (MAN) periods of the FRC_{Apnea} and $RBR_{Matched}$ protocols.

*Significantly different from BSL, $P < 0.05$; †Significantly different from $RBR_{Matched}$, $P < 0.01$.

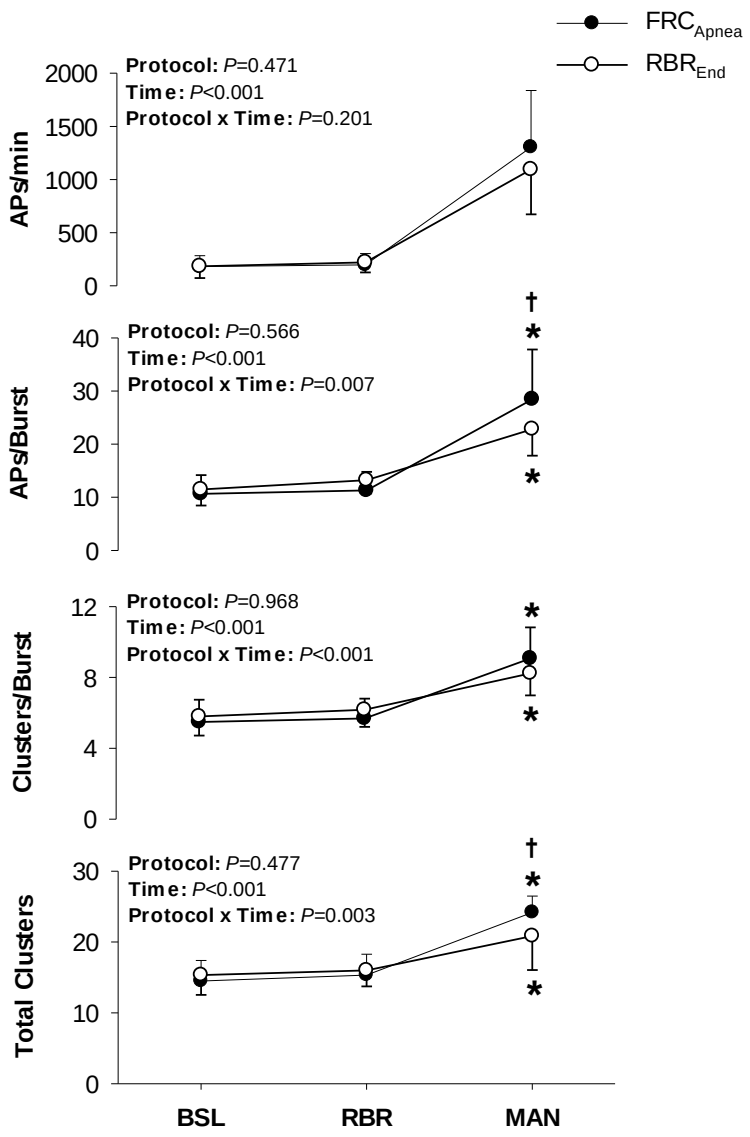

Figure 5.3: Sympathetic action potential (AP) recruitment during baseline (BSL), initial rebreathe (RBR), and maneuver (MAN) periods of the FRC_{Apnea} and RBR_{End} protocols.

*Significantly different from BSL, $P < 0.05$; †Significantly different from RBR_{End}, $P < 0.01$.

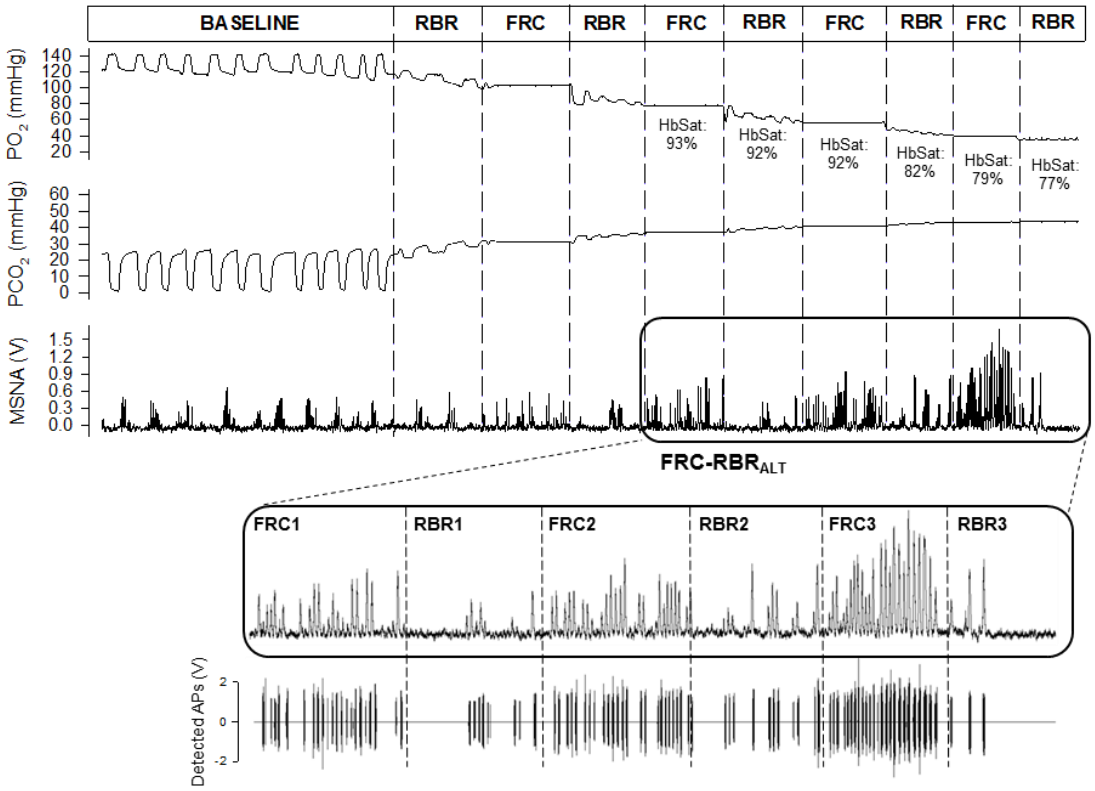

Figure 5.4: Representative recordings of the integrated muscle sympathetic nerve activity (MSNA) neurogram and detected action potentials (APs) (and associated chemoreflex stimuli) from one individual during the alternating functional residual capacity (FRC) apnea and rebreathe (RBR) protocol (i.e., FRC-RBR$_{ALT}$).

PO_2, partial pressure of oxygen; PCO_2, partial pressure of carbon dioxide; HbSat, hemoglobin saturation. Highlighted (i.e., boxed) area represents the portion of the maneuver used for analysis.

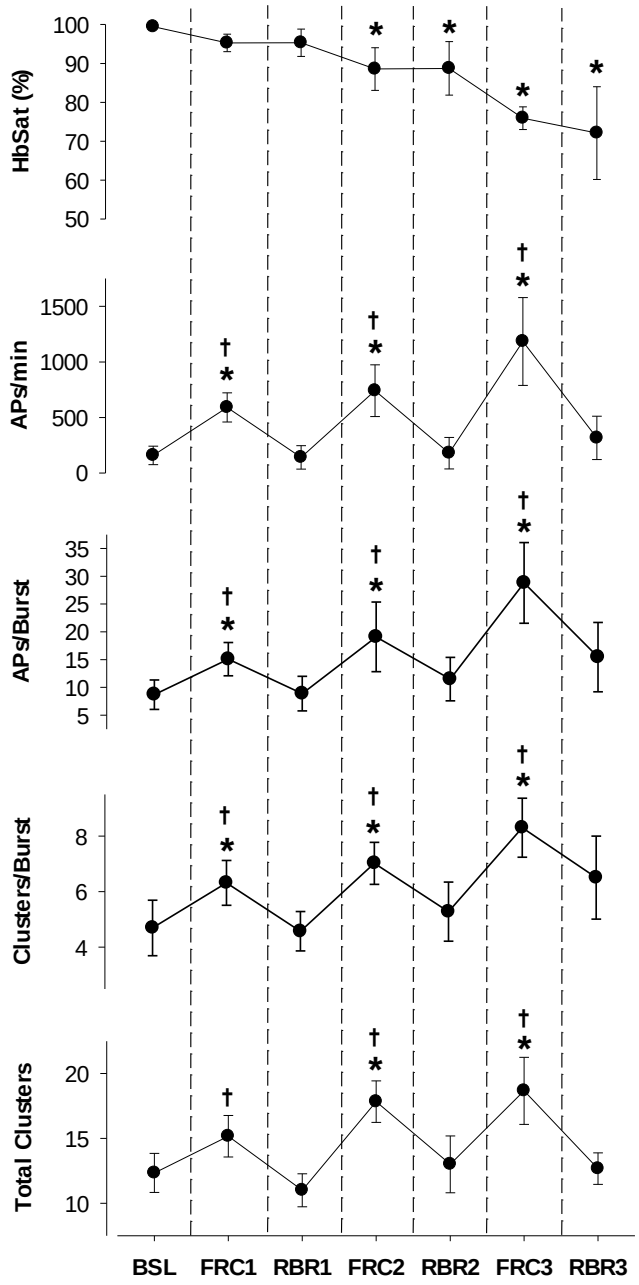

Figure 5.5: Sympathetic action potential (AP) recruitment during baseline (BSL) and alternating periods of apnea at functional residual capacity (FRC) and rebreathe (RBR).

HbSat, hemoglobin saturation. *Significantly different from BSL, $P < 0.001$; †Significantly different from corresponding RBR, $P < 0.001$.

5.4 Discussion

The current study was designed to study the dissociated influences of chemoreceptor stimuli (i.e., hypoxia and hypercapnia) and ventilation on sympathetic AP recruitment patterns during chemoreflex stress. First, we demonstrate that during similar levels of (high) chemoreflex stress, the act of ventilation *per se* restrained the increased firing of already-active, lower-threshold axons, and furthermore, inhibited the recruitment of latent, higher-threshold axons that appeared during apnea. Second, recruitment of previously-silent axons was observed during severe chemoreflex stimulation induced by the continued rebreathe protocol; however, sympathetic AP recruitment was still restrained as compared to apnea. Finally, during alternating periods of apnea and rebreathe, the act of rebreathing between apneas was associated with a rapid and complete withdrawal of sympathetic AP recruitment, despite the ever-increasing chemoreflex stimulus. As such, it appears that the sympathoinhibitory effect of ventilation during chemoreceptor activation extends to the central recruitment strategies used by the sympathetic nervous system to respond to homeostatic stress, whereby both the frequency of neural discharge and recruitment of latent axons are restrained/inhibited in the presence of ventilation, even at excessive levels of chemoreflex stress.

The sympathoexcitatory response to voluntary apnea is robust, and indeed, includes a powerful stimulus for efferent sympathetic axonal recruitment (Steinback *et al.* 2010*b*; Breskovic *et al.* 2011; Badrov *et al.* 2015; Badrov *et al.* 2016*a*). Chemoreceptor activation is believed to form a primary mechanism driving this response. Nevertheless, previous work demonstrates that the absence of ventilation

during apnea acts to augment this sympathetic drive (Somers *et al.* 1989*a*,*b*; Steinback *et al.* 2010*a*). Certainly, albeit indirectly, ventilation has been shown to be a powerful within-breath modulator of sympathetic neural recruitment (Seals *et al.* 1990). Specifically, during deep breathing, the typical observation of increased and decreased MSNA during expiration and inspiration, respectively (Eckberg *et al.* 1985), was extended to show that, over multiple breaths, MSNA inhibition during inspiration was compensated for by augmented burst amplitude during expiration (Seals *et al.* 1990). Therefore, the total MSNA response was not affected. Furthermore, since burst size reflects AP content (Ninomiya *et al.* 1993; Salmanpour *et al.* 2011), ventilation affects sympathetic AP synchronization and recruitment of additional and/or larger sympathetic axons (Ninomiya *et al.* 1993; Salmanpour *et al.* 2011). Our current results support the conjecture that ventilation modulates sympathetic postganglionic axonal recruitment and extend this conclusion to include high/severe levels of chemoreflex stress.

The current data illustrate, like never before, the unfailing ability of inhalation to inhibit sympathetic activity across a wide range of chemoreflex stress, at least acutely, and to inhibit AP recruitment even during what likely are the most severe cases of chemoreflex stress that can be imposed voluntarily. Specifically, replicating earlier studies (Steinback *et al.* 2010*b*; Badrov *et al.* 2015; Badrov *et al.* 2016*a*), the large increases in neural outflow during apnea were associated with increases in the within-burst firing frequency of already-recruited sympathetic fibers, as well as the recruitment of latent (i.e., not present at baseline) sub-populations of larger-sized axons. However, for similar levels of hypoxia and hypercapnia, but in the presence of ventilation (i.e.,

during $RBR_{Matched}$), these neural recruitment patterns were not achieved. Indeed, $RBR_{Matched}$ was associated with a lower firing frequency and a restrained increase in the number of APs per integrated burst, such that, overall, sympathetic AP frequency increased approximately 700% during FRC_{Apnea}, but only about 300% during $RBR_{Matched}$. Furthermore, the capacity of the sympathetic nervous system to recruit latent neural sub-populations was inhibited during $RBR_{Matched}$, despite the same chemoreflex load, indicating the profound effect of ventilation on AP recruitment patterns.

Nonetheless, the current data do support the idea that the sympathoinhibitory effect of ventilation is less effective at more severe levels of chemoreflex stress. Specifically, latent axons were recruited during the more severe chemoreflex stress induced by the continued rebreathe protocol, despite the presence of ventilation (i.e., RBR_{End}). Interestingly, in this scenario (i.e., FRC_{Apnea} vs. RBR_{End}) the total integrated MSNA response was similar between protocols but the underlying patterns of AP recruitment differed by maneuver. These data highlight the importance of studying AP behaviour and support the notion that these latent, higher-threshold axons, are reserved for severe stress scenarios (Badrov *et al.* 2015).

The protocol alternating between FRC and rebreathing further enforces the role of ventilation in AP recruitment, across many levels of progressive chemoreflex stress. In this case, all occurrences of rebreathe, despite no relief of chemical drive, were associated with an inhibition of sympathetic AP discharge to baseline levels. Specifically, while each apnea was associated with increased within-burst firing of lower-threshold axons and recruitment of latent, larger-sized axons, each subsequent

period of rebreathe was accompanied by a total withdrawal of this sympathetic AP recruitment. This withdrawal of sympathetic drive following the resumption of breathing in the face of similar and/or elevated chemical drive is consistent with findings from the integrated MSNA neurogram (Watenpaugh *et al.* 1999; Steinback *et al.* 2010*a*; Seitz *et al.* 2013). For example, Steinback et al. (2010*a*) found that sympathetic burst activity was silenced during brief periods of rebreathe following apnea. Furthermore, Seitz et al. (2013) demonstrated an immediate inhibition of MSNA following the break point of end-expiratory apnea, which was not influenced by whether subjects inhaled room air or asphyxic gas upon the resumption of breathing.

Therefore, the present data support previous findings that indicate ventilation *per se* is responsible for the sympathoinhibition across a wide range of chemoreflex stress. However, acute periods of rebreathe following apnea were associated with complete withdrawal of AP discharge, whereas when rebreathe was allowed to continue (i.e., RBR_{End} protocol), sympathetic axonal recruitment did occur over time, albeit still at lesser levels than apnea. These observations suggest that the sympathoinhibitory influence of breathing may be robust acutely, but perhaps, less effective over time as the chemoreflex load continues to extreme levels.

The mechanisms underlying the ventilatory restraint of sympathetic axonal recruitment during high levels of chemoreflex stress remain unknown and cannot be elucidated from the current results. Possible contributors include lung-stretch receptor feedback (Somers *et al.* 1989*b*) and perceptual factors associated with the stress experienced during prolonged breath-holding (Fowler, 1954; Heusser *et al.* 2009). Stated differently, the volitional effort *not* to breathe coupled with the growing desire-

to-breathe during voluntary apnea may result in a greater perception of stress than that of rebreathing, thereby influencing sympathetic drive. Callister et al. (1992) have shown that levels of perceived stress influence directly the sympathetic response during cognitive challenge. However, stress-induced sympathetic responses related to such prolonged breath-holds and chemoreflex duress produced by these elite breath-hold competitors has not been quantified. However, components of the current observations argue against a "stress" determinant of sympathetic drive during apnea. First, all participants were instructed to engage in and continue each protocol until they achieved ~85% of their self-perceived 'maximal' tolerance for the maneuver. As such, the FRC_{Apnea} and RBR_{End} protocols were 'matched' for levels of perceived stress, whereby greater AP recruitment was still observed during apnea. Second, we deliberately studied breath-hold divers who are uniquely trained to endure this level of stress and perform these maneuvers often. Thus, the fact that these were not 'maximal' efforts, combined with the participants' familiarity with the maneuvers, likely suggests that levels of perceived stress during voluntary apnea were not maximal. However, we acknowledge that the perceptual levels of stress magnitude in sympathetic activation in the context of apneas are not known. Finally, albeit in a volitional handgrip contraction and metaboreflex activation model, we have found that a central perceptual component has little to do with actual axonal recruitment, as opposed to the effects of peripheral-reflex mechanisms (Badrov *et al.* 2016*b*). Therefore, we do not regard a specific role of perceptual factors in the current results as important in the observations. Furthermore, whether a baroreflex mechanism contributed to the divergent sympathetic recruitment responses between conditions is unknown, but unlikely. Specifically, the differing AP

recruitment responses persisted despite large and similar (or slightly greater during apnea) increases in MAP during both maneuvers. Therefore, it is likely that resetting of the arterial baroreflex occurred during both maneuvers (Muenter Swift *et al.* 2003), the magnitude of which might be greater during apnea. Nonetheless, ventilation appears to modulate sympathetic axonal recruitment during high and even severe chemoreflex stress. The mechanisms mediating this restraint on sympathetic neural recruitment will require additional study.

In summary, the present study demonstrated that the sympathetic axonal recruitment strategies that are normally observed during apnea are largely restrained by the act of ventilation *per se*, despite similar and/or greater levels of high, and even, extreme, chemoreflex stress. Specifically, during severe levels of hypoxia and hypercapnia, both the frequency of within-burst firing of already-active sympathetic fibres and the recruitment of sub-populations of previously-silent, higher-threshold axons are restrained in the presence of ventilation. Therefore, the robust increases in sympathetic nerve activity seen during apnea are largely influenced by the lack of breathing itself, rather than the increasing chemical drive, although the latter undoubtedly plays a role (Hardy *et al.* 1994). Nonetheless, the pronounced sympathetic neural recruitment in response to apnea, and in turn, the large systemic vascular resistance and blood pressure response may lend important mechanistic insight into observed relationship between obstructive sleep apnea and cardiovascular disease (Kasai *et al.* 2012).

5.5 References

Badrov MB, Lalande S, Olver TD, Suskin N & Shoemaker JK (2016*a*). Effects of aging and coronary artery disease on sympathetic neural recruitment strategies during end-inspiratory and end-expiratory apnea. *Am J Physiol Heart Circ Physiol* **311**, H1040-H1050.

Badrov MB, Olver TD & Shoemaker JK (2016*b*). Central vs. peripheral determinants of sympathetic neural recruitment: insights from static handgrip exercise and postexercise circulatory occlusion. *Am J Physiol Regul Integr Comp Physiol* **311,** R1013-R1021.

Badrov MB, Usselman CW & Shoemaker JK. (2015). Sympathetic neural recruitment strategies: responses to severe chemoreflex and baroreflex stress. *Am J Physiol Regul Integr Comp Physiol* **309,** R160-R168.

Breskovic T, Steinback CD, Salmanpour A, Shoemaker JK & Dujic Z (2011). Recruitment pattern of sympathetic neurons during breath-holding at different lung volumes in apnea divers and controls. *Auton Neurosci* **164,** 74-81.

Callister R, Suwarno NO & Seals DR (1992). Sympathetic activity is influenced by task difficulty and stress perception during mental challenge in humans. *J Physiol* **454,** 373-387.

Darnall RA & Guyenet P (1990). Respiratory modulation of pre- and postganglionic lumbar vasomotor sympathetic neurons in the rat. *Neurosci Lett* **119,** 148-152.

Eckberg DL, Nerhed C & Wallin BG (1985). Respiratory modulation of muscle sympathetic and vagal cardiac outflow in man. *J Physiol* **365,** 181-196.

Fowler WS (1954). Breaking point of breath-holding. *J Appl Physiol* **6,** 539-545.

Guyenet PG (2014). Regulation of breathing and autonomic outflows by chemoreceptors. *Compr Physiol* **4**, 1511-1562.

Guyenet PG, Stornetta RL, Abbott SBG, Depuy SD, Fortuna MG & Kanbar R (2010). Central CO_2 chemoreception and integrated neural mechanisms of cardiovascular and respiratory control. *J Appl Physiol* **108,** 995-1002.

Hagbarth KE & Vallbo AB (1968). Pulse and respiratory grouping of sympathetic impulses in human muscle nerves. *Acta Physiol Scand* **74,** 96-108.

Hardy JC, Gray K, Whisler S & Leuenberger U (1994). Sympathetic and blood pressure responses to voluntary apnea are augmented by hypoxemia. *J Appl Physiol* **77,** 2360-2365.

Haselton JR & Guyenet PG (1989). Central respiratory modulation of medullary sympathoexcitatory neurons in rat. *Am J Physiol Regul Integr Comp Physiol* **256,** R739-R750.

Heusser K, Dzamonja G, Tank J, Palada I, Valic Z, Bakovic D, Obad A, Ivancev V, Breskovic T, Diedrich A, Joyner MJ, Luft FC, Jordan J & Dujic Z (2009). Cardiovascular regulation during apnea in elite divers. *Hypertension* **53,** 719-724.

Kara T, Narkiewicz K & Somers VK (2003). Chemoreflexes – physiology and clinical implications. *Acta Physiol Scand* **177,** 377-384.

Kasai T, Floras JS & Bradley TD (2012). Sleep apnea and cardiovascular disease: a bidirectional relationship. *Circulation* **126,** 1495-1510.

Leuenberger U, Jacob E, Sweer L, Waravdekar N, Zwillich C & Sinoway L (1995). Surges of muscle sympathetic nerve activity during obstructive apnea are linked to hypoxemia. *J Appl Physiol* **79,** 581-588.

Leuenberger UA, Brubaker D, Quraishi S, Hogeman CS, Imadojemu VA & Gray KS (2005). Effects of intermittent hypoxia on sympathetic activity and blood pressure in humans. *Auton Neurosci* **121,** 87-93.

Lim K, Burke SL, Moretti JL & Head GA (2015). Differential activation of renal sympathetic burst amplitude and frequency during hypoxia, stress and baroreflexes with chronic angiotensin treatment. *Exp Physiol* **100,** 1132-1144.

Macefield VG & Wallin BG (1999). Firing properties of single vasoconstrictor neurones in human subjects with high levels of muscle sympathetic activity. *J Physiol* **516,** 293-301.

Malpas SC, Bendle RD, Head GA & Ricketts JH (1996). Frequency and amplitude of sympathetic discharges by baroreflexes during hypoxia in conscious rabbits. *Am J Physiol Heart Circ Physiol* **271,** H2563-H2574.

Malpas SC & Ninomiya I (1992*a*). Effect of asphyxia on the frequency and amplitude modulation of synchronized renal nerve activity in the cat. *J Auton Nerv Syst* **40,** 199-205.

Malpas SC & Ninomiya I (1992*b*). Effect of chemoreceptor stimulation on the periodicity of renal sympathetic nerve activity in anesthetized cats. *J Auton Nerv Syst* **37,** 19-28.

Morgan BJ, Crabtree DC, Palta M & Skatrud JB (1995). Combined hypoxia and hypercapnia evokes long-lasting sympathetic activation in humans. *J Appl Physiol* **79,** 205-213.

Morgan BJ, Denahan T & Ebert TJ (1993). Neurocirculatory consequences of negative intrathoracic pressure vs. asphyxia during voluntary apnea. *J Appl Physiol* **74,** 2969-2975.

Muenter Swift N, Cutler MJ, Fadel PJ, Wasmund WL, Ogoh S, Keller DM, Raven PB & Smith ML (2003). Carotid baroreflex function during and following voluntary apnea in humans. *Am J Physiol Heart Circ Physiol* **285,** H2411-H2419.

Ninomiya I, Malpas SC, Matsukawa K, Shindo T & Akiyama T (1993). The amplitude of synchronized cardiac sympathetic nerve activity reflects the number of activated pre- and postganglionic fibers in anesthetized cats. *J Auton Nerv Syst* **45,** 139-147.

Numao Y, Koshiya N, Gilbey MP & Spyer KM (1987). Central respiratory drive-related activity in sympathetic nerves of the rat: the regional differences. *Neurosci Lett* **81,** 279-284.

Saito M, Mano T, Iwase S, Koga K, Abe H & Yamazaki Y (1988). Responses in muscle sympathetic activity to acute hypoxia in humans. *J Appl Physiol* **65,** 1548-1552.

Salmanpour A, Brown LJ & Shoemaker JK (2010). Spike detection in human muscle sympathetic nerve activity using a matched wavelet approach. *J Neurosci Methods* **193,** 343-355.

Salmanpour A, Brown LJ, Steinback CD, Usselman CW, Goswami R & Shoemaker JK (2011). Relationship between size and latency of action potentials in human muscle sympathetic nerve activity. *J Neurophysiol* **105,** 2830-2842.

Scott DW (1979). On optimal and data-based histograms. *Biometrika* **66,** 605-610.

Seals DR, Suwarno NO & Dempsey JA (1990). Influence of lung volume on sympathetic nerve discharge in normal humans. *Circ Res* **67,** 130-141.

Seals DR, Suwarno NO, Joyner MJ, Iber C, Copeland JG & Dempsey JA (1993). Respiratory modulation of muscle sympathetic nerve activity in intact and lung denervated humans. *Circ Res* **72,** 440-454.

Seitz MJ, Brown R & Macefield VG (2013). Inhibition of augmented muscle vasoconstrictor drive following asphyxic apnoea in awake human subjects is not affected by relief of chemical drive. *Exp Physiol* **98,** 405-414.

Somers VK, Mark AL, Zavala DC & Abboud FM (1989*a*). Contrasting effects of hypoxia and hypercapnia on ventilation and sympathetic activity in humans. *J Appl Physiol* **67,** 2101-2106.

Somers VK, Mark AL, Zavala DC & Abboud FM (1989*b*). Influence of ventilation and hypocapnia on sympathetic nerve responses to hypoxia in normal humans. *J Appl Physiol* **67,** 2095-2100.

St. Croix CM, Satoh M, Morgan BJ, Skatrud JB & Dempsey JA (1999). Role of respiratory motor output in within-breath modulation of muscle sympathetic nerve activity in humans. *Cir Res* **85,** 457-469.

Steinback CD, Breskovic T, Frances M, Dujic Z & Shoemaker JK (2010*a*). Ventilatory restraint of sympathetic activity during chemoreflex stress. *Am J Physiol Regul Integr Comp Physiol* **299,** R1407-R1414.

Steinback CD, Salmanpour A, Breskovic T, Dujic Z & Shoemaker JK (2010*b*). Sympathetic neural activation: an ordered affair. *J Physiol* **588,** 4825-4836.

Usselman CW, Luchyshyn TA, Gimon TI, Nielson CA, Van Uum SHM & Shoemaker JK (2013). Hormone phase dependency of neural responses to chemoreflex-driven sympathoexcitation in young women using hormonal contraceptives. *J Appl Physiol* **115,** 1415-1422.

Watenpaugh DE, Muenter NK, Wasmund WL, Wasmund SL & Smith ML (1999). Post-apneic inhalation reverses apnea-induced sympathoexcitation before restoration of blood oxygen levels. *Sleep* **22,** 435-440.

Wesseling KH, Jansen JR, Settels JJ & Schreuder JJ (1993). Computation of aortic flow from pressure in humans using a nonlinear, three-element model. *J Appl Physiol* **74,** 2566-2573.

Chapter 6

6 General Discussion

6.1 Overview

The SNS represents a fundamental system of control through which homeostatic adjustments to physiological stress are achieved, occurring largely through the reflexive regulation of blood pressure and blood flow. In turn, this process (i.e., neural control of the circulation) is characterized by a highly integrative and finely-tuned system that is layered with multiple levels of unique, albeit complex, control. Briefly, these include post-ganglionic sympathetic nerve outflow, neurotransmitter release, and the end-organ vascular response. Indeed, since the first human recordings of efferent sympathetic nerve activity in the late 1960's (Hagbarth & Vallbo, 1968), integrative physiologists have been interested in the patterned nature of sympathetic neural discharge and, in turn, its implication for, and role in, the neurovascular control complex. Stated differently, the patterning of neural discharge reflects the strategies used by the CNS to fine-tune sympathetic outflow, and ultimately, control systemic vascular resistance and blood pressure, thereby maintaining homeostasis in the face of physiological perturbation. As such, in the current dissertation, we investigated recruitment strategies in efferent post-ganglionic sympathetic nerve activity with the hopes of gaining greater insight into one of the complex mechanisms by which sympathetic neuro-circulatory control is governed.

6.2 Major Findings

The series of studies contained herein investigated the neural coding patterns employed by the SNS to alter efferent sympathetic outflow in response to homeostatic

challenge, and further, the modifiers of, and mechanisms of control underlying these recruitment strategies. Overall, these studies support the working hypothesis and confirm that neural coding principles operate within the SNS. Specifically, these reflect the ability to increase discharge frequency or rate of already-active, lower-threshold axons (i.e., rate coding), recruit latent, higher-threshold neural sub-populations (i.e., population coding), as well as modify acutely synaptic delays and/or central processing times (i.e., temporal coding) in response to reflex-mediated sympathoexcitatory stress.

A major finding of this series of studies was the ability of the SNS to recruit sub-populations of previously silent (i.e., not active at baseline), larger amplitude, and faster conducting sympathetic axons in response to severe physiological stress. In turn, this recruitment option appears to be a fixed, reflex-independent recruitment strategy available to the SNS, as this pattern was observed during severe chemoreflex- (i.e., *Studies 1, 3, and 4*), baroreflex- (i.e., *Study 1*), and metaboreflex- (i.e., *Study 2*) mediated sympathoexcitation. These data of latent, but recruitable, higher-threshold axons are consistent with rat work in which approximately 20% of post-ganglionic C-fibres are quiet at rest (Habler *et al.* 1994), and are further supported by the concept that C-fibre diameter variations (~0.5 to 2.0 um) exist within the human peroneal nerve (Tompkins *et al.* 2013). However, recruitment of latent axons was not observed during preliminary studies using more modest levels of baroreceptor unloading (i.e., −60 mmHg LBNP) (Salmanpour *et al.* 2011*a*), or in the current dissertation, during low levels of metaboreflex activation (i.e., the first three minutes of SHG exercise; *Study 3*). In these low- to moderate- stress situations, sympathetic outflow was elevated primarily through the increased firing of axons already-active at baseline. Therefore, it appears

that the option to recruit latent neural sub-populations is reserved for severe stress scenarios requiring high sympathetic drive. In this sense, original hypotheses from Macefield and colleagues (Macefield & Wallin, 1999), in which they suggested that recruitment of new axons may be a primary mechanism by which sympathetic activation is achieved, are confirmed presently. However, it appears that a threshold for recruitment of these latent sub-populations exists that varies with stress severity (i.e., reserved for severe stress). Therefore, during low- to moderate- levels of stress, the SNS elevates sympathetic neural drive through increased firing of lower-threshold axons (i.e., those already-active at baseline), whereas during severe stress scenarios, latent sub-populations of higher-threshold sympathetic axons are also recruited to help achieve the high levels of sympathetic outflow necessary to maintain cardiovascular homeostasis. As such, the SNS operates on a principle of ordered recruitment, similar to that of the skeletal motor system during the generation of ever-increasing muscular contraction force (i.e., Henneman's size principle) (Henneman *et al.* 1965). Furthermore, results from *Study 2* suggest that peripheral-reflex mechanisms play a dominant role in mediating this recruitment option. Specifically, latent, higher-threshold axons were present (i.e., recruited) towards the end of fatiguing SHG exercise, and importantly, persisted throughout the PECO phase (i.e., in the absence of central, volitional factors). However, this important finding pertains to a metaboreflex-model, and, therefore, whether this conclusion applies across all reflexes will require future study. Yet, central factors likely play a small and insignificant role during LBNP (i.e., *Study 1*), lending further support to the concept that peripheral sensory mechanisms are responsible for mediating this recruitment strategy. Nonetheless, the

present studies confirm the presence of neural coding patterns in the SNS, reflecting both rate- and population coding strategies in response to acute reflex-mediated sympathoexcitatory stress.

Another major and novel finding of this series of studies is that, in addition to actual recruitment, the SNS exhibits a third strategy to alter efferent sympathetic outflow in response to physiologic stress; that is, the ability to modify acutely synaptic delays and/or central processing times. Specifically, the AP cluster size-latency profile was shifted acutely downward during maximal voluntary apnea (i.e., *Studies 1 and 3*) and towards the end of fatiguing SHG exercise (i.e., minutes four and five; *Study 2*), such that the latency of all corresponding APs with similar peak-to-peak amplitudes (i.e., AP clusters) was reduced during severe stress. Stated differently, lower-threshold axons were recruited with a shorter latency during reflex-mediated stress. In line with these observations, a similar systemic downward shift in the AP cluster size-latency profile was found during the Valsalva maneuver (Salmanpour *et al.* 2011*b*). These findings suggest the possibility of a neural short-cut somewhere within the neural reflex-arc; however, the exact mechanism(s) and/or source(s) of these synaptic delay changes cannot be discerned from the current analyses and will require future study. Interestingly, in contrast to voluntary apnea (i.e., *Studies 1 and 3*) and SHG exercise (i.e., *Study 2*), during −80 mmHg LBNP-induced baroreceptor unloading (i.e., *Study 1*), the AP cluster size-latency profile was shifted acutely upward, such that all APs were recruited with a slower latency during lower body suction. The physiological relevance of this observation is unknown. Nevertheless, the common pattern of a systemic shift to shorter reflex latency during maximal voluntary apnea (i.e., *Studies 1 and 3*), the

Valsalva maneuver (Salmanpour *et al.* 2011*b*), and towards the end of fatiguing SHG exercise, but not during PECO (*i.e., Study 2*), suggests that central, perceptual factors may play a role in mediating the synaptic delay component of sympathetic neural discharge. Furthermore, just like for that observed in the recruitment of latent neural sub-populations, it seems that a threshold level of stress (or perception of stress) exists for this recruitment option; that is, despite central, volitional factors being active throughout all five minutes of SHG (i.e., *Study 2*), a downward shift in the AP cluster size-latency profile was not observed until minutes four and five of exercise, when levels of perceived stress were likely quite high. Nonetheless, in line with early theories from Wallin *et al.* (1994), it appears that acute malleability of synaptic delays and/or central processing times exists as an option available to the SNS to alter sympathetic drive.

Furthermore, findings from *Study 3* provide the first insight into the malleability of these sympathetic neural recruitment strategies with increasing age and cardiovascular disease. Importantly, it was demonstrated that the sympathetic dysregulation commonly observed at rest with age and cardiovascular disease extends to the neural coding patterns used by the SNS to respond to acute physiologic stress. Specifically, while the ability to acutely modify synaptic delays and/or central processing times appears preserved, both the ability to increase within-burst firing frequency of already-recruited axons, and importantly, the capacity of the SNS to recruit latent sub-populations of higher-threshold axons are reduced with healthy aging and perhaps lost altogether with CAD. Therefore, aging, and even more so, cardiovascular disease, impairs sympathetic axonal recruitment during apneic stress.

However, future study is needed to assess recruitment responses to additional reflex stimuli (i.e., baroreflex, metaboreflex, cold pressor test, etc.) to determine if the presently observed impairment in neural discharge patterns with aging and cardiovascular disease is specific to the apnea maneuver itself, or whether it represents a generalized impairment across reflexes.

Finally, results from *Study 4* suggest that, while voluntary apnea appears to provide the most robust stimulus for sympathetic neural recruitment (Steinback *et al.* 2010), the response is largely due to the lack of ventilation itself. That is, increased firing of already-active axons, and also, the recruitment of latent, higher-threshold axons, is largely restrained/inhibited by the act of breathing, despite similar and/or greater levels of severe chemoreflex stress. Therefore, the lack of ventilation *per se*, rather than the increasing chemical drive, appears largely responsible for the robust increases in sympathetic nerve activity observed during apnea.

6.3 Perspectives and Significance

The findings of the studies contained herein enhance our understanding of how the SNS is activated during reflex-mediated physiological stress, and, importantly, provide a novel perspective on sympathetic neural recruitment that may offer additional insight into the complex nature of sympathetic neurovascular control in health and disease. For example, the patterning of sympathetic neural discharge likely exerts important influences on neurotransmitter release which, in turn, likely affects the end-organ homeostatic response. Indeed, the pattern of nerve discharge frequency appears to affect neurotransmitter release, whereby ATP is dominantly released during low frequency nerve activation (Todorov *et al.* 1994), followed by NE release at higher

frequencies (Stjärne & Brundin, 1977), and finally, NPY release at even higher frequencies (Pernow *et al.* 1989). However, the effect of increased firing probabilities and recruitment of latent axons on neurotransmitter release patterns and the end-organ vascular response (i.e., 'neurovascular transduction') remains to be determined. Yet, it appears reasonable that these recruitment strategies may code for and/or combine to elicit different functional responses within the end-organ, that, in turn, optimize the ability of the SNS to buffer acute homeostatic perturbation. Indeed, efforts from the integrated MSNA neurogram have demonstrated that total burst activity, likely reflective of the integration and details of these sympathetic axonal recruitment patterns (i.e., increased firing probability, latent neural sub-populations, synaptic delays, etc.), influence directly the magnitude of decrease in leg vascular conductance (Fairfax *et al.* 2013). Nonetheless, the exact role(s) of these recruitment strategies available to the SNS in the overall sympathetic neuro-circulatory control complex remains to be discovered.

Furthermore, the data from this dissertation suggest that there are implications of these recruitment strategies for cardiovascular disease, which, by extension, may provide novel mechanistic insight into the aberrant sympathetic control seen in certain cardiovascular-related pathologies. For example, findings of exaggerated sympathetic and pressor responses to exercise in certain pathologies like hypertension (Delaney *et al.* 2010) and chronic heart failure (Notarius *et al.* 2001; Murai *et al.* 2009) point to abnormal central features of sympathetic neural recruitment. Yet, how these observations integrate with the current observations of diminished recruitment in CAD patients remains to be investigated. Nonetheless, the current analytical technique may

offer a novel and innovative approach in the understanding of the mechanisms contributing to abnormal sympathetic discharge patterns in humans. Certainly, these important issues warrant further study.

6.4 Conclusion

In conclusion, the series of studies contained within this dissertation confirm the presence of neural coding patterns in efferent post-ganglionic sympathetic nerve activity, and further, offer novel insight into the recruitment strategies used by the SNS to respond to homeostatic challenge. Specifically, in response to acute physiological stress, the SNS has options to increase the firing frequency of already-active, lower-threshold axons, recruit latent sub-populations of larger-sized, higher-threshold axons, as well as modify acutely synaptic delays and/or central processing times. The recruitment of latent neuronal sub-populations represents a reflex-independent strategy within the SNS that is reserved for severe stress scenarios requiring high sympathetic outflow, and further, is likely mediated via peripheral-reflex sensory mechanisms. However, it appears that the capacity of the SNS to recruit these latent axons is reduced with aging and perhaps lost altogether in cardiovascular disease. In contrast, the synaptic delay component of efferent nerve discharge is reflex-specific, is influenced by central, perceptual factors, and appears preserved with increasing age and cardiovascular disease.

6.5 References

Delaney EP, Greaney JL, Edwards DG, Rose WC, Fadel PJ & Farquhar WB (2010). Exaggerated sympathetic and pressor responses to handgrip exercise in older hypertensive humans: role of the muscle metaboreflex. *Am J Physiol Heart Circ Physiol* **299,** H1318-H1327.

Fairfax ST, Padilla J, Vianna LC, Davis MJ & Fadel PJ (2013). Spontaneous bursts of muscle sympathetic nerve activity decrease leg vascular conductance in resting humans. *Am J Physiol Heart Circ Physiol* **304,** H759-H766.

Habler H, Janig W, Krummel M & Peters O (1994). Reflex patterns in postganglionic neurons supplying skin and skeletal muscle of the rat hindlimb. *J Neurophysiol* **72,** 2222-2236.

Hagbarth KE & Vallbo AB (1968). Pulse and respiratory grouping of sympathetic impulses in human muscle nerves. *Acta Physiol Scand* **74,** 96-108.

Henneman E, Somjen G & Carpenter DO (1965). Functional significance of cell size in spinal motoneurons. *J Neurophysiol* **28,** 560-580.

Macefield VG & Wallin BG (1999). Firing properties of single vasoconstrictor neurones in human subjects with high levels of muscle sympathetic activity. *J Physiol* **516,** 293-301.

Murai H, Takamura M, Maruyama M, Nakano M, Ikeda T, Kobayashi D, Otowa K, Ootsuji H, Okajima M, Furusho H, Takata S & Kaneko S (2009). Altered firing pattern of single-unit muscle sympathetic nerve activity during handgrip exercise in chronic heart failure. *J Physiol* **587,** 2613-2622.

Notarius CF, Atchison DJ & Floras JS (2001). Impact of heart failure and exercise capacity on sympathetic response to handgrip exercise. *Am J Physiol Heart Circ Physiol* **280,** H969-H976.

Pernow J, Schwieler J, Kahan T, Hjemdahl P, Oberle J, Wallin BG & Lundberg J (1989). Influence of sympathetic discharge pattern on norepinephrine and neuropeptide Y release. *Am J Physiol Heart Circ Physiol* **257,** H866-H872.

Salmanpour A, Brown LJ, Steinback CD, Usselman CW, Goswami R & Shoemaker JK (2011*a*). Relationship between size and latency of action potentials in human muscle sympathetic nerve activity. *J Neurophysiol* **105,** 2830-2842.

Salmanpour A, Frances MF, Goswami R & Shoemaker JK (2011*b*). Sympathetic neural recruitment patterns during the Valsalva maneuver. *Conf Proc IEEE Eng Med Biol Soc* **2011,** 6951-6954.

Steinback CD, Salmanpour A, Breskovic T, Dujic Z & Shoemaker JK (2010). Sympathetic neural activation: an ordered affair. *J Physiol* **588,** 4825-4836.

Stjärne L & Brundin J (1977). Frequency-dependence of 3H-noradrenaline secretion from human vasoconstrictor nerves: modification by factors interfering with α- or β-adrenoceptor or prostaglandin E2 mediated control. *Acta Physiol Scand* **101,** 199-210.

Todorov LD, Bjur RA & Westfall DP (1994). Temporal dissociation of the release of the sympathetic co-transmitters ATP and noradrenaline. *Clin Exp Pharmacol Physiol* **21,** 931-932.

Tompkins RP, Melling CW, Wilson TD, Bates BD & Shoemaker JK (2013). Arrangement of sympathetic fibers within the human common peroneal nerve: implications for microneurography. *J Appl Physiol* **115,** 1553-1561.

Wallin BG, Burke D & Gandevia S (1994). Coupling between variations in strength and baroreflex latency of sympathetic discharges in human muscle nerves. *J Physiol* **474,** 331-338.

Appendix A: Ethics Approval

Western

Office of Research Ethics

The University of Western Ontario
Room 4180 Support Services Building, London, ON, Canada N6A 5C1
Telephone: (519) 661-3036 Fax: (519) 850-2466 Email: ethics@uwo.ca
Website: www.uwo.ca/research/ethics

Use of Human Subjects - Ethics Approval Notice

Principal Investigator: Dr. K. Shoemaker
Review Number: 16912 **Review Level:** Full Board
Review Date: February 23, 2010 **Approved Local # of Participants:** 30
Protocol Title: Sex-specific hormone levels and reflex sympathoexcitation
Department and Institution: Kinesiology, University of Western Ontario
Sponsor: NSERC # 217916-2008
Ethics Approval Date: March 12, 2010 **Expiry Date:** December 31, 2012
Documents Reviewed and Approved: UWO Protocol, Letter of information & consent form & Advertisement
Documents Received for Information:

This is to notify you that The University of Western Ontario Research Ethics Board for Health Sciences Research Involving Human Subjects (HSREB) which is organized and operates according to the Tri-Council Policy Statement: Ethical Conduct of Research Involving Humans and the Health Canada/ICH Good Clinical Practice Practices: Consolidated Guidelines; and the applicable laws and regulations of Ontario has reviewed and granted approval to the above referenced study on the approval date noted above. The membership of this REB also complies with the membership requirements for REB's as defined in Division 5 of the Food and Drug Regulations.

The ethics approval for this study shall remain valid until the expiry date noted above assuming timely and acceptable responses to the HSREB's periodic requests for surveillance and monitoring information. If you require an updated approval notice prior to that time you must request it using the UWO Updated Approval Request Form.

During the course of the research, no deviations from, or changes to, the protocol or consent form may be initiated without prior written approval from the HSREB except when necessary to eliminate immediate hazards to the subject or when the change(s) involve only logistical or administrative aspects of the study (e.g. change of monitor, telephone number). Expedited review of minor change(s) in ongoing studies will be considered. Subjects must receive a copy of the signed information/consent documentation.

Investigators must promptly also report to the HSREB:

a) changes increasing the risk to the participant(s) and/or affecting significantly the conduct of the study;
b) all adverse and unexpected experiences or events that are both serious and unexpected;
c) new information that may adversely affect the safety of the subjects or the conduct of the study.

If these changes/adverse events require a change to the information/consent documentation, and/or recruitment advertisement, the newly revised information/consent documentation, and/or advertisement, must be submitted to this office for approval.

Members of the HSREB who are named as investigators in research studies, or declare a conflict of interest, do not participate in discussion related to, nor vote on, such studies when they are presented to the HSREB.

[redacted]

Chair of HSREB: Dr. Joseph Gilbert
FDA Ref. #: IRB 00000940

Ethics Officer to Contact for Further Information			
☙ Janice Sutherland (jsutherl@uwo.ca)	☐ Elizabeth Wambolt (ewambolt@uwo.ca)	☐ Grace Kelly (grace.kelly@uwo.ca)	☐ Denise Grafton (dgrafton@uwo.ca)

This is an official document. Please retain the original in your files.

cc: ORE File

Western Research

Research Ethics

Use of Human Participants - Revision Ethics Approval Notice

Principal Investigator: Dr. Kevin Shoemaker
File Number:102782
Review Level: Delegated
Protocol Title: Effect of central blood volume manipulation on the cardiac output contribution to the exercise pressor reflex
Department & Institution: Health Sciences\Kinesiology,Western University
Sponsor: Natural Sciences and Engineering Research Council

Ethics Approval Date: December 23, 2013 **Expiry Date:**December 31, 2014
Documents Reviewed & Approved & Documents Received for Information:

Document Name	Comments	Version Date
Increase in number of local Participants	The number of participants has been revised to 33 from 16 in order to achieve complete data sets.	
Revised Western University Protocol		
Revised Letter of Information & Consent	V2	

This is to notify you that The University of Western Ontario Research Ethics Board for Health Sciences Research Involving Human Subjects (HSREB) which is organized and operates according to the Tri-Council Policy Statement: Ethical Conduct of Research Involving Humans and the Health Canada/ICH Good Clinical Practice Practices: Consolidated Guidelines; and the applicable laws and regulations of Ontario has reviewed and granted approval to the above referenced revision(s) or amendment(s) on the approval date noted above. The membership of this REB also complies with the membership requirements for REB's as defined in Division 5 of the Food and Drug Regulations.

The ethics approval for this study shall remain valid until the expiry date noted above assuming timely and acceptable responses to the HSREB's periodic requests for surveillance and monitoring information. If you require an updated approval notice prior to that time you must request it using the University of Western Ontario Updated Approval Request Form.

Members of the HSREB who are named as investigators in research studies, or declare a conflict of interest, do not participate in discussion related to, nor vote on, such studies when they are presented to the HSREB.

The Chair of the HSREB is Dr. Joseph Gilbert. The HSREB is registered with the U.S. Department of Health & Human Services under the IRB registration number IRB 00000940.

[redacted]

Ethics Officer to Contact for Further Information

Erika Basile (ebasile@uwo.ca)	Grace Kelly (grace.kelly@uwo.ca)	Mina Mekhail (mmekhail@uwo.ca)	Vikki Tran (vikki.tran@uwo.ca)

This is an official document. Please retain the original in your files.

Research Western

Use of Human Participants - Ethics Approval Notice

Principal Investigator: Dr. Kevin Shoemaker
Review Number: 17810
Review Level: Full Board
Approved Local Adult Participants: 200
Approved Local Minor Participants: 0
Protocol Title: Architecture of Cortical Somatosensory and Autonomic Neural Networks Supporting Muscular Movement: Impacts of Vascular Disease and Exercise Interventions.
Department & Institution: Kinesiology,University of Western Ontario
Sponsor: Canadian Institutes of Health Research

Ethics Approval Date: June 09, 2011 **Expiry Date:** December 31, 2016

Documents Reviewed & Approved & Documents Received for Information:

Document Name	Comments	Version Date
UWO Protocol		
Letter of Information & Consent		2011/06/06
Advertisement		
Advertisement		
Other	Patient recruitment letter	
Other	Control group recruitment letter	
Advertisement		
Other	3 - Day food recall	

This is to notify you that the University of Western Ontario Health Sciences Research Ethics Board (HSREB) which is organized and operates according to the Tri-Council Policy Statement: Ethical Conduct of Research Involving Humans and the Health Canada/ICH Good Clinical Practice Practices: Consolidated Guidelines; and the applicable laws and regulations of Ontario has reviewed and granted approval to the above referenced study on the approval date noted above. The membership of this HSREB also complies with the membership requirements for REB's as defined in Division 5 of the Food and Drug Regulations.

The ethics approval for this study shall remain valid until the expiry date noted above assuming timely and acceptable responses to the HSREB's periodic requests for surveillance and monitoring information. If you require an updated approval notice prior to that time you must request it using the UWO Updated Approval Request form.

Member of the HSREB that are named as investigators in research studies, or declare a conflict of interest, do not participate in discussions related to, nor vote on, such studies when they are presented to the HSREB.

The Chair of the HSREB is Dr. Joseph Gilbert. The UWO HSREB is registered with the U.S. Department of Health & Human Services under the IRB registration number IRB 00000940.

[redacted]

Ethics Officer to Contact for Further Information

___ Janice Sutherland (jsutherl@uwo..ca)	____Grace Kelly (grace.kelly@uwo.ca)	✓Shantel Walcott (swalcot@uwo.ca)

This is an official document. Please retain the original in your files.

Western Research

Research Ethics

Use of Human Participants - Ethics Approval Notice

Principal Investigator: Dr. Kevin Shoemaker
File Number:103838
Review Level: Full Board
Approved Local Adult Participants:0
Approved Local Minor Participants:0
Protocol Title: Central motor pathways affecting cardiovascular arousal.
Department & Institution: Health Sciences\Kinesiology,Western University
Sponsor:
Ethics Approval Date: July 11, 2013
Ethics Expiry Date: May 31, 2016

Documents Reviewed & Approved & Documents Received for Information:

Document Name	Comments	Version Date
Other	Approval Letter from the University of Split (translated version) - Received for information	2013/05/03
Response to Board Recommendations	Response to HSREB Comments and Queries	2013/05/30
Response to Board Recommendations	Response to Special Query regarding roles of investigators, and participant recruitment location	2013/05/30
Letter of Information & Consent	Revised LOI, CLEAN	2013/05/30
Western University Protocol		

This is to notify you that the University of Western Ontario Health Sciences Research Ethics Board (HSREB) which is organized and operates according to the Tri-Council Policy Statement: Ethical Conduct of Research Involving Humans and the Health Canada/ICH Good Clinical Practice Practices: Consolidated Guidelines; and the applicable laws and regulations of Ontario has reviewed and granted approval to the above referenced study on the approval date noted above. The membership of this HSREB also complies with the membership requirements for REB's as defined in Division 5 of the Food and Drug Regulations.

The ethics approval for this study shall remain valid until the expiry date noted above assuming timely and acceptable responses to the HSREB's periodic requests for surveillance and monitoring information. If you require an updated approval notice prior to that time you must request it using the University of Western Ontario Updated Approval Request form.

Member of the HSREB that are named as investigators in research studies, or declare a conflict of interest, do not participate in discussions related to, nor vote on, such studies when they are presented to the HSREB.

The Chair of the HSREB is Dr. Joseph Gilbert. The HSREB is registered with the U.S. Department of Health & Human Services under the IRB registration number IRB 00000940.

[redacted]

Ethics Officer to Contact for Further Information

Erika Basile (ebasile@uwo.ca)	Grace Kelly (grace.kelly@uwo.ca)	Shantel Walcott (swalcot@uwo.ca)

This is an official document. Please retain the original in your files.

Western University, Research, Support Services Bldg., Rm. 5150
London, ON, Canada N6A 3K7 t. 519.661.3036 f. 519.850.2466 www.uwo.ca/research/services/ethics

SCHOOL OF MEDICINE
UNIVERSITY OF SPLIT
Ethics Committee

Class: 003-08/14-03/0001
Reg. no.: 2181-198-03-04-14-0039

Split, 11 September 2014

CERTIFICATE
of the Ethics Committee that research project application:

Cerebrovascular regulation during apnea in elite breath-hold divers

submitted by professor Željko Dujić to Ethics Committee of the University of Split School of Medicine, entitled Cerebrovascular regulation in elite divers but with identical experimental protocol was approved though three different requests for approval.
The research in question was approved on 11 September 2013 (Class: 003-08/13-03/0003, Reg. no.: 2181-198-03-04-13-0032).
Two requests for expansion of the approval were submitted subsequently due to the expansion of the experimental protocol. Both applications were revised and approved by the Ethics committee (03 March 2014; Class: 003-08/14-03/0001, Reg. no.: 2181-198-03-04-14-0011 te 08 April 2014; Class: 003-08/14-03/0001, Reg. no.: 2181-198-03-04-14-0015)

According to the provisions of Article 16 of the School of Medicine in Split Code of Ethics, the Committee decided that the research **Cerebrovascular regulation during apnea in elite breath-hold divers** is **in accordance with the provisions of the Code of Ethics** which regulate research on human subjects in scientific, research and professional work and with the ethical principles of Declaration of Helsinki.

Committee Chair:

[redacted]

Professor Miroslav Simunić

Deliver to:
- Professor Željko Dujic x2
- Ethics Committee of the School of Medicine archive
- School archive

Appendix B: Rights of Authors of APS Articles

Copyright

The APS Journals are copyrighted for the protection of authors and the Society. The Mandatory Submission Form serves as the Society's official copyright transfer form.

Rights of Authors of APS Articles

- For educational purposes only:
  - Authors may republish parts of their final-published version articles (e.g., figures, tables), without charge and without requesting permission, provided that full acknowledgement of the source is given in the new work.
  - Authors may use their articles (in whole or in part) for presentations (e.g., at meetings and conferences). These presentations may be reproduced on any type of media in materials arising from the meeting or conference such as the proceedings of a meeting or conference. A copyright fee will apply if there is a charge to the user or if the materials arising are directly or indirectly commercially supported.
- Posting of the accepted or final version of articles or parts of articles is restricted and subject to the conditions below:
  - ***Theses and dissertations.*** APS permits whole published articles to be reproduced without charge in dissertations and posted to thesis repositories. Full citation is required.
  - ***Open courseware.*** Articles, or parts of articles, may be posted to a public access courseware website. Permission must be requested from the APS. A copyright fee will apply during the first 12 months of the article's publication by the APS. Full citation is required.
  - ***Websites.*** Authors may not post a PDF of the accepted or final version of their published article on any website including social and research networking platforms; instead, links may be posted to the article on the APS journal website (see exception to authors' own institution's repository, as note below).
  - ***Institutional repositories (non-theses).*** Authors may deposit their accepted, peer-reviewed manuscripts into an institutional repository providing:
    - the APS retains copyright to the article[1]
    - a 12 month embargo period from the date of final publication of the article is observed by the institutional repository and the author
    - a link to the published article on the APS website is prominently displayed with the article in the institutional repository
    - the article is not used for commercial purposes
    - Self-archived articles posted to repositories are without warranty of any kind

    [1]Unless it is published under the APS *AuthorChoice* open access option, which allows for immediate public access under a Creative Commons license (CC BY)

    (See also the APS Policy on Depositing Articles in PMC.)

Curriculum Vitae

Name: Mark B. Badrov

Post-secondary Education and Degrees:

Western University
London, Ontario, Canada
2012-2017 PhD (Integrative Physiology of Exercise)

University of Windsor
Windsor, Ontario, Canada
2010-2012 MHK (Applied Human Performance)

McMaster University
Hamilton, Ontario, Canada
2006-2010 BKin (Honours Kinesiology)

Honours and Awards:

Peñáz-Wesseling Award for Systemic Hemodynamics, $2500
2015

Canada Graduate Scholarships – Michael Smith Foreign Study Supplement, $6000
2015

Canadian Institutes of Health Research Frederick Banting and Charles Best Canada Graduate Scholarship – Doctoral Research Award, $105,000
2013-2016

Western Graduate Research Scholarship, $45 000
2012-2016

Graduate Research Excellence Award, $250
2012

Outstanding Graduate Research Award
2012

Verdecchia Family Scholarships in Health Sciences Award, $1000
2012

University of Windsor Faculty of Graduate Studies Research Grant, $500
2011

Ontario Graduate Scholarship Award, $15 000
2011-2012

University of Windsor Dean's Honour Role
2010-2012

University of Windsor Postgraduate Tuition Scholarship, $18000
2010-2012

Summa Cum Laude Distinction, McMaster University
2010

Dr. Harry Lyman Hooker Scholarship, $1000
2009

McMaster University Dean's Honour List
2006-2010

Marauder Scholar Award, McMaster University
2006

Related Work Experience

Clinical Research Assistant
Children's Health Research Institute
London Health Sciences Centre
2016 –

Research Assistant
Laboratory for Brain and Heart Health
Western University
2015 –

Research Assistant
Neurovascular Research Laboratory
Western University
2012-2016

Teaching Assistant
Western University
2012-2014

Research Assistant
Physical Activity and Cardiovascular Research Laboratory
University of Windsor
2010-2012

Graduate Teaching Assistant
University of Windsor
2010-2012

Publications:

Peer-Reviewed Articles

1. Zamir M, **Badrov MB**, Olver TD & Shoemaker JK (2017). Cardiac baroreflex variability and resetting during sustained mild effort. *Front Physiol* **8,** 246.

2. **Badrov MB**, Olver TD & Shoemaker JK (2016). Central versus peripheral determinants of sympathetic neural recruitment: insights from static handgrip exercise and postexercise circulatory occlusion. *Am J Physiol Regul Integr Physiol* **311,** R1013-R1021.

3. **Badrov MB**, Lalande S, Olver TD, Suskin N & Shoemaker JK (2016). Effects of aging and coronary artery disease on sympathetic neural recruitment strategies during end-inspiratory and end-expiratory apnea. *Am J Physiol Heart Circ Physiol* **311,** H1040-H1050.

4. **Badrov MB**, Freeman SR, Zokvic MA, Millar PJ & McGowan CL (2016). Isometric exercise training lowers resting blood pressure and improves local brachial artery flow-mediated dilation equally in men and women. *Eur J Appl Physiol* **116,** 1289-1296.

5. Coverdale NS, **Badrov MB** & Shoemaker JK (2016). Impact of age on cerebrovascular dilation versus reactivity to hypercapnia. *J Cereb Blood Flow Metab* **37,** 344-355.

6. Shoemaker JK, **Badrov MB**, Al-Khazraji BK & Jackson DN (2016). Neural control of vascular function in skeletal muscle. *Compr Physiol* **6,** 303-329.

7. Norton KN, **Badrov MB**, Barron CC, Suskin N, Heinecke A & Shoemaker JK (2015). Coronary artery disease affects cortical circuitry associated with brain-heart integration during volitional exercise. *J Neurophysiol* **114,** 835-845.

8. **Badrov MB**, Usselman CW & Shoemaker JK (2015). Sympathetic neural recruitment strategies: responses to severe chemoreflex and baroreflex stress. *Am J Physiol Regul Integr Physiol* **309,** R160-168.

9. **Badrov MB**, Bartol CL, DiBartolomeo MA, Millar PJ, McNevin NH & McGowan CL (2013). Effects of isometric handgrip training dose on resting blood pressure and resistance vessel endothelial function in normotensive women. *Eur J Appl Physiol* **113,** 2091-2100.

10. **Badrov MB**, Horton S, Millar PJ & McGowan CL (2013). Cardiovascular stress reactivity tasks successfully predict the hypotensive response of isometric handgrip training in hypertensives. *Psychophysiology* **50,** 407-414.

11. **Badrov MB**, Millar PJ & McGowan CL (2010). Role of isometric handgrip training in the management of hypertension: Insights from cardiovascular stress reactivity testing. *Crit Rev Phys Rehabil Med* **22,** 13-27.

Peer-Reviewed Abstracts

1. Al-Khazraji BK, Badrov MB, Vording JL, Birmingham TB & Shoemaker JK (2017). Osteoarthritis patients exhibit cerebrovascular control impairment similar to ischemic heart disease patients. *Osteoarthritis Cartilage* **25,** S343.

2. **Badrov MB**, Wood KN, Lalande S, Suskin N & Shoemaker JK (2016). Exaggerated pressor and sympathetic responses to short-duration static handgrip in coronary artery disease patients: Effect of six-months of cardiac rehabilitation. *Clin Auton Res* **26,** 357.

3. Limberg JK, Holbein WW, **Badrov MB**, Joyner MJ & Shoemaker JK (2016). Contribution of the carotid chemoreflex to sympathetic discharge patterns in healthy humans. *Clin Auton Res* **26,** LB6.

4. **Badrov MB**, Norton KN, Lalande S, Suskin N & Shoemaker JK (2016). Effect of six months of cardiac rehabilitation on autonomic function in coronary artery disease patients. *FASEB J* **30,** 756.5.

5. Abbott KC, **Badrov MB**, Elfassy J, Moir EM, Fischer SA, Fischer LK, Fraser DD & Shoemaker JK (2016). Cardiac autonomic function is impaired in adolescents with mild traumatic brain injury. *FASEB J* **30,** LB724.

6. **Badrov MB**, Lalande S & Shoemaker JK (2015). Effects of healthy aging and coronary artery disease on sympathetic axonal recruitment strategies during prolonged end-inspiratory apnea. *Auton Neurosci* **192,** 113-114.

7. Pearl MD, Zokvic MA, Somani YB, **Badrov MB**, Hanik SE, Baross AW, Swaine IL, Milne KJ & McGowan CL (2015). Using bilateral and unilateral exercise to better understand the blood pressure lowering effects of isometric handgrip training: preliminary findings. *Appl Physiol Nutr Metab* **40,** S51-S52.

8. Coverdale NS, **Badrov MB** & Shoemaker JK (2015). Impaired middle cerebral artery and cerebrovascular vasodilation in healthy aging. *FASEB J* **29,** 645.5.

9. **Badrov MB**, Usselman CW & Shoemaker JK (2015). Sympathetic axonal recruitment during severe chemoreflex stress in humans. *FASEB J* **29,** 653.4.

10. Somani YB, Hanik SE, **Badrov MB**, Baross AW, Swaine IL, Milne KJ & McGowan CL (2014). Can blood pressure reactivity to a 2-minute isometric handgrip task predict reductions in ambulatory blood pressure? *Appl Physiol Nutr Metab* **39,** S43.

11. **Badrov MB**, Usselman CW & Shoemaker JK (2014). Sympathetic neural recruitment during severe chemoreflex stimulation. *FASEB J* **28,** LB732.

12. Somani Y, Hanik SE, Malandruccalo A, Freeman S, Caruana N, **Badrov MB**, Baross A, Swaine I, Milne K & McGowan CL (2014). Isometric handgrip (IHG) training-induced reductions in resting blood pressure: reactivity to a 2-minute handgrip task identifies responders and non-responders in young normotensive individuals. *FASEB J* **28,** LB661.

13. Freeman SR, **Badrov MB**, Seifarth J, Hanik SE, Millar PJ, Milne KJ & McGowan CL (2014). Brachial artery flow-mediated constriction and dilation in response to a cardiovascular stress: potential influence of age. *FASEB J* **28,** LB683.

14. **Badrov MB**, Usselman CW, Luchyshyn TA, Gimon TI, Nielson CA & Shoemaker JK (2013). Sympathetic neural recruitment patterns during −80 mmHg lower body negative pressure. *Appl Physiol Nutr Metab* **38,** 1021-1022.

15. **Badrov MB**, Freeman SR, Millar PJ & McGowan CL (2013). Sex-differences in the effects of isometric handgrip training on resting blood pressure and resistance vessel function. *FASEB J* **27,** 1132.21.

16. Hanik SE, **Badrov MB**, Stiller-Moldovan CL, DiBartolomeo MA, Millar PJ, Clarke D, McNevin NH & McGowan CL (2012). Isometric handgrip training induces equal blood pressure reductions in normotensive males and females without influencing heart rate variability. *Can J Cardiol* **28,** S118-S119.

17. **Badrov MB**, DiBartolomeo M, Stiller-Moldovan CL, Clarke D, Millar PJ & McGowan CL (2011). Isometric handgrip training lowers resting arterial blood pressure and improves global heart rate variability in young, normotensive individuals. *Appl Physiol Nutr Metab* **36,** S300.